L-PYRROLIDINE-2-CARBOXYLIC ACID SULFATE (LPCAS): A NEW IONIC LIQUID FOR THE SYNTHESIS OF 1,8-DIOXOOCTAHYDROXANTHENES

Vaibhav W. Godse,[a] Sahebrao S. Rindhe,[b] László Kótai,[c] Yogesh W. More[c] [d], Rajeeta D. Ingle[d]and Rajendra P. Pawar[d]*

Keywords: 1,8-dioxooctahydroxanthenes, L-pyrrolidine-2-carboxylic acid sulfate (LPCAS), eco-friendly, solvent free, ionic liqud

A clean, simple, highly efficient and eco-friendly benign method for the synthesis of 1, 8-dioxooctahydroxanthene derivatives utilizing novel bronsted acidic ionic liquid; L-Pyrrolidine-2-carboxylic acid sulfate (LPCAS) as reagent been reported. Distinguishing features of the methodology are excellent yield of products in shorter reaction time, cleaner reaction profile, environmentally friendly nature and the use of inexpensive reagent.

*Corresponding Authors
E-mail addresses: rppawar@yahoo.com
Telephone: +91-240-2367335; Fax: +091-240-2367335.
[a] Department of Chemistry, NACS College, Ahmednagar, 414001, Maharashtra, India.
[b] Department of Chemistry, R K M Mahavidyalaya, Ahmednagar, 414001, Maharashtra, India.
[c] Institute of Materials and Environmental Chemistry,Research Centre for Natural Sciences, Hungarian Academy of Sciences, Budapest, 1171, Magyar Tudósok krt. 2.
[d] Department of Chemistry, Deogiri College, Aurangabad, 431005, Maharashtra, India.

Introduction

Organic synthesis commonly includes the use of variety of solvents which are mostly harmful to the environment and human being. Multistep reactions for the synthesis of organic compounds multiply consuming of solvents and reagents, which generates a demand to design and develop environmentally benign multi-component and solvent-free green organic transformations.

Multicomponent reactions (MCR) are processes, in which three or more reactants are combined in one pot to produce products that incorporate substantial portion of all the components; naturally comply with many of these stringent requirements for ideal organic synthesis.

Xanthene derivatives have been attracted various researchers due to significant value in pharmaceutical aspect. 1,8-dioxooctahydroxanthene derivatives have different biological potential as such antibacterial,[1] antiviral[2] and anti-inflammatory,[3] etc. 1,8-dioxo-octahydroxanthene derivatives have medicinal significance. The basic scaffold of these heterocycles could be an attractive model for the identification of new and potential anticancer agents.[4] Literature survey also shows that such derivatives have activities concern with antiplasmodial,[5] antagonists for drug resistant leukemia lines,[6] pH-sensitive fluorescent materials,[7] laser technologies,[8] etc. These compounds are also used as precursors in the synthesis of various organic compounds and dyes.[9,10]

Numerous methods have been reported for efficient and facile synthesis of 1,8-dioxooctahydroxanthenes by using different catalyst, including DBSA.[11] cellulose sulfonic acid.[12] $CaCl_2$,[13] $[Et_3NH][HSO_4]$,[14] $SiCl_4$,[15] ceric ammonium nitrate (CAN),[16] Amberlyst-15,[17] nano-TiO_2,[18] Fe-Montmorillonite,[19] $SmCl_3$,[20] trimethylsilyl chloride,[21] $H_3PW_{12}O_{40}$-MCM-41,[22][bmim]HSO_4,[23] CAN supported on HY-zeolite,[24] [Hbim]BF_4.[25]

These reported methods have various disadvantages and to overcome these problems, we have developed a green protocol for efficient synthesis of 1,8-dioxoocta-hydroxanthenes using a Brönsted acidic ionic liquid, L-pyrrolidine-2-carboxylic acid sulphate LPCAS)[26] Scheme1). Ionic liquids (ILs) are environmental friendly reaction media or catalysts with many excellent advantages such as negligible volatility and good thermal stability.

In the present work, L-pyrrolidine-2-carboxylic acid sulfate as environmentally benign component has been used for the first time in the synthesis of bioactive1,8-dioxo-octahydroxanthene derivatives via multicomponent reaction of aldehydes and dimedone under solvent free conditions (Scheme1).

Experimental Procedure

All the reagents were purchased from Aldrich/Merck and used without further purification. Melting points were obtained by using digital melting point apparatus EQ730 (Equiptronics) and uncorrected. Progress of reactions and the purity of product formation were monitored on thin layer chromatography using silica gel as stationary phase and hexane/ethyl acetate 8:2 as eluent. The products were characterized by comparing melting points and spectral data with authentic melting points and spectroscopic data (IR, ^{1}H NMR). IR spectra were recorded on schimadzu IR Solution 150SUI spectrophotometer using KBr pellet; values are expressed in cm^{-1}. NMR spectra were recorded on Bruker 400 MHz spectrometer using appropriate solvent and TMS as an internal standard. Chemical shift were expressed in ppm.

Table 1. Synthesis of 1,8-dioxooctahydroxanthenederivatives catalyzed by LPCAS (3a-j).

Sr. No.	Aldehyde	Time (mins)	Yield (%)	Melting Point (°C) Observed	Reported	References
3a	Benzaldehyde	05	95	202-204	205-206	[27]
3b	4-Nitro bennzaldehyde	10	95	220-222	221-223	[12]
3c	4-hydroxy benzaldehyde	25	85	240-242	241-243	[12]
3d	4-chloro benzaldehyde	05	85	232-234	231-233	[27]
3e	4-Methoxy benzaldehyde	05	95	238-240	241-243	[12]
3f	1-Naphthaldehyde	15	85	230-232	231-233	[16]
3g	4-Dimethylamino benzaldehyde	15	92	220-222	224-226	[11]
3h	2-hydroxy-1-naphthaldehyde	60	85	256-257	--------	This Work
3i	9-Anthraldehyde	50	85	280	---------	This Work
3j	4-Hydroxy-3-methoxy benzaldehyde	55	90	222-224	226-228	[28]

Mass spectra were scanned on a Jeol JMSD-300 spectrometer.

General procedure for synthesisof 1,8-dioxooctahydro-xanthenederivatives

To a mixture of the appropriate aldehyde (1 mmol), 5,5-dimethyl-1,3-cyclohexanedione (2 mmol) and L-pyrrolidine-2-carboxylic acid sulfate (LPCAS) (1 mmol) was added and the mixture was stirred at 100˚C for appropriate time (Scheme 1). The progress of reaction was monitored on TLC. After completion of reaction, the reaction mixture was cooled to room temperature and water (10 ml) was added. Separated solid was filtered and the crude was recrystallized from ethanol to give the pure product. Similarly the other derivatives were also prepared using same procedure and reported in Table 1.

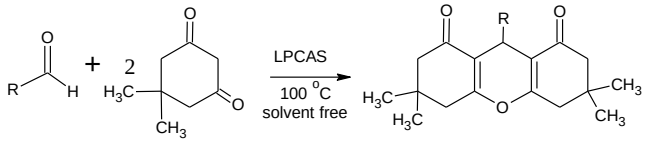

1a-1j **2** **3(a-j)**

Scheme1. Synthesis of 1,8-dioxooctahydroxanthenederivatives.

Spectral data of selected compounds

The known compounds 3a-g and 3j were identified comparing their physical and spectroscopical data with the reference data.11,12,16,27,28

Compound 3h: FTIR (KBr) (cm 1):3420, 3180, 3056, 2941, 2891, 1643, 1622, 1583, 1373, 1359, 1261, 1234, 1197, 1028, 1010, 746. ^{1}H NMR (400 MHz, DMSO): δ ppm 0.80 (s 3H), 0.92 (s 3H), 0.99 (s 3H), 1.08 (s 3H), 2.06-2.10 (d 2H), 2.27-2.31 (d 2H), 2.38-2.42 (d 2H), 2.51-2.63 (d 2H), 3.39 (brs 1H), 7.18-7.20 (d 1H), 7.35-7.43 (m 2H), 7.71-7.73 (d 1H), 7.79-7.81 (d 1H), 8.19-8.21 (brs 1H), 5.57 (s 1H). ^{13}C NMR (400 MHz, DMSO): 195.80, 147.98, 131.56, 130.47, 128.07, 127.53, 126.23, 117.31, 116.59, 110.68, 50.60, 40.53, 31.67, 31.37, 29.34, 27.55, 25.93. m/z: 417.2.

Compound 3i:FTIR (KBr) (cm ^{1}): 3320, 3130,2986, 2887, 2870, 1661, 1573, 1469, 1371, 1229, 1147, 1014, 1109, 1031,863,732.^{1}H NMR (400 MHz, DMSO): δ ppm 0.85 (s 3H), 0.97 (s 3H), 1.05 (s 3H), 1.29 (s 3H), 2.16-2.21 (m 2H), 2.25-2.31 (m 2H), 2.33-2.46 (m 2H), 2.58-2.66 (m 2H), 4.52 (s 1H), 7.30-7.46 (m 2H), 7.48-7.69 (m 2H), 7.78-7.88 (m 1H), 8.0-8.12 (dd1H), 8.45-8.51 (dd 1H), 8.86 (d 1H), 8.99-9.01 (d 1H). ^{13}C NMR (400 MHz, DMSO): 196.92, 162.90, 135.28, 134.51, 131.46, 131.24, 130.72, 129.34, 129.05, 128.76, 128.44, 128.02,126.75,126.02, 125.83, 125.49, 125.06, 124.95, 124.63, 124.35, 124.19, 123.99, 123.44, 114.31, 111.99, 111.30, 110.07. m/z: 450.21.

Result and discussions

To determine suitable conditions for this transformation, a mixture of benzaldehyde (1 mmol), 5,5-dimethyl-1,3-cyclohexanedione (2 mmol) and LPCAS (1mmol) was added to 25 ml round bottom flask and stirred at 100^{0}C under solvent free conditions.The progress of reaction was monitored by TLC.After completion of reaction, the mixture was cooled to room temperature and 10 ml water was added. Separated solid was filtered, recrystallized product was characterized by IR, ^{1}H and ^{13}C-NMR and Mass spectra.

The efficiency of IL media has been determined and compared with those of reported acid catalysts/reagents in the synthesis of 3,3,6,6-tetramethyl-9-(4-phenyl)-1,8-dioxo-octahydroxanthene (**3a**). The comparison of various reported reagent is summarized in (Table2).

In presence of $[Et_3NH][HSO_4]$, the reaction proceeds at 100 °C within 30 minutes offering 92% yield of the product under solvent free condition (entry 3, Table 2). In presence of *β*-CD-BSA in water the reaction mixture on heating for 15 minutes afforded 95 % of product (entry 1, Table 2). Also by using sonochemical synthesis method in the presence of catalyst $[Hbim]BF_4$ in methanol at 25-30 °C within 45 minutes (entry 14, Table 2).

Similarly in presence of L-proline in dichloromethane at 60 °C, the same reaction proceeds in 360 minutes offering 78 % of product (entry 18, Table 2). Whereas, in presence of $[bmim]ClO_4$ the reaction proceeds at 100 °C within 40 minutes offering 92% yield of the product under solvent free condition (entry 19, Table 2).

Table 2. Comparison of the present catalytic system with some reported protocols in the model reaction between benzaldehyde and dimedone.

Entry	Aldehyde	Conditions	Time	Yield(%)	Ref.
1	*β*-CD-BSA	H_2O	15	95	[29]
2	DBSA	H_2O/100°C	360	94	[11]
3	$[Et_3NH][HSO_4]$	Solvent free/100 °C	30	92	[14]
4	Cellulose sulfonic acid	Solvent free/110 °C	300	95	[12]
5	MCM-41-SO_3H	H_2O/90°C	60	50	[22]
6	$HClO_4$-SiO_2	H_2O/100°C	60	68	[32]
7	Amberlyst-15	CH_3CN/reflux	300	94	[17]
8	Trimethyl silyl chloride	CH_3CN/reflux	480	72	[30]
9	Fe^{3+}-montmorillonite	EtOH/100°C	360	93	[19]
10	CAN supported HY-zeolite	Solvent free/80 °C	45	93	[24]
11	Fe_3O_4@SiO_2-imid-PMA	EtOH/reflux	75	94	[21]
12	Nano-TiO_2	Solvent free/100 °C	15	96	[18]
13	$CaCl_2$	DMSO/90°C	300	87	[13]
14	$[Hbim]BF_4$	Methanol/ ultrasonic irradiation	45	85	[25]
15	$[HBim]HSO_4$	Solvent free /reflux	210	76	[23]
16	Tetrachloro silane	Dichloromethane/60-70 °C	180	92	[15]
17	$SmCl_3$	Solvent free/120 °C	480	98	[20]
18	L-Proline	$ClCH_2CH_2Cl$/60°C	360	78	[31]
19	$[bmim]ClO_4$	Solvent free/100 °C	40	92	[33]
20	L-Pyrrolidine-2-carboxylic acid sulfate(LPCAS)	Solvent free/100 °C	5	95	This work

But surprisingly when the reaction is carried out using ionic liquid L-pyrollidine-2-carboxylic acid sulfate at 100 °C under solvent free condition, it proceeds within 5 minutes and offering the product in 95 % (entry 20, Table 2).

All the above results have showed that, the L-pyrollidine-2-carboxylic acid sulfate proved its efficiency in terms of product yield and reaction times (Table-2). All the known synthesized compounds were confirmed by comparing their melting points with standards and new compounds were confirmed by spectroscopic data (IR, ^1H NMR). An advantage of the novel ionic liquid (L-pyrrolidine-2-carboxylic acid sulfate) is; its cost and more efficiency as compare to other reported ionic liquids.

Conclusions

In summary, we have developed a new eco-friendly procedure for the synthesis of 1, 8-dioxo-octahydroxanthenes via one pot condensation of aromatic aryl aldehydes and dimedone using LPCAS as a ionic liquid reagent under solvent free conditions. The hopeful points for the presented methodology are including a simple procedure, high catalytic activity, short reaction time, excellent yields. This approach therefore represents a precious addition to the existing processes for the synthesis of 1, 8-dioxo-octahydro xanthenes.

Acknowledgements

The authors are thankful to **Dr. S. N. Thore,** Principal Deogiri College, Aurangabad, and **Dr. B. H. Zaware,** Principal New Arts, Comm. & Science, College, Ahmednagar for constant encouragement and providing necessary facilities. The authors are also thankful to the Director, SAIF, Punjab University, Chandigarh for providing spectral data.

References

[1]El-Brashy, A. M., El-Sayed Metwally, M., El-Sepai, F. A., *Farmaco*, **2004**, *59*, 809–817. https://doi.org/10.1016/j.farmac.2004.07.001

[2]Chibale, K., Visser, M., Schalkwyk, D. V., Smith, P. J., Saravanamuthu A. and Fairlamb, A. H., *Tetrahedron*, **2003**, *59*, 2289–2296. https://doi.org/10.1016/s0040-4020(03)00240-0

[3]Poupelin, J. P.,Saint-Rut, G.,Fussard-Blanpin, O., Narciss, G., Ernouf,G. U. and Lacroix, R., *Eur. J. Med. Chem.*, **1978**, *13*, 67-71. https://doi.org/10.1055/s-1975-23879

[4]Mulakayala, N., Murthy, P. V. N. S.,Rambabu, D., Aeluri, M., Adepu, R., Krishna, G.R.,Reddy, C. M., Prasad, K.R.S., Chaitanya, M., Kumar, C. S., Basaveswara Rao M. V., Pal, M., *Bioorg. Med. Chem. Lett.*, **2012**,*22*, 2186–2191. https://doi.org/10.1016/j.bmcl.2012.01.126

[5]Zelefack, F., Guilet, D., Fabre, N., Bayet, C., Chevalley, S., Ngouela, S., Lenta, B. N., Valentin, A., Tsamo, E. and Dijoux-Franca, M. G., *J. Nat. Prod.*, **2009**, *72*, 954. https://doi.org/10.1021/np8005953

[6]Nguyen, H. T., Lallemand, M. C.,Boutefnouchet, S., Michel, S. and Tillequin, F., *J. Nat. Prod.*, **2009**, *72*, 527. https://doi.org/10.1021/np800644y

[7]Knight, C. G. and Stephens, T., *Biochem. J.*, **1989**, *258(3)*, 683-687. https://doi.org/10.1042/bj2580683

[8]Ahmad, M., King, T. A., Ko, D. K., Cha, B. H., Lee, J., *Appl. Phys.*, **2002**, *35*, 1473–1476. https://doi.org/10.1088/0022-3727/35/13/303

[9]Bhowmik, B. B., Ganguly, P., *Spectrochim. Acta*, **2005**, *61*, 1997–2003. https://doi.org/10.1016/j.saa.2004.07.031

[10]Zolfigol, M. A., Moosavi-Zare, A. R., Arghavani-Hadi, P., Zare, A., Khakyzadeh, V. and Darvishi, G., *RSC Adv*., **2012**, *2*, 3618. https://doi.org/10.1039/c2ra00014h

[11]Jin, T. S., Zhang, J. S., Xiao, J. C., Wang, A. Q. and Li, T. S., *Synlett*, **2004**, *5*, 866-870. https://doi.org/10.1055/s-2004-820022

[12]Oskooie, H. A., Tahershamsi, L., Heravi, M. M., Baghernejad, B., *E.-J. Chem.*, **2010**, *7*, 717. https://doi.org/10.1155/2010/936107

[13]Ilangovan, A., Muralidharan, S., Sakthivel, P., Malayappasamy, S., Karuppusamy, S., Kaushik, M. P., *Tetrahedron Lett.*, **2013**, *54*, 491. https://doi.org/10.1016/j.tetlet.2012.11.058

[14]Zhou, Z.and Deng, X., *J. Mol. Catal. A*: *Chem.*, **2013**, *367*, 99-102. https://doi.org/10.1016/j.tetlet.2012.11.058

[15]Soliman, H. A. and Salama, T. A., *Chin. Chem. Lett.*,**2013**, *24(5)*, 404-406. https://doi.org/10.1016/j.cclet.2013.03.021

[16]Mulakayala, N., Pavan Kumar, G., Rambabu, D., Aeluri, M., Rao M. V. B. and Pal, M., *Tetrahedron Lett.*,**2013**, *53(51)*, 6923-6926. https://doi.org/10.1016/j.tetlet.2012.10.024

[17]Das, B., Thirupathi, P., Mahender, I., Reddy V. S. and Rao, Y. K., *J. Mol. Catal., A*: *Chem.*, **2006**, *247(1-2)*, 233-239. https://doi.org/10.1016/j.molcata.2005.11.048

[18]Khazaei, A., Reza Moosavi-Zare, A., Mohammadi, Z., Zare, A., Khakyzadeh, V., Darvishi, G., *RSC Adv.*, **2013**, *3*, 1323. https://doi.org/10.1039/c2ra22595f

[19]Song, G. Y.,Wang, B., Luo H.and Yang, L., *Catal. Commun.*,**2007**, *8(4)*, 673-676. https://doi.org/10.1016/j.catcom.2005.12.018

[20]Llangovan, A., Malayappasamy, S., Muralidharan S. and Maruthamuthu, S., *Chem. Central J.*, **2011**, *5*, 81. https://doi.org/10.1186/1752-153x-5-81

[21]Kantevari, S., Bantu,R.and Nagarapu, L., *ARKIVOC* Part (XVI), **2006**, 136-148. https://doi.org/10.3998/ark.5550190.0007.g15

[22]Karthikeyan, G. and Pandurangan, A., *J. Mol. Catal. A*: *Chem.*, **2009**, 311, 1-2, 36-45. https://doi.org/10.1016/j.molcata.2009.06.020

[23]Niknam, K. and Damya, M., *J. Chin. Chem. Soc.*, **2009**, *56(3)*, 659-665. https://doi.org/10.1002/jccs.200900098

[24]Sivaguru, P. and Lalitha, A., *Chin. Chem. Lett.*, **2014**, *25*, 321. https://doi.org/10.1016/j.cclet.2013.11.043

[25]Vankatesan, K., Pujari, S. S., Lahoti, R. J. and Srinivasan, K. V., *Ultrasonic Sonochem.*, **2008**, *15(4)*, 548-553. https://doi.org/10.1016/j.ultsonch.2007.06.001

[26]Godse, V. W.,Darandale, S. N., Rindhe, S. S., Parandkar, Y. R., Desai, R. D., Zaware, B. H., Jadhav, S. S. and Pawar. R. P., *Eur. Chem. Bull.*, **2016**, *5(7)*, 280-282. DOI: 10.17628/ECB.2016.5.280

[27]Pohlers, G. and Scaiano, J. C., *Chem. Mater.*,**1997**, *9(12)*, 3222-3230. https://doi.org/10.1021/cm970587p

[28]Ma, J., Li, J., Tang, R., Zhou, X., Wu, Q., Wang, C., Zhang, M., Li, Q., *Chin. J. Org. Chem.*, **2007**, *27*, 640-642.

[29]Gong, K., Wang, H., Wang, S., Wang, Y., Chen, J., *Chin. J. Catal.*, 2015, *36*, 1249–1255. https://doi.org/10.1016/s1872-2067(15)60888-9

[30]Esmaeilpour, M., Javidi, J., Dehghani, F. and Dodeji, F. N., *New J. Chem.*, **2014**, *38*, 5453. https://doi.org/10.1039/c4nj00961d

[31]Das, B., Kashanna, J.,Kumar, R. A. and Jangili, P., *Synth. Commun.*,**2012**, *42*, 2876. https://doi.org/10.1080/00397911.2011.571804

[32]Kantevari, S., Bantu, R., Nagarapu, L., *J. Mol. Catal. A*, **2007**, *269*, 53. https://doi.org/10.1016/j.molcata.2006.12.039

[33]Makone, S. and Mahurkar, S., *Green Sustain. Chem.*,**2013**, *3*, 27-32. https://doi.org/10.4236/gsc.2013.34a005

Received: 14.12.2016.
Accepted: 12.02.2017.

GENOTYPIC DISTINCTIONS OF VARIABILITY OF BIOCHEMICAL COMPOSITION OF FRUITS OF *VACCINIACEAE* SPECIES UNDER CONDITIONS OF BELARUS

Zhanna Rupasova,[a]* Aleksandr Yakovlev,[a] Nikolay Pavlovsky,[a] Vladimir Titok,[a] Vladimir Reshetnikov,[a] Tamara Vasilevskaya,[a] Natalia Krinitskaya,[a] Elizaweta Tishkovskaya,[a] and Anton Volotovich[b]

Keywords: Biochemical composition, genotypic variability, highbush blueberry (*V. corymbosum* L.), lingonberry (*V. vitis-idaea* L.), cranberry (*Oxycoccus macrocarpus* (Ait.) Pers.).

Result of research of quantitative characteristics of biochemical composition of fruits of 30 taxons of 3 *Vacciniaceae* species (such as *V. corymbosum L.* (highbush blueberry), *V. vitis-idaea* L. (lingonberry) and *Oxycoccus macrocarpus* (Ait.) Pers. (cranberry)) inter-specific distinctions of a degree of stability of its separate components to complex influence of meteorological factors are revealed by 32 parameters (traits) describing the contents in fruits of some organic acids, carbohydrates, phenolic compounds, terpenoids and major mineral elements are presented. The cultivars possessing by the greatest and accordingly by the least levels of dependence on abiotic factors are identified.

* Corresponding Authors
E-Mail: J.Rupasova@cbg.org.by
[a] Central Botanical Garden of the National Academy of Sciences of Belarus, 2v, Surganova Str., 220012, Minsk, Republic of Belarus
[b] Polessky State University, 4, Pushkin Str., 225710, Pinsk, Republic of BelarusIntroduction

The major aspect of researches connected with in-depth study of species of berry plants is the estimation of complex biochemical composition of fruits in a long-term cycle of the supervision, which gives to us the information not only about its genotypic features, but also about the degree of dependence on hydrothermal regime during the period of fruits maturing and of parameters about accumulation of wide spectrum of the useful substances determining organoleptic properties of berry production. The response of the introduced species to influence of complex meteorological factors particularly the extremely unstable character of weather conditions during vegetation of plants and maturing of their fruits, peculiar to the Belarus region, can noticeably influence on the rates of accumulation of those or other compounds. This information may lead to correcting action to enhance their nutritious and vitamin values. In the last few years, the Central Botanical Garden of the NAS of Belarus has introduced new taxons of 3 *Vacciniaceae* species (*V. corymbosum L.* (highbush blueberry), *V. vitis-idaea* L. (lingonberry) and *Oxycoccus macrocarpus* (Ait.) Pers. (cranberry). It has created additional opportunities to increase the varieties offered for breeding to select the most perspective variety. The selection may be made on nutritious and vitamin values of the berry production as defined by its biochemical composition and also on the degree of constancy of biochemical composition in the face of influence of complex meteorological factors.

It is, however, expected that there will long-term stable genotypic distinctions. It will enable to designate cultivars which exhibit least dependence on abiotic factors. The object of this work is to establish quantitatively the degree of dependence of biochemical composition of fruits of investigated *Vacciniaceae* species on the hydrothermal regime of a season

Experimentals

Studies have been done during the years 2006-2008, on the plant material received at Gantsevichi research station of Central Botanical Garden of the NAS of Belarus (the Brest region). Intra- and inter-seasonal weather conditions during July-September, the active period of maturing of fruits of *Vacciniaceae* species, varied considerably. It has not created conditions stability of biochemical compositions of their fruits. The lowest temperature during the given period was recorded in 2008, and the highest one in 2006. All of three seasons were characterized by plentiful atmospheric precipitates with extremely non-uniform distribution in time.

Table 1. Values of hydrothermal factor (Htf) during formation and maturing of fruits of plants of *Vacciniaceae* species (Percentage deviation from the mark is given in the second line).

Year	May	June	July	Aug.	Sep.	Mean
2006	1.8	1.1	1.6	3.0	0.8	1.7
	120.0	73.3	100.0	200.0	44.4	106.2
2007	1.4	1.0	5.4	0.4	0.8	1.8
	93.3	66.7	337.5	26.7	44.4	112.5
2008	2.3	0.7	2.4	1.3	3.8	2.1
	153.3	46.7	150.0	86.7	211.1	131.2
Mean of 3 years	1.5	1.5	1.6	1.5	1.8	1.6

Most objective integrated representation about the character of a weather situation within the years of supervision, on our opinion, can be made on monthly values of the hydrothermal factor determined by a ratio of amount of atmospheric precipitation dropped out and the sum of active temperatures above 10 °C.[1] Our estimates are given in table

1, and according to Seljaninov's gradation of a degree of humidity of any area, in 2006 May and July were characterized by sufficient humidity, June and September had drought and only August had excess humidity. In 2007, May experienced sufficient humidity, June, August and September had mainly by dry weather and only July had large excess of humidity. In 2008, May, July and particularly September were characterized by the excess humidity combined with the low background temperature. August differed by having sufficient humidity whereas June had droughty.

The samples for the investigation comprised of mature fruits of 16 cultivars of *Vaccinium corymbosum L.* (early-maturing: *Bluetta*, *Northblue*, *Weymouth*, *Duke*, *Reka*, *Earliblue*, *Patriot*, *Spartan*, *Puru*, *Nui*, mid-ripening: *Bluecrop*, *Northland*, *Toro*, *Jersey*; late-ripening: *Elizabeth* and *Coville*), of 10 cultivars of *V. vitis-idaea* L. (*Koralle*, *Red Pearl*, *Rubin*, *Erntedank*, *Erntesegen*, *Erntekrone*, *Ammerland*, *Masovia*, *Sanna*, *Sussi*) and of 4 cultivars of *Oxycoccus macrocarpus* (Ait.) Pers. (*Stevens*, *Ben Lear*, *McFarlin*, *Piligrim*).

Biochemical composition of fruits of above-mentioned taxons has been analysed for 32 parameters. In the average fresh samples of a plant vegetative material the contents of dry matter was determined in accordance to GOST.[2] Vitamin C was determined by the standard indophenolic method and organic acid by the volumetric method.[3] In the samples of fruits, after being dried at 65 °C, nitrogen, phosphorus, potassium were determined by the method of Fomenko and Nesterov,[4] calcium, magnesium by the complexometric method,[3] glucose, fructose, sucrose by Zavadskaja's process,[5] pectin substances (water-soluble pectin and protopectin) by carbazolic method.[3] Total anthocyanins was determined by construction of a calibration curve with crystal cyanidin.[6] Cyanidin was obtained from fruits of black chokeberry and was purified,[7] a formula given by Tanchev[8] was used in calculations. Anthocyanins was determined by the method of Shnajdman and Afanaseva,[9] total flavonoids by the method of Sarapuu and Mijdla,[10] catechines by a photometric method with vanillin reagent,[11] chlorogenic acids by the method of paper chromatography,[12] tannins by titirimetric method of Levental,[13] lignins by the modified method of Klason,[3] benzoic acid by Kalebin and Kolesnik's method,[14] fixed oils by Sapunov and Fedunjak's method[15] triterpene acids (in recalculation on ursolic acid) by Simonjan's method.[16]

All analytical definitions are carried out in thrice-repeated biological repeatability by Laboratory of Plant Chemistry of Central Botanical Garden of the NAS of Belarus. The data are statistically processed with use of program MS Excel.

For the estimation of genotypic variability of parameters of accumulation of the specified compounds in a spectrum of investigated taxons in a long-term cycle of supervision we were guided by variation coefficient values (V) of the examined traits. The comparative analysis of the materials has enabled us to establish which biochemical characteristics of fruits of the introduced species are less susceptible to the external influences and which are more susceptible. It is also possible to define the integrated degree of susceptible to the external influences of all the investigated taxons. It is well established that a degree of variation of a specific trait is proportional to its dependence on investigated factors, here on meteorological factor. By estimations of Sennov and Kovjazin,[17] the variability of for biological properties is considered small if it is within the limits of 11-30 % and considered big if exceeds 31%. By consideration of the information presented in our paper, we should consider active reaction of introduced species on the breeding process, allowing in the certain measure to resist to it and to regulate the biochemical composition of generative organs within the limits of genetically determined ranges of a variation of each trait. It has permitted the basis to narrow the border of designated above small variability of row for examined parameters up to 10 %. Its average range was characterized by a level of variability within the limits of 11-20 %, and maximal over 20 %. The accepted gradation of levels of variability of analyzed traits coincides with the recommended for biological objects gradation by Zajtsev.[18]

Results and discussion

We have observed a very wide range of variation in long-term cycle of observations averaged for the varietals series introduced species 32 quantitative indicators of the biochemical composition of fruits in table 2, indicating a significant impact on the abiotic factors. The greatest number of parameters with the maximal values for all of investigated species is observed in the hottest season of 2006. The hot season stimulated accumulation of the majority of useful substances such as organic acids, vitamin C, soluble sugars, bioflavonoid, pectin, terpenoids and phosphorus compounds. The largest number of parameters with the minimal values is foundfor *V. corymbosum L.* cultivars in 2007 and for *V. vitis-idaea* L. and *Oxycoccus macrocarpus* (Ait.) Pers. cultivars in 2008. In all the species, accumulation of benzoic and chlorogenic acids in fruits was the maximum in 2007 indicated by maximal values of a sugar-acid index. Similarly, accumulation of flavonols and most of the macronutrients was the maximum in 2008.

An analysis of data presented in Tables 3 and 4, has revealed a wide ranges of changes in variation coefficients of biochemical composition of fruits of investigated taxa of *Vacciniaceae* species in a long-term cycle of supervision. It testifies to a different level of their dependence on a hydrothermal regime of a season and allowed to designate the traits possessed by the greatest and accordingly by the least degree of this dependence.

Within the years of supervision the majority of parameters of biochemical composition of fruits of *V. corymbosum L.*, irrespective of maturing terms, were inherent of average (V=11-20 %) and high (V>20 %) levels of variability (accordingly for 16-44 % and 44-69 % of parameters). Only for 9-22 % of parameters the levels of variability were low (V<10 %). Biochemical composition of fruits of investigated taxons of *Oxycoccus macrocarpus* (Ait.) Pers. species has been noted by similarity of individual share of analyzed traits within the limits of each level of variability (low level for 12-25 %, average level for 19-38 % and high level for 40-63 % of parameters)

Table 2. Range of changes of averaged quantitative characteristics of biochemical composition of fruits (in dry substance) for *Vacciniaceae* cultivar rows in a long-term cycle of supervision.

Chemical composition	***V. corymbosum L.***	***V. vitis-idaea* L.**	***O. macrocarpus* (Ait.) Pers.**
Dry matter, %	13.90-14.10	14.90-16.90	10.30-12.50
Organic acid, %	3.80-6.70	14.60-19.30	20.60-36.10
Vitamin C, mg %	426.60-604.80	304.30-670.80	463.60-495.10
Glucose, %	4.49-5.34	5.65-5.95	5.18-6.96
Fructose, %	7.26-18.74	6.85-10.54	1.37-6.86
Sucrose, %	0.56-3.19	0.86-2.09	0.36-0.51
Total sugar, %	12.79-27.25	14.72-18.27	6.91-12.69
Fructose/ Glucose ratio	1.70-3.60	1.20-1.90	0.30-1.30
Monose/Disaccharide ratio	7.90-22.70	6.50-17.40	24.60-28.10
Sugar-acid index	2.50-6.50	0.80-1.30	0.30-0.60
Hydropectin, %	1.98-2.37	2.56-3.03	2.22-2.54
Protopectin, %	2.60-3.45	3.45-3.84	3.56-5.40
Total pectins, %	4.77-5.71	6.01-6.73	6.10-7.65
Protopectin/Hydropectin ratio	1.20-1.80	1.30-1.50	1.40-2.50
Anthocyanins, mg %	2.00-17.10	1.60-3.90	6.70-12.00
Leucoanthocyanins, mg %	12.10-24.10	29.70-32.70	25.10-37.70
Total anthocyanic pigments, mg %	14.10-41.20	32.80-36.60	34.80-49.70
Catechines, mg %	570.10-984.30	710.00-1777.80	1067.10-1823.30
Flavonols, mg %	1626.00-1890.60	1618.90-2227.50	1349.10-3112.90
Flavonols/Catechines ratio	1.90-3.40	1.10-3.70	1.40-3.00
Total bioflavonols, mg %	2501.80-2776.00	2970.30-3719.80	2596.00-4227.00
Chlorogenic acids, mg %	781.40-800.30	484.90-838.10	486.80-700.50
Benzoic acid, %	1.11-1.18	1.14-1.65	1.12-1.49
Tannins, %	1.21-1.83	1.98-2.45	1.76-2.01
Lignins, %	11.30-11.70	10.70-11.90	10.00-13.20
Fixed oils, %	3.17-3.61	5.16-6.09	4.43-5.35
Triterpene acids, %	2.49-3.22	2.58-3.41	2.09-3.44
Nitrogen, %	0.76-1.10	1.19-1.24	0.85-1.03
Phosphorus, %	0.14-0.17	0.14-0.18	0.13-0.16
Potassium, %	0.53-0.76	0.51-0.90	0.58-0.80
Calcium, %	0.31-0.42	0.32-0.39	0.24-0.30
Magnesium, %	0.08-0.11	0.08-0.11	0.08-0.10

For fruits of *V. vitis-idaea* L. the essential increase in a time-row, in comparison with the previous *Vacciniaceae* species, of a relative share of traits with small variability (up to 16-41 %) has been shown. It exclusively possible due to decrease of levels of variability of traits with high variability up to 35-53 % (Table 3 and Table 4), that testifies about the less susceptibility of biochemical composition of fruits of these cultivars to complex influence of abiotic factors.

In our opinion, it is connected with participation in breeding process of the *V. vitis-idaea* L. cultivars of its wild-growing forms selected on the European continent in woodlands of Sweden, Finland, Holland, Germany, Poland and other countries, which are similar by character of soil-climatic conditions to those of Belarus, whereas *V. corymbosum L.* and *Oxycoccus macrocarpus* (Ait.) Pers. are natives from remote North American continent with essentially differing set of climatic and natural factors.[18] It is quite natural, that at adaptation of plants under different conditions leads to more susceptibility to abiotic changes. Thus some of the parameters of biochemical composition of fruits were characterized by relative stability of a level of variability within the limits of cultivar rows of all of three investigated *Vacciniaceae* species.

In the majority of cases the conformity of a level of variability of these parameters of the certain area of the accepted gradation took place only at separate taxons, and frequently the range of changes of a level of variability of traits within the limits of cultivar row covered all of three areas of the shown gradation.

In our view, the most objective representation about a degree of variability of quantity traits of biochemical composition of fruits in varietals rows of investigated *Vacciniaceae* species can give the value of variation coefficient averaged in a 3-years cycle of supervision. The variability of traits, testifying to their stability to atmospheric influences are presented in table 5. In this case it is possible to divide the analyzed traits into 3 groups, according to a level of genotypic variability:

(1) with low variability (V=8.2-10.9 % at a blueberry; V=6.7-9.0 % at a cowberry; V=5.9-10.4 % at a cranberry);

(2) with average variability (V=12.2-20.0 % at a blueberry; V=11.1-20.0 % at a cowberry; V=11.3-18.4 % at a cranberry);

Table 3. Averaged variation coefficients (%) of quantitative characteristics of biochemical composition of fruits for *Vaccinium corymbosum L.* cultivars in a long-term cycle of supervision ((1 – Bluetta, 2 – Northblue, 3 – Weymouth, 4 – Duke, 5 – Reka, 6 – Earliblue, 7 - Spartan, 8 - Puru, 9 - Nui, 10 - Patriot, 11 - Bluecrop, 12 - Northland, 13 - Toro, 14 - Jersey, 15 - Elizabeth, 16 - Coville)

Chemical composition	**Early-maturing**										**Mid-ripening**				**Late-ripening**	
	1	**2**	**3**	**4**	**5**	**6**	**7**	**8**	**9**	**10**	**11**	**12**	**13**	**14**	**15**	**16**
Dry matter	8.7	9.7	7.6	7.4	9.2	16.6	8.5	3.6	3.8	14.6	8.1	6.3	10.4	9.9	3.4	3.0
Organic acid	28.9	20.5	16.0	19.3	39.6	61.3	54.5	39.3	9.3	43.2	24.9	13.1	33.8	63.2	55.3	52.1
Vitamin C	36.0	45.5	54.2	46.7	15.1	36.3	5.4	8.0	15.9	26.4	15.5	42.5	17.2	32.1	25.9	6.4
Glucose	19.1	17.9	18.3	17.9	15.3	32.6	17.9	13.5	12.6	10.1	4.7	10.4	11.5	14.6	18.5	16.9
Fructose	45.2	37.4	40.0	34.5	31.7	46.8	32.0	36.4	41.6	54.4	51.9	40.5	50.3	49.5	51.3	54.3
Sucrose	64.9	68.8	69.5	62.8	65.1	66.9	74.6	54.5	64.2	68.7	73.1	69.8	82.0	80.8	64.9	63.6
Total sugar	38.8	35.6	36.6	33.2	30.8	32.4	32.8	33.3	37.8	38.7	40.7	33.1	36.7	40.0	36.5	36.5
Fructose/ Glucose ratio	39.6	23.1	32.1	16.9	18.9	60.1	15.4	25.1	29.3	52.5	48.1	38.7	53.4	48.3	58.9	61.6
Monose/Disaccharide ratio	57.4	61.0	72.7	67.4	56.0	40.3	87.7	43.8	54.5	43.3	53.4	65.8	74.0	83.5	57.8	55.1
Sugar-acid index	51.1	32.8	26.1	31.8	53.2	26.8	70.7	53.9	47.0	60.7	50.0	44.9	51.3	66.7	74.5	67.8
Hydropectin	20.8	5.4	19.0	21.6	8.5	23.8	29.0	6.5	13.9	26.1	6.8	31.8	8.2	32.7	21.8	30.4
Protopectin	35.6	37.0	29.6	18.5	32.8	25.6	20.6	22.7	26.3	14.9	23.5	17.7	15.7	22.3	5.2	24.3
Total pectins	27.8	22.1	14.3	18.8	22.4	14.9	14.5	14.4	19.1	19.9	11.1	23.4	12.0	26.1	13.0	21.6
Protopectin/Hydropectin ratio	28.4	32.9	49.9	11.4	25.5	45.5	47.1	20.0	18.2	14.4	32.2	13.6	6.0	19.5	18.7	31.9
Anthocyanins	91.7	112.6	47.3	62.9	81.7	62.1	88.1	119.0	118.3	73.5	90.9	109.8	124.1	102.3	101.6	72.2
Leucoanthocyanins	26.2	34.8	46.6	41.3	33.1	50.7	15.2	16.2	17.0	37.1	34.6	45.7	68.6	55.0	46.3	27.1
Total anthocyanic pigments	45.9	62.8	45.4	46.7	38.7	39.8	41.4	44.9	55.0	48.8	42.8	65.7	85.7	68.3	67.2	40.2
Catechines	30.3	31.2	36.4	35.6	43.6	14.6	25.9	37.3	21.3	17.7	26.2	46.6	34.1	43.7	39.8	44.8
Flavonols	11.7	18.9	17.0	13.4	7.7	5.8	16.1	15.2	5.8	9.1	14.8	7.3	9.1	3.7	10.5	8.2
Flavonols/Catechines ratio	39.3	42.7	52.2	56.8	52.6	17.9	37.4	50.7	26.6	19.6	22.3	48.0	50.7	58.5	53.4	55.9
Total bioflavonols	7.1	14.4	3.6	7.5	8.8	2.3	7.9	4.3	4.7	8.4	15.2	18.2	9.2	11.7	8.4	19.1
Chlorogenic acids	11.5	28.6	10.9	19.4	21.3	12.8	23.6	12.2	12.4	16.9	12.2	9.6	11.8	27.8	3.0	27.8
Benzoic acid	6.7	5.9	18.8	21.9	5.5	11.2	15.5	13.3	21.7	7.6	15.6	16.3	13.1	7.9	11.4	7.5
Tannins	10.6	20.7	32.6	30.1	12.2	23.3	38.8	31.9	31.9	17.7	33.4	15.0	21.8	37.8	27.6	16.6
Lignins	18.7	27.3	12.4	13.4	16.5	4.1	7.9	24.7	9.4	15.2	7.4	13.2	7.3	2.5	1.6	13.8
Fixed oils	24.9	38.2	14.4	20.7	34.0	38.7	25.0	12.9	20.0	15.0	23.7	20.3	31.9	11.2	21.6	18.0
Triterpene acids	19.5	27.3	24.3	14.9	21.5	14.0	6.2	11.5	8.9	24.4	6.4	16.9	23.4	9.4	20.2	20.6
Nitrogen	26.7	24.3	16.8	8.4	12.3	19.1	31.4	31.9	23.7	13.9	21.1	28.4	19.5	12.0	15.3	17.8
Phosphorus	5.6	9.9	8.7	13.1	8.1	10.0	16.4	9.4	7.4	22.7	13.3	30.2	31.2	30.6	10.4	24.7
Potassium	23.5	22.4	23.5	12.1	10.4	13.8	18.2	15.4	25.8	14.4	7.5	21.8	25.5	20.6	32.5	32.8
Calcium	6.8	5.4	10.2	17.3	15.9	9.4	11.8	19.7	15.0	16.4	26.5	18.9	18.7	11.8	19.5	21.5
Magnesium	17.6	12.4	22.2	11.2	15.8	26.0	15.8	23.9	11.1	19.2	16.4	13.3	12.5	19.2	18.3	16.4
V mean	**28.9**	**30.9**	**29.0**	**26.7**	**27.0**	**28.3**	**29.8**	**27.2**	**25.9**	**27.7**	**27.3**	**31.2**	**33.1**	**35.1**	**31.7**	**31.6**

Table 4. Averaged variation coefficients (%) of quantitative characteristics of biochemical composition of fruits for *Vaccinium vitis-idaea* L. and *Oxycoccus macrocarpus* (Ait.) Pers. cultivars in a long-term cycle of supervision (1 - Koralle, 2 - Red Pearl, 3 - Rubin, 4 - Erntedank, 5 - Erntesegen, 6 - Erntekrone, 7 - Ammerland, 8 - Masovia, 9 - Sanna, 10 - Sussi, 11 - Stevens 12 - Ben Lear, 13 - Mc Farlin, 14 - Piligrim)

Chemical composition	***Vaccinium vitis-idaea* L. cv.**									***Oxycoccus macrocarpus* (Ait.) Pers. cv.**				
	1	**2**	**3**	**4**	**5**	**6**	**7**	**8**	**9**	**10**	**11**	**12**	**13**	**14**
Dry matter	14.6	5.3	3.7	7.8	8.4	11.3	5.1	11.9	10.2	1.7	13.0	2.0	6.2	15.6
Organic acid	19.1	22.0	15.2	20.2	16.6	39.8	9.0	7.5	6.8	12.5	35.1	18.7	17.2	25.0
Vitamin C	42.7	28.9	33.9	57.3	45.7	62.0	4.7	29.6	31.2	21.7	8.8	5.3	1.6	7.9
Glucose	11.4	6.1	6.0	7.0	6.6	8.7	4.6	5.1	9.7	6.4	17.1	16.4	19.3	16.4
Fructose	20.9	28.0	21.1	27.2	23.4	24.6	17.9	32.6	2.4	1.7	60.4	72.0	67.6	53.8
Sucrose	45.7	23.4	36.6	28.4	48.0	48.4	50.2	47.2	78.7	64.1	19.7	6.1	26.2	59.2
Total sugar	11.6	14.7	13.8	17.6	13.0	13.2	13.4	20.2	5.2	4.8	27.5	29.7	33.0	32.4
Fructose/ Glucose ratio	29.0	28.8	16.2	23.1	30.4	31.2	18.0	30.7	12.0	8.1	75.4	103.7	87.0	61.1
Monose/Disaccharide ratio	41.8	30.5	48.7	38.1	60.6	69.3	64.3	63.4	80.5	65.0	42.8	25.5	24.4	51.4
Sugar-acid index	19.3	40.6	30.7	35.3	22.1	41.7	4.9	27.7	12.0	7.7	43.3	25.0	44.6	58.1
Hydropectin	4.8	6.4	10.6	7.5	12.1	7.5	9.4	22.7	6.7	2.4	28.2	11.0	1.4	6.1
Protopectin	4.9	12.5	21.5	11.2	17.8	10.5	10.3	18.6	1.5	23.0	29.5	28.1	23.2	7.6
Total pectins	1.4	8.0	16.3	9.6	8.5	2.7	9.3	13.6	2.5	15.3	15.7	17.7	15.0	6.6
Protopectin/Hydropectin ratio	39.5	13.3	16.5	4.3	26.2	18.2	8.3	31.5	6.7	21.4	51.7	33.1	21.5	7.4
Anthocyanins	88.4	40.9	27.3	86.9	117.5	139.1	46.9	86.6	4.3	141.4	52.5	23.2	49.8	22.3
Leucoanthocyanins	13.4	38.7	33.8	3.0	63.6	39.6	11.7	49.5	51.3	13.0	40.2	11.4	26.6	17.3
Total anthocyanic pigments	18.5	38.3	33.0	7.3	65.9	46.3	9.8	50.1	100.4	86.9	40.8	5.7	30.3	17.4
Catechines	32.5	9.1	35.7	67.1	48.1	97.0	50.3	55.7	97.1	54.8	46.1	24.8	36.7	32.8
Flavonols	25.1	16.6	15.8	22.5	11.0	13.0	16.3	7.5	23.4	28.6	48.5	57.7	56.6	37.0
Flavonols/Catechines ratio	51.2	27.3	55.5	96.3	45.8	83.1	81.1	51.5	108.5	76.1	79.6	53.9	66.3	63.5
Total bioflavonols	13.1	5.2	6.7	21.0	18.7	38.2	12.5	24.4	36.7	1.1	30.5	32.0	25.9	11.1
Chlorogenic acids	9.6	31.4	40.6	28.3	27.8	10.5	36.4	30.6	33.1	19.1	22.1	10.5	24.3	24.1
Benzoic acid	5.6	15.1	22.0	20.2	6.9	26.1	16.9	28.0	27.1	46.8	20.0	21.6	9.8	15.0
Tannins	9.0	42.9	9.9	16.2	8.7	46.9	14.0	40.1	21.9	8.7	20.0	8.4	10.6	2.7
Lignins	12.9	2.4	2.1	18.5	4.6	5.5	4.8	4.9	26.7	5.2	31.3	19.5	10.0	1.7
Fixed oils	11.0	6.8	4.4	7.7	16.5	16.9	14.4	23.1	3.9	11.2	7.8	8.3	9.8	14.5
Triterpene acids	9.8	11.9	15.8	12.6	13.0	13.6	23.7	15.8	14.4	20.7	32.5	12.6	32.8	26.3
Nitrogen	4.8	7.0	6.6	3.6	7.6	9.3	2.0	8.6	12.6	4.8	6.7	14.8	11.4	12.2
Phosphorus	7.4	19.7	7.4	16.5	17.6	3.7	19.5	22.5	4.9	5.7	0	6.3	17.6	16.4
Potassium	24.5	30.5	30.1	30.1	32.8	39.5	40.2	32.5	22.0	25.5	21.4	18.6	17.9	15.5
Calcium	14.8	14.7	12.9	4.4	12.7	11.5	15.2	13.6	3.7	7.6	12.3	13.4	9.0	18.4
Magnesium	18.3	16.4	16.4	16.4	10.0	16.4	11.1	19.2	14.1	22.3	18.3	18.3	22.2	13.3
V mean	**21.1**	**20.1**	**20.8**	**24.2**	**27.1**	**33.6**	**20.5**	**29.0**	**27.3**	**26.1**	**31.2**	**23.6**	**26.7**	**24.1**

(3) with high variability (*V* = 20.9-75.9 % at a blueberry; *V*=20.1-48.6 % at a cowberry; *V*=20.4-40.3 % at a cranberry).

The analysis of data resulted in Table 5 revealed that in some cases similarity of parameters of variability of the analyzed traits describing a degree of inter-seasonal distinctions in a long-term cycle of supervision at all of investigated cultivars of *Vacciniaceae* species. So the least expressive (within the limits of low variability) they have appeared only in a single instance, for the dry substances contents in fruits. The generality of an average level of the shown distinctions notes parameters of accumulation in fruits of calcium and magnesium. For a much greater set of parameters like contents of sucrose, of anthocyanins, of catechines and also of ratio of fractions of soluble sugars, of bioflavonols, and of values of a sugar-acid index at all of investigated *Vacciniaceae* species have been established a high level of variability in a time row.

At the same time the results of long-term supervision revealed that the taxons of *Vacciniaceae* species possess the greatest susceptibility and consequently the least stability of biochemical composition of fruits to external influences A degree of variability of biochemical composition of fruits as a whole in a long-term cycle of supervision for all the cultivars of *Vacciniaceae* species has been determined. The data, presented in tables 3 and 4 indicated that variation coefficients in a spectrum of cultivars of investigated *Vacciniaceae* species are 25.9 % for blueberry, for cowberry it is 20.1-33.6 % and 23.6-31.2 % for cranberry.

It has been determined, on the basis of the values of the variation coefficients, that all the taxons can be arranged in the following order of degree of stability of biochemical composition of fruits against the atmospheric influences in a long-term cycle of supervision:

For cultivars of *Vaccinium corymbosum L.*:

Nui>Duke>Reka=Puru=Bluecrop>Patriot>Earliblue > Bluetta = Weymouth > Spartan > Northblue = Northland > Coville = Elizabeth > Toro > Jersey

For cultivars of *Vaccinium vitis-idaea* L.:

RedPearl>Ammerland>Rubin>Koralle>Erntedank>Sussi> Erntesegen=Sanna>Masovia>Erntekrone

For cultivars of *Oxycoccus macrocarpus* (Ait.) Pers.:

Ben Lear>Piligrim>McFarlin>Stevens

Table 5. Averaged variation coefficients (%) of quantitative characteristics of biochemical composition of fruits for *Vacciniaceae* cultivar rows in a long-term cycle of supervision

Chemical composition	***V. corymbosum***	***L.V. vitisidaea***	***Oxycoccus macrocarpus (Ait.) Pers.***
Dry matter	8.2	8.0	9.2
Organic acid	35.9	16.8	24.0
Vitamin C	26.8	35.8	5.9
Glucose	15.7	7.2	17.3
Fructose	43.6	20.0	63.4
Sucrose	68.4	47.1	27.8
Total sugar	35.8	12.8	30.6
Fructose/ Glucose ratio	38.9	22.8	81.8
Monose/Disaccharide ratio	60.9	56.2	36.0
Sugar-acid index	50.6	24.2	42.8
Hydropectin	19.1	9.0	11.7
Protopectin	23.3	13.2	22.1
Total pectins	18.5	8.7	13.8
Protopectin/Hydropectin ratio	26.0	18.6	28.4
Anthocyanins	91.1	77.9	37.0
Leucoanthocyanins	37.2	31.8	23.9
Total anthocyanic pigments	52.5	45.6	23.6
Catechines	33.1	54.7	35.1
Flavonols	10.9	18.0	50.0
Flavonols/Catechines ratio	42.8	67.6	65.8
Total bioflavonols	9.4	17.8	24.9
Chlorogenic acids	16.4	29.7	20.2
Benzoic acid	12.5	21.5	16.6
Tannins	25.1	21.8	10.4
Lignins	12.2	8.8	15.6
Fixed oils	23.2	11.6	10.1
Triterpene acids	16.8	15.1	26.0
Nitrogen	20.2	6.7	11.3
Phosphorus	15.7	12.5	10.1
Potassium	20.0	30.8	18.4
Calcium	15.3	11.1	13.3
Magnesium	17.0	16.1	18.0

Table 6. Positions of characteristics of biochemical composition of fruits of *Vacciniaceae* species in a row of strengthening of inter-seasonal distinctions in the parameters of their accumulation

Chemical composition	***V. corymbosum L.***	***V. vitisidaea* L.,**	***Oxycoccus macrocarpus* (Ait.) Pers.**
Dry matter	1	3	2
Organic acid	23	14	19
Vitamin C	20	26	1
Glucose	7	2	12
Fructose	27	18	30
Sucrose	31	28	22
Total sugar	22	10	24
Fructose/ Glucose ratio	25	21	32
Monose/Disaccharide ratio	30	30	26
Sugar-acid index	28	22	28
Hydropectin	13	6	7
Protopectin	17	11	16
Total pectins	12	4	9
Protopectin/Hydropectin ratio	19	17	23
Anthocyanins	32	32	27
Leucoanthocyanins	24	25	18
Total anthocyanic pigments	29	27	17
Catechines	21	29	25
Flavonols	3	16	29
Flavonols/Catechines ratio	26	31	31
Total bioflavonols	2	15	20
Chlorogenic acids	9	23	15
Benzoic acid	5	19	11
Tannins	18	20	5
Lignins	4	5	10
Fixed oils	16	8	3
Triterpene acids	10	12	21
Nitrogen	15	1	6
Phosphorus	8	9	4
Potassium	14	24	14
Calcium	6	7	8
Magnesium	11	13	13

At the same time specific features of the variability were inherent to each cultivars of *Vacciniaceae* species even within the limits of exact area of its gradation. For revealing sequence of analyzed traits in ascending order a level of their variability in a long-term cycle of the supervision, specifying on strengthening of inter-seasonal distinctions, it has been decided to position each of traits according to increase in values of the variation coefficients (Table 6). It is apparent from the data that the least expressive inter-seasonal distinctions at *V. corymbosum L.* are established for the contents in fruits of dry matter, of flavonols and of total bioflavonoid, of lignins and of benzoic acid, whereas the most expressive ones are established are anthocyanins, total anthocyanic pigments, sucrose, monose to disaccharide ratio and also the sugar-acid index. The least expressed inter-seasonal distinctions at *V. vitis-idaea* L. cultivars are nitrogen, glucose, dry matter and pectin, and also lignins, whereas the most expressed ones are anthocyanins, catechines, sucrose, ratio of bioflavonoid fractions, and also monose to disaccharide ratio. The least significant inter-seasonal distinctions in *Oxycoccus macrocarpus* (Ait.) Pers. cultivars are vitamin C, fixed oils, phosphorus, of the dry matter is tannins, whereas the most significant ones are fructose, flavonols, ratio of bioflavonoid fractions, monose to disaccharide ratio, and also values of the sugar-acid index.

Biochemical composition of fruits of the majority of early-maturing cultivars of blueberry has higher stability to a hydrothermal regime of a season, than the mid-ripening and late-ripening cultivars. Thus the biochemical composition of fruits of the 4 early-maturing cultivars such as *Reka*, *Puru*, *Nui* and *Duke* are the most steady, surpassing the zoned *Bluetta* cultivar. The least steady in this respect are *Spartan* and *Northblue* cultivars.

At the same time among mid-ripening cultivars of *Vaccinium corymbosum L.* the zoned *Bluecrop* cultivar is characterized by the least dependence on weather factors. Among the others of mid-ripening cultivars of a blueberry, the *Patriot* cultivar has the most expressed stability. *Toro* and *Jersey* cultivars were characterized by the least stability. The two late-ripening cultivars (*Coville* and *Elizabeth*) have the least steadiness.

In a cultivar row of *Vaccinium vitis-idaea* L. *Ammerland*, *Rubin* and especially *Red Pearl* were characterized by the greatest stability of biochemical composition of fruits. The zoned *Koralle*. *Masovia* and *Erntekrone* are characterized by the least stability of this trait.

Among taxons of *Oxycoccus macrocarpus* (Ait.) Pers. *Ben Lear* cultivar were characterized by the most steadiness of biochemical composition of fruits to external influences and *Stevens* were characterized by the least one of this trait.

Conclusion

As a result of comparative research of levels of variability of 32 quantitative characteristics of biochemical composition of fruits of 30 taxons of 3 *Vacciniaceae* species (*V. corymbosum L.*, *V. vitis-idaea* L. and *Oxycoccus macrocarpus* (Ait.) Pers.) in a long-term cycle of supervision, it has been established, that the *Oxycoccus macrocarpus* (Ait.) Pers. characterizes by the most expressed stability of biochemical composition of fruits to complex influence of abiotic factors.

The least expressive inter-seasonal distinctions in the biochemical composition of dry matter of fruits of highbush blueberry are flavonols and total bioflavonoid, lignins and benzoic acid, whereas the most expressive ones are anthocyanins, total anthocyanic pigments, sucrose, monose to disaccharide ratio, and sugar-acid index. The least expressed inter-seasonal distinctions in biochemical composition of dry matter of fruits of lingonberries are nitrogen, glucose, lignins and pectin, whereas the most expressed ones are anthocyanins, atechines, sucrose, ratio of bioflavonoid fractions and monose to disaccharide ratio. The least significant inter-seasonal distinctions in biochemical composition of dry matter of fruits of cranberry are vitamin C, fixed oils, phosphorus, tannins, whereas the most significant ones are fructose, flavonols, ratio of bioflavonol fractions, monose to disaccharide ratio and sugar-acid index.

The majority of early-maturing cultivars of a highbush blueberry have higher stability of biochemical composition of fruits to the hydrothermal regime of a season, than the mid-ripening and late-ripening cultivars. Thus, the biochemical composition of fruits of the 4 early-maturing cultivars such as *Reka*, *Puru*, *Nui* and *Duke* are the most steady, surpassing the zoned *Bluetta* cultivar. The least steady biochemical composition of fruits hasbeen observed in *Spartan* and *Northblue* cultivars. Among mid-ripening cultivars of highbush blueberry the zoned *Bluecrop* and *Patriot* show dependence on weather factors. *Toro* and *Jersey* cultivars have the least stability of biochemical composition of fruits, differing from the two late-ripening *Coville* and *Elizabeth* being the least steady.

In a cultivar row of *Vaccinium vitis-idaea* L. *Ammerland*, *Rubin* and especially *Red Pearl* were characterized by the greatest stability of biochemical composition of fruits in a long-term cycle of supervision, surpassing the zoned *Koralle*. *Masovia* and *Erntekrone* were characterized by the least stability in this regard.

Among taxons of *Oxycoccus macrocarpus* (Ait.) Pers. *Ben Lear* cultivar is the most steady to external influences and zoned Stevens is the least one.

References

[1]Seljaninov, G. T., *Climatic zoning of the USSR for the agricultural purposes*. In: Memory of academician L. S. Berg, **1955**, pp. 187-225. [In Russian].

[2]*Methods for determination of total solids or moisture: GOST (State Standard)* 28561-90, **2011**. Fruit and vegetable products. pp. 75-85. Moscow. (In Russian).

[3]Ermakova, A.I. (Ed.), *Methods for biochemical studies of plants*, Leningrad. Russia, **1987**, 430. [In Russian].

[4]Fomenko, K. P., Nesterov N. N., *Chem. Agric.*, **1971**, *10*, 72-74.

[5]Zavadskaja, I. G., Gorbacheva G. I., Mamushina N. S., *The Technique of a quantitative paper chromatography of sugars, organic acids and amino acids at plants*, Moscow-Leningrad, USSR, **1962**, 17-26.

[6]Swain, T., Hillis, W. J., *Sci. Food Agric*. **1959**, *10 (1)*, 63-68. https://doi.org/10.1002/jsfa.2740100110

[7]Skorikova, Y. G., Shaftan, E. A., *Proc. 3rd All-union Seminar Biol. Active (Therapeutic) Subst. Fruit and Berries*, Sverdlovsk, USSR, **1968**, 451-461.

[8]Tanchev, S. S., *Anthocyanins in fruits and vegetables*, Moscow, Russia, **1980**, 304.

[9]Shnajdman L. O., Afanasjeva V. S., *Proc. 9th Mendeleev. Congr. Gen. Appl. Chem.*, **1965**, 79-80.

[10]Sarapuu, L., Mijdla H., *Uch. West Tart. SU*, **1971**, *256*, 111-113.

[11]Zaprometov, M. N., *Biochemistry of catechins*, Moscow, USSR, **1964**, 325.

[12]Mzhavanadze, V. V., Targamadze I. L., Dranik L. I., *Proc. Acad. Sci. GSSR*, **1971**, *63*, 205-210.

[13]*The State pharmacopoeia of the USSR*, Moscow, USSR, **1987**, *1*, 286-287.

[14]Kalebin, M. I., and Kolesnik A. A., *Research of fresh fruits, vegetables and products of their processing*. In: Tserevitinov F.V. Research of foodstuff, **1949**, pp. 218-245, Moscow, USSR [In Russian].

[15]Sapunov, V. A., Fedunjak I. I., *Methods* of an estimation of forages and the zootechnical analysis, **1958**, 190 p. [In Russian].

[16]Simonjan, A. V., Shinkarenko A. L., Oganesyan E. T., *Chem. Nat. Compd.*, **1972**, 3, 293-295. [In Russian] https://doi.org/10.1007/bf00563731

[17]Sennov, S. N., Kovjazin V. F., *Forestry*, **1990,** 91 p., Leningrad, Russia [In Russian].

[18]Zaitsev, G. N., *The technique of biometric calculations. Mathematical Statistics in Experimental Botany*, **1973**, 256 p. Moscow, USSR [In Russian].

[19]Kurlovich, T. V., *Cranberry, blueberry, cowberry*, **2007**, 200 p. Moscow, Russia [In Russian].

Received: 04.11.2016.
Accepted: 13.02.2017.

STRUCTURAL, ELECTRICAL AND OPTICAL STUDIES OF NEWLY SYNTHESIZED STEROIDAL IMIDAZOLE BASED NICKEL MOLYBDATE COMPOSITE

Ayaz Mahmood Dar[a]*, Shafia Mir[b], Urfi Ishrat[a], Shamsuzzaman[a]

Keywords: Steroidal imidazole, Band gap, Conductivity, Impedance, SEM

The synthesis of the steroidal imidazole and nickel molybdate based composite membrane is described. The fabricated composite material was characterized by using FT-IR, XRD, PSA and SEM and has been investigated for its functional, diffusive, structural, electrical and optical properties. The SEM showed that membrane has random non-preferential orientation with no visible cracks and appeared to be composed of dense and loose aggregation of small particles. No impurity peak was observed in the XRD pattern showing the single phase composite formation. The IR spectra showed the characteristic absorption peaks of different functional groups present in the composite. It was observed that real impedance decreased with the increase in frequency while AC conductivity gradually increased with the increase in frequency of applied AC due to hopping phenomenon. It was also confirmed that with the increase in frequency, the dielectric constant decreased and became almost constant at high frequencies for both compositions. The UV-vis spectrum of the synthesized composite indicate band gap energy of about 3.1 eV showing a weak blue shift compared to 4.6 eV for the bulk. Due to their optical and electrical properties, nano phase composite is promising candidate for use as selectivity of different cations.

*Corresponding Authors: Ayaz Mahmood Dar
E-Mail: ayazchem09@gmail.com
[a] Department of Chemistry, Aligarh Muslim University, Aligarh 202002, India
[b] Department of Chemistry, Govt Degree College Kulgam 192231, University of Kashmir, J&K, India

Introduction

Self-assembly of organic compounds with cholesteryl groups has proved to be attractive in the field of nanotechnology research. Some steroid derivatives are known to form ordered structures which indicate thermotropic and lyotropic liquid crystalline while other derivatives form monolayers, multilayers and micelles.[1] The steroid molecule undergoes rapid uncatalyzed transmembrane and intermembraneous transfer.[2,3] The bulk effects of cholesterol on membrane phase transitions and, as a consequence, on membrane fluidity and permeability have been well documented.[4,5] In addition, the ordered arrays of steroid molecules or mesogens result in the formation of liquid crystalline (LC) mesophases during which orientation order arises from parallel arrangement of cholesterol while positional order is obtained from attractive forces that hold the assembly together.[6-9]

The behavior of membrane systems has been extensively investigated by studying the transport properties of artificial membrane[10,11] and some of the recent analytical and electronic techniques have added impetus to such investigations. In recent years, many organic compounds and their composites with strong acid functionality such as polyarylene ether sulfone[12,13] and sulfonated poly (ether, ether ketone) (SPEEK) [14-17] have showed excellent stabilities and electrochemical properties. However, these membranes require a high pressure humidification system in order to keep liquid water in the polymer matrix.[18] In these membranes, the choice of both these components is a problem of material selection, such as polymer-chain rigidity, free volume and the altered interface, all of which influence transport through the membrane. These membranes have several advantages over organic ion-exchangers example; their ability to withstand ionizing radiations and very high temperature without undergoing degradation and their remarkably high selectivity for heavy toxic metals.[19, 20]

An organic-inorganic composite membrane (asymmetric membrane) is comprised of more than one material and structure and is usually prepared by multi-step method. The top and sub layer of the membrane can be originated from different polymeric materials with different structures, with each layer able to be optimizing independently. Usually, the top is a thin dense polymer skin formed over a microporous support with a thickness around 0.15 to 1 μm. A major benefit of such hybrid research activities is linked to synergistic effects of organic and inorganic matrix with desired and improved properties in comparison to own unique properties of each components, offering specific advantages of the excellent separation performances, optimum thermal and chemical stability, adaptability to the harsh conditions and membrane forming ability.[21-24] Here in we report the synthesis of the composite membrane comprised of steroidal imidazole and nickel molybdate and study its structural, electrical and optical properties.

Experimental

Cholesterol, oxalyl chloride, trisodium molybdate and titanium chloride were purchased from Merck and Sigma-Aldrich with purity of 99.90% and used without further purification. The IR spectra were recorded on KBr pellets with Perkin Elmer RXI Spectrometer (without microscope) and values are given in cm^{-1}. 1H and 13C NMR spectra were run in $CDCl_3$ on a JEOL Eclipse (400 MHz) instrument with TMS as internal standard and values are given in ppm (δ). Mass spectra were recorded on a JEOL SX 102/DA-6000 Mass Spectrometer.

Synthesis of nickel molybdate by sol-gel method

The nickel molybdate was prepared by sol-gel method[25] by taking a 0.2 mol trisodium molybdate and mix with 0.2 mol titanium chloride ($TiCl_3$) with continuous stirring. The pH of the mixture was adjusted at 7 by adding 1 M HNO_3 or NH_3 solutions. The mixing ratio of the reactants was 1:1 (v/v). The nickel molybdate precipitate obtained was washed with deionized water to removed free electrolyte and then dried at 100 °C.

Synthesis of [4, 5-dioxo-2-thioxoimidazole-1-yl] 6-imino-5α-cholestane

To a solution of steroidal thiosemicarbazone (1.5 mmol) in absolute ethanol (20 mL), an equimolar amount of oxalyl chloride was added. The reaction mixture was refluxed for 9 h. The progress and completion of the reaction was monitored by thin layer chromatography. After completion of reaction the excess solvent was removed to three fourths of the original volume under reduced pressure. The reaction mixture was then taken in diethyl ether, washed with water and dried over anhydrous sodium sulphate. Evaporation of solvents and recrystallization from methanol afforded respective product. [26]

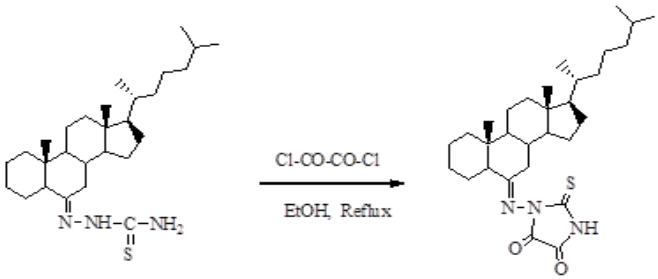

Scheme 1. Showing the formation of steroidal thioxoimidazole

Characterization of data

White powder; yield: 70 %, Mol. Formula $C_{30}H_{47}N_3O_2S$, IR (KBr) ν cm^{-1}: 3310 (NH), 1687, 1675 (C=O), 1518 (C=N), 1236 (C=S), 1029 (C-N); ^{1}H NMR (400 MHz, $CDCl_3$, ppm): δ 7.8 (s, 1H, N*H*, exchangeable with D_2O), 1.17 (s, 3H, C_{10}-C*H*$_3$), 0.72 (s, 3H, C_{13}-C*H*$_3$), 0.94 & 0.84 (other methyl protons); ^{13}C NMR (100 MHz, $CDCl_3$, ppm): δ 182 (C=S), 163.6 (C=O), 161.3 (C=O), 154.3 (C=N); ESI MS: m/z 513 [$M^{+\cdot}$].

Preparation of membrane from steroidal imidazole and nickel molybdate

The dried precipitate of nickel molybdate was grounded into fine powder by pestle mortar and then sieved through 200 mesh (granule size ≤ 0.075mm) with grounded steroidal imidazole used as a binder. The optimum quantity of binder was embedded in order to get membrane of adequate mechanical strength. The membrane prepared by embedding 25 % of binder was most suitable for this experiment. Those containing large amount of binder (> 25 %) did not give reproducible results while those containing lesser amount (< 20 %) were quite unstable. The mixture was kept into cast die and then placed in an oven maintain at 200 °C for about half an hour to equilibrate the reaction mixture, then die was transferred to a pressure device (SL-89, UK) with pressure maintained at 60 MPa.

Fourier Transform Infrared Spectroscopy (FTIR)

FTIR spectra of pure steroidal imidazole, nickel molybdate and composite were taken by KBr disc method at room temperature after drying the sample at 40 ºC. The grinding was done using pestle and mortar. To avoid scattering, the particle size of the grounded mixture was limited up to 2 μm.

XRD analysis

The crystallinity, structure and crystal size of pure nickel molybdate and composite were determined with Rigaku Diffractometer (2400) using graded *d*-space elliptical side-by-side multilayer optics, monochromatic Cu Kα radiation λ = (0.15406 nm) in 2θ range from 20 °C to 80 °C and an imaging plate (R-Axis IV).

SEM analysis

The membrane morphology had been studied using scanning electron microscopy.[27,28] The information obtained from SEM images provided guidance in the preparation of well-ordered precipitates.-, The composite pore structure, micro/macro porosity, homogeneity, thickness, cracks and surface texture/morphology had been studied. [29, 30]

Particle size analysis

The particle size of composite was analyzed by using laser diffraction. The sample had been mixed with distilled water using ultrasonic treatment. The pre-requisite for understanding the performance of a composite membrane is its complete physico-chemical characterization, which involves the determination of all parameters like thickness, porosity, swelling, water content which affects its electrical properties. The above parameters are shown in **Table 1.**

Table 1. Physico-chemical characterization of composite membrane

Parameterss	Result
Thickness of the membrane (cm)	0.075
Water Content as % weight of wet membrane	0.074
Porosity	0.113
Swelling of %weight wet membrane	No swelling

The membrane did not show any dispersion in water and in other electrolyte solutions as there was no swelling found in the membrane.

Result and Discussion

Structural properties

The size of the suspended particle had been measured by laser. The average particle size comes out to be 1157.88, 1473.33 and 1448.46 nm. The reason for such a high value is the preparation method. Sol-gel method gives a uniform and smaller particle size (Figure 1). SEM surface image of the composite membrane of nickel molybdate and steroidal imidazole was taken at 60 MPa pressure and are shown in Figure 2A and the cross-sectional SEM micrograph of the surface is shown in Figure 2B. Membrane had random non-preferential orientation with no visible cracks and appeared to be composed of dense and loose aggregation of small particles. The membrane is macroscopically uniform in thickness and porous in nature. The pores are in the form of uniform capillaries that extend throughout the membrane, and are evenly distributed throughout the surface of the membrane.

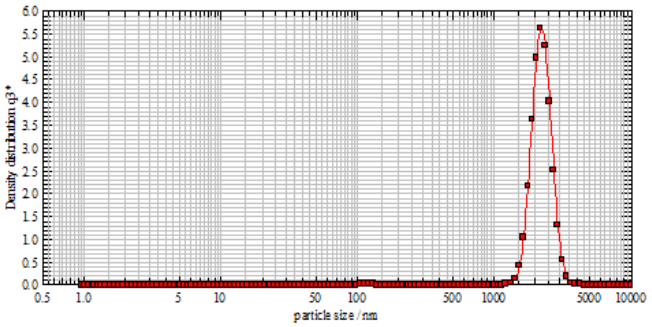

Figure 1. The graph shown particle size analysis of the composite.

The thickness is still large as compared to the pore radius and it is assumed that the membrane and adjacent solution (interface) are in equilibrium. The distribution of charge density and mobile species within the pores is assumed to be uniform.

The peak position of the sample at 44.31º and 55.71º shows the presence of nickel molybdate in composite which was confirmed from the ICDD card No. 070356 and the presence of peak position of steroidal imidazole at 21.7º in composite was confirmed from the ICDD card no. 470787. Further, no other impurity peak was observed in the XRD pattern showing the single phase composite formation. The typical XRD patterns of the pure nickel molybdate,[31] and its composite with steroidal imidazole are shown in Figure S1 (Supplementary Material).

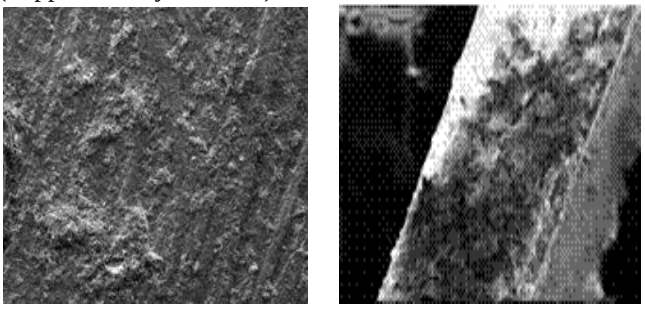

(A) (B)

Figure 2. SEM images of surface (**A**) and cross-sectional surface (**B**) of composite

The IR spectra displays absorption bands in the range of 745, 821 and 964 cm^{-1}, which shows the presence of Mo-O group (Figure S2a, Supplementary material) in nickel molybdate. The Fig. S2b shows absorption peaks at *v* 1687 and 1685 cm^{-1} for two (C=O) groups and absorption peak at 1515 and 1236 cm^{-1} for (C=N) and C=S, respectively. These peaks confirms the presence of steroidal imidazole fragment. The IR spectrum S2c (Supplementary material) shows the combination of peaks of nickel molybdate and steroidal imidazole, which confirms the formation of composite [32-34]

Electrical properties

The electrical properties such as impedance analysis, AC conductivity, dielectric constant and dielectric loss of nickel molybdate and of steroidal imidazole are determined using impedance spectroscopy.

The nickel molybdate powder was pressed into pellets of 13 mm diameter and 0.84 mm thickness and composite powder was pressed into pellet of 0.49 mm thickness for electrical measurements. Dielectric and impedance spectroscopy measurements were carried out in the frequency range 1 kHz to 1 MHz using LCR meter (Agilent 48). The pellets were coated on adjacent faces with silver paste, thereby forming parallel plate capacitor geometry. The value of dielectric constant (ε′) is calculated using the the following formula:

$$\varepsilon' = \frac{c_p d}{\varepsilon_0 A} \qquad (1)$$

where,

ε_0 = permittivity of free space,

d = thickness of pellet,

A= cross sectional area of the flat surface of the pellet,

c_p= capacitance of the specimen in Farad (F)

The complex dielectric constant (ε″) of the samples was calculated using the relation, as follows:

$$\varepsilon'' = \varepsilon' \tan\delta \qquad (2)$$

where tan δ is the dielectric loss which is proportional to the loss of energy from the applied field into the sample and is therefore called as dielectric loss

The AC conductivity of the samples was determined using the relation:

$$\sigma_{ac} = \varepsilon' \varepsilon_0 \omega \tan\delta \qquad (3)$$

where, ω is the angular frequency

Table 2. Variation in different electrical parameters as a function of composite

Material	R_{gb} (Ω)	C_{gb} (F)	ω_{gb}	τ_{gb}
Ni-molybdate	5.3668E13	3.954E-20	4.712E5	2.122E-6
Composite	5.4128E6	3.2387E-13	4.7124E5	2.122E-06

Impedance analysis

The electrical behavior of composite had been studied over a wide range of frequencies at room temperature using AC technique of complex impedance spectroscopy. The electrical property of a material is exhibited by the appearance of semicircular arcs in Nyquist plots. **Figure 5** shows the complex impedance plots (Nyquist plots) of pure nickel molybdate and composite. It is evident that both the samples show single semicircular behavior, which suggests the predominance of grain boundary resistance over the grain resistance in both. The literature mentions that the resistivity of a polycrystalline material increases with decreasing grain size.[35]

Accordingly, smaller grains imply a larger number of insulating grain boundaries which act as a barrier to the flow of electrons. Smaller grains also imply smaller grain-grain surface contact area and therefore a reduced electron flow. In both samples the contribution of the grain boundary becomes dominant and grain contribution is not seen. This is the reason for which only single semicircular arc appears in Cole-Cole plots of both samples. In terms of impedance plots, each semicircular arc can be modeled by an equivalent circuit consisting of a resistor (R) and a capacitor (C) connected in parallel. The complex impedance of a system can be written as the sum of real and imaginary part, as follows:

$$Z^* = Z' + jZ'' \qquad (4)$$

where, Z' and Z'' are given by the following relations:

$$Z' = \frac{R_g}{1+(\omega_g{}^2 C_g{}^2 R_g{}^2)} + \frac{R_{gb}}{1+(\omega_{gb}{}^2 C_{gb}{}^2 R_{gb}{}^2)} \qquad (5)$$

$$Z'' = \frac{R_g{}^2 \omega_g C_g}{1+(\omega_g{}^2 C_g{}^2 R_g{}^2)} + \frac{R_{gb}{}^2 \omega_{gb} C_{gb}}{1+(\omega_{gb}{}^2 C_{gb}{}^2 R_{gb}{}^2)} \qquad (6)$$

where,

R_a, R_{ab}, C_a, C_{ab} are the resistance and capacitance of the grain and grain boundary, respectively, while

ω_a and ω_{ab} are the frequencies at the peaks of the semicircles for grain and grain boundary, respectively.

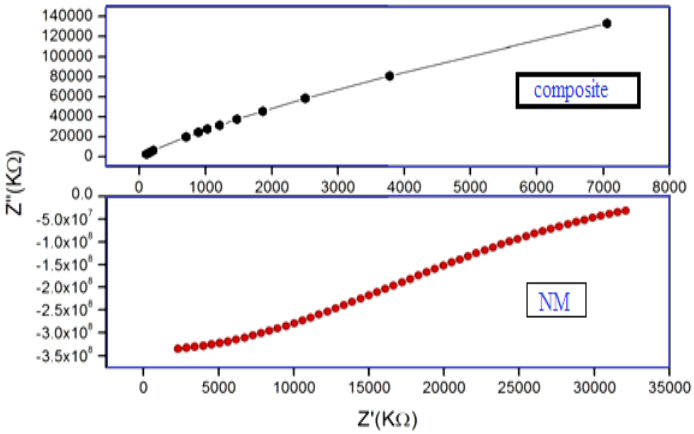

Figure 5. Nyquist plots for different compositions at room temperature (NM-nickel molybdate)

The resistance values are obtained from the circular arc intercepts on *Z*-axis, while the capacitance values can be derived from the maximum height of the circular arcs. The capacitances and the relaxation time can be calculated for the grain and grain boundary by the expressions as follows:

$$C_g = \frac{1}{R_g \omega_g}, \quad C_{gb} = \frac{1}{R_{gb} \omega_{gb}}, \quad \tau_g = \frac{1}{\omega_g} = C_g R_g,$$

$$\tau_{gb} = \frac{1}{\omega_{gb}} = C_{gb} R_{gb} \qquad (7)$$

where,

R_g, R_{gb}, C_g, C_{gb} are the resistance and capacitance of the grain and grain boundary, respectively.

ω_g and ω_{gb} are the frequencies at the peaks of the semicircles for grain and grain boundary, respectively.

τ_g, and τ_{gb} are the time constants of an RC circuit of the grain and grain boundary, respectively.

The grain and grain boundary parameters like resistance and capacitance are obtained by analyzing the impedance data using nonlinear least square fitting method and are shown in Table 2.

It has been observed that grain boundary resistance R_{gb} decreases while the capacitance C_{gb} increases with the addition of steroidal imidazole in nickel molybdate.

The variation in real part of impedance (Z') as a function of frequency is shown in Figure 6. It can be observed that Z' decreases with the increase in frequency for all the composition. This is due to increase in conductivity with frequency resulting from hopping phenomenon.

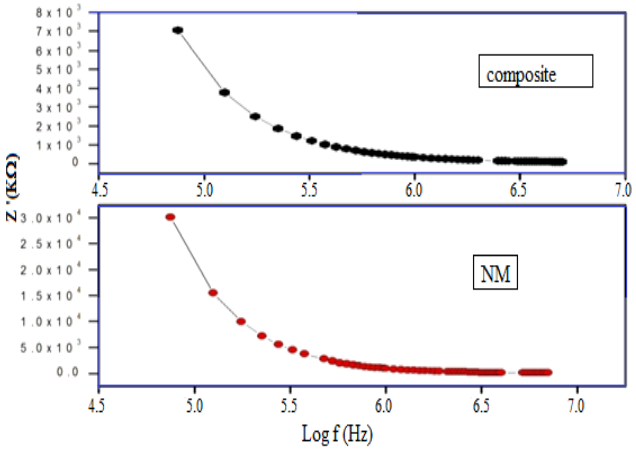

Figure 6. Variation in real impedance (Z′) as a function of frequency and composition (NM-nickel molybdate)

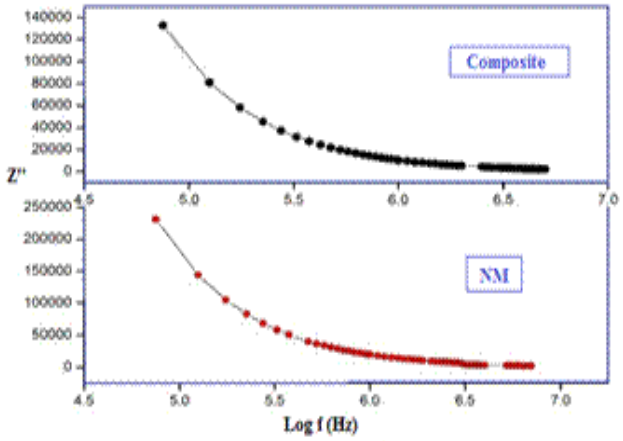

Figure 7. Variation in imaginary impedance Z″ with frequency for different compositions (NM-nickel molybdate)

It is seen from **Figure 7** that Z′ had strong frequency dependence in the lower frequency and show frequency independent behavior in the higher frequency region. This can be attributed to the fact that low frequency region corresponds to high resistivity due to the effectiveness of resistive grain boundaries in this region. **Figure 7** shows the variation in reactive part of impedance (Z′) as a function of frequency and composition.

It shows the same behavior as that of Z′. Z″ increases with the addition of steroidal imidazole in composite due to the decrease in C_{gb} as shown in **Table 2**. This can be attributed to the fact that Z″ is inversely proportional to capacitance as shown below:

$$Z'' = \frac{1}{j\omega C} \qquad (8)$$

Thus, as the steroidal imidazole is added in composite, C_{gb} decreases leading to the increase in Z″. The j represents the phase shift or phase angle between voltage and current.

A.C conductivity

The variation in electrical conductivity with frequency for different compositions at room temperature is shown in Figure 8. It is clear from the Figure that the AC conductivity increases with the increase in frequency for both compositions. The total conductivity of the system is given by:

$$\sigma = \sigma_0(T) + \sigma(\omega, T) \qquad (9)$$

Here, first term on R.H.S is DC conductivity which is independent of frequency. The second term is pure AC conductivity due to the electron hopping between the metal ions. It has been observed that AC conductivity gradually increases with the increase in frequency of applied AC field because the increase in frequency enhances the electron hopping frequency.

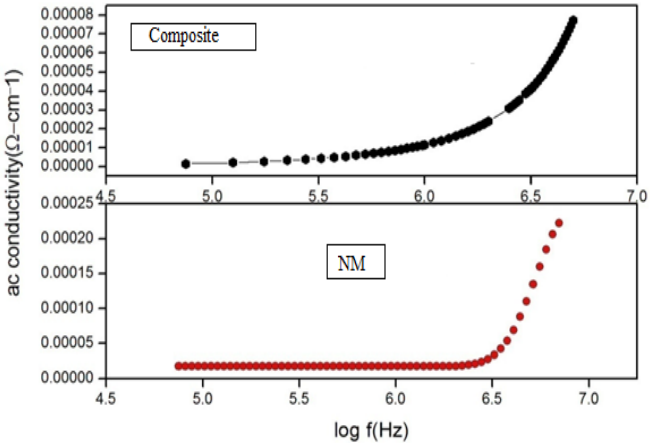

Figure 8. Variation in AC conductivity with frequency for different compositions (NM-nickel molybdate)

Dielectric properties

The complex dielectric permittivity of pure nickel molybdate and composite was measured as a function of frequency at room temperature by equation 10.

$$\varepsilon^* = \varepsilon' - i\varepsilon'' \qquad (3.10)$$

where

ε is real part of dielectric constant and describes the stored energy while

ε" is the imaginary part of the dielectric constant, which describes the dissipated energy.

The dielectric constant ε^* is used as a function of frequency for both nickel molybdate and composite is shown in Figure 9. The *i* (iota) is the imaginary constant that defines the imaginary part of dielectric constant in the equation 10. It is shown that with increase in frequency, the dielectric constant decreases and becomes almost constant at high frequencies for both compositions.

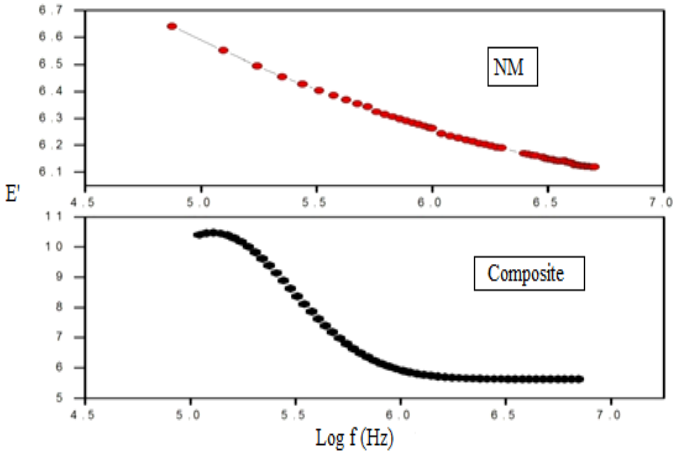

Figure 9. Variation in dielectric constant ε' as a function of frequency and composition (NM-nickel molybdate)

This behavior can be explained using Maxwell-Wagner interfacial model. According to this model, a dielectric medium is considered to be composed of double layers, well conducting grains which are separated by poorly conducting or resistive grain boundaries. Under the application of external electric field, the charge carriers can easily migrate the grains but are accumulated at the grain boundaries. This process can produce large polarization and high dielectric constant. The higher value of dielectric constant can also be explained on the basis of interfacial/space charge polarization due to non-homogeneous dielectric structure. Loss tangent or loss factor *tan δ* represents the energy dissipation in the dielectric system. The **Figure 10** shows the variation in dielectric loss factor with frequency at room temperature.

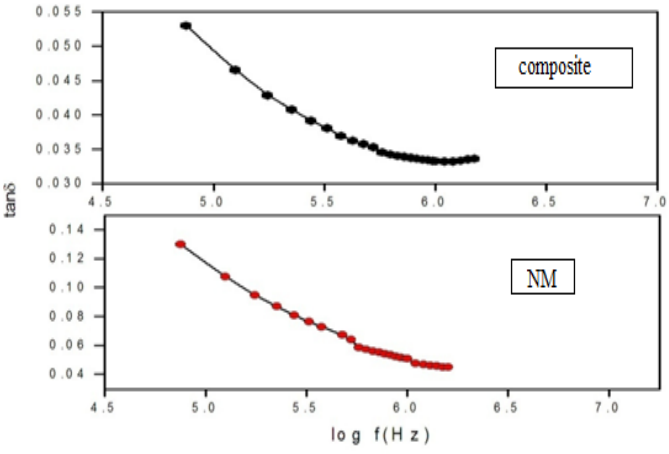

Figure 10. Variation in loss tangent tan δ with frequency for all the compositions (NM-nickel molybdate)

It had been observed that *tan δ* decreases with the increase in frequency, which may be due to the space charge polarization. One semicircle for composite suggests the dominance of grain boundary resistance. Moreover, the grain boundary resistance *Rgb* is found to decrease, while capacitance *Cgb* is observed to increase with addition of steroidal imidazole. The AC conductivity shows the frequency dependent behavior. The data reveals that the dielectric constant and *tan δ* exhibit the normal dielectric behavior and decreases with the increase in frequency.

Optical properties

In order to describe the photo-absorption behavior of the nickel molybdate and composite, certain amount of samples were uniformly dispersed in ethanol and then UV-visible absorption spectra were recorded. Figure 11 shows the UV-vis absorption spectra of nickel molybdate and composite.

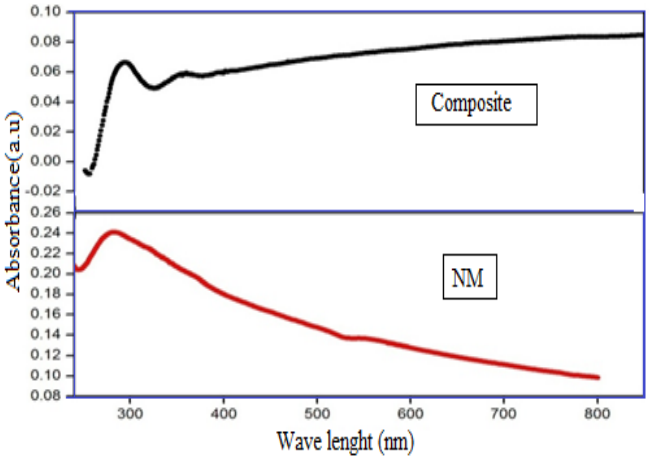

Figure 11. UV-vis absorption spectrum of nickel molybdate and composite (NM-nickel molybdate)

It can be seen that an extremely strong absorption occurs at the wavelength 250 nm and 295 nm for nickel molybdate and composite, respectively, but relatively strong absorption in the visible region (400 nm) for composite can also be seen (**Figure 11)**. This increase in the wavelength in UV-vis absorption spectra of composite may be due to the presence of unsaturation in the functional groups present in the imidazole moiety of the steroidal molecule. The band gap energy calculated by extrapolating the best linear fit (shown in Figure 12a and 12b) was found to be 4.6 eV and 3.1 eV for nickel molybdate and composite, respectively.

The decrease in the band gap energy of composite than nickel molybdate is due to the presence of unsaturated carbonyl groups in steroidal imidazole which may cause conjugation with the lone pairs of electrons of NH that leads to the decrease in the energy gap between the HOMO and LUMO in the molecule. Thus energy of maximum wavelength is required to cause the absorption, hence red shift is observed in composite.

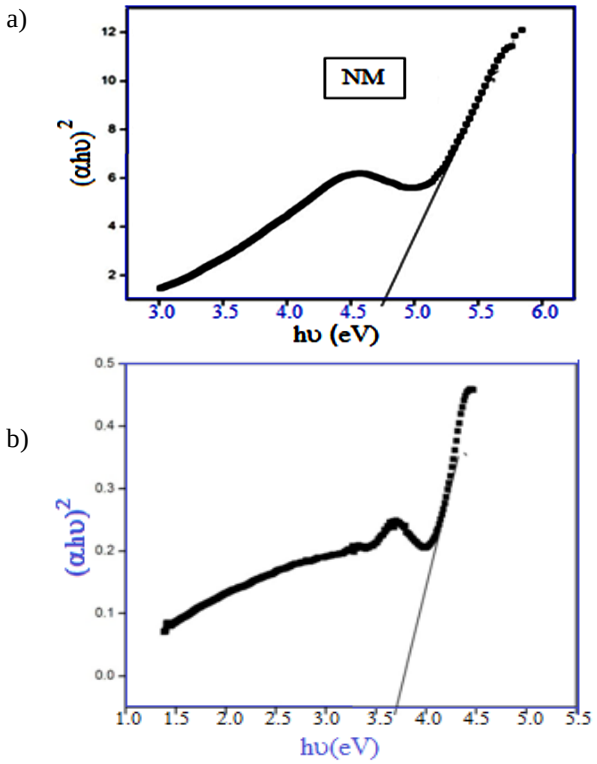

Figure 12a. The optical band gap energy of (a) nickel molybdate (NM) (b) Composite

Conclusion

In this work, sample characterization had been done by XRD, FTIR and SEM. Steroidal imidazole based composite membrane of nickel molybdate was quite stable and did not show any dispersion in water and in other electrolyte solutions. From the optical absorption spectra, the band gap of nickel molybdate and composite of nickel molybdate and steroidal imidazole was found to be 4.6 eV and 3.1 eV, respectively. The decrease in the band gap shows that the conductivity of composite had been increased. The electrical behavior of composite had been studied over a wide range of frequencies. One semicircle for sample suggested that there is a dominance of grain boundary resistance in the samples. Moreover, the grain boundary resistance R_{gb} is found to decrease, while grain boundary capacitance C_{gb} is increase in case of composite as compared to pure nickel molybdate. The AC conductivity shows the frequency dependent behavior. The data reveals that the dielectric constant and *tan* δ exhibited the normal dielectric behavior and decreases with the increase in frequency.

Acknowledgements

The authors are thankful to the Chairman Department of Chemistry for providing research facilities, All India Institute of Medical Sciences (AIIMS), New Delhi for SEM micrograms and Department of Applied Physics (AMU) for X-ray diffraction and particle size analysis is also acknowledged.

References

[1]Yusa, S. I., *Int. J. Polym. Sci.*, **2011**, 1.

[2]Backer, J. M., Dawidowicz, E. A., *J. Biol. Chem.*, **1981**, *256*, 586.

[3]Backer, J. M., Dawidowicz, E. A., *Biochemistry*, **1981**, *20*, 3805. https://doi.org/10.1021/bi00516a021

[4]Shimshick, E. J., McConnell, H. M., *Biochem. Biophys. Res. Commun.*, **1973**, *53*, 446. https://doi.org/10.1016/0006-291X(73)90682-7

[5]Estep, T. N., Mountcastle, D. B., Biltonen, R. L., Thompson, T. E., *Biochemistry*, **1978**, *17*, 1984. https://doi.org/10.1021/bi00603a029

[6]Drummond, C. J., Fong, C., *Curr. Opin. Colloid Interface Sci.*, **1999**, *4*, 449. https://doi.org/10.1016/S1359-0294(00)00020-0

[7]Mannock, D. A., McElhaney, R. N., *Curr. Opin. Colloid Interface Sci.*, **2004**, *8*, 426. https://doi.org/10.1016/j.cocis.2004.01.009

[8]Thiemann, T., Vill, V., *J. Phys. Chem.*, **1997**, *26*, 291.

[9]Hao, J. Q., Li, H., Zhu, X. X., *Chin. J. Org. Chem.*, **2004**, *24*, 1129.

[10]Lakshminaraynaih, N., Siddiqui, F. A., *Biophys. J.*, **1971**, *11*, 603.

[11]Kobatake, Y., Kamo, N., *Prog. Polym. Sci. Jpn.*, **1972**, *5*, 257.

[12]Wang, F., Hickner, M., Kim, Y. S., Zawodzinski, T. A., McGrath, J. E., *J. Membrane Sci.*, **2002**, *197*, 231. https://doi.org/10.1016/S0376-7388(01)00620-2

[13]Kreuer, K. D., *J. Membrane Sci.*, **2001**, *185*, 29. https://doi.org/10.1016/S0376-7388(00)00632-3

[14]Kaliaguine, S., Mikhailenko, S. D, Wang, K. P., Xing, P., Robertson, G., Guiver, M. C., *Catal. Today*, **2003**, *82*, 213. https://doi.org/10.1016/S0920-5861(03)00235-9

[15]Alberti, G., Casciola, M., Massinelli, L., Bauer, B., *J. Membrane Sci.*, **2001**, *185*, 73. https://doi.org/10.1016/s0376-7388(00)00635-9

[16]Ahmad, M. I., Zaidi, S. M. J., Rahman, S. U., *Desalination*, **2006**, *193*, 387. https://doi.org/10.1016/j.desal.2005.06.069

[17]He, R., Li, Q., Jensen, J. O., Bjerrum, N. J., *J. Polym Sci. A: Polym. Chem.*, **2007**, *45*, 2989. https://doi.org/10.1002/pola.22053

[18]Nabi, S. A., Shallo, A. H., Khan. A. M., Ganie, S., *Colloid Surf. A: Physicochem. Aspect.*, **2007**, *302*, 241. https://doi.org/10.1016/j.colsurfa.2007.02.034

[19]Zhang, H., Pang, J. H., Wang, D., Li, A., Li, X., Jiang, Z., *J. Membrane Sci.*, **2005**, *264*, 56. https://doi.org/10.1016/j.memsci.2005.04.021

[20]Lakshminarayanah, N., *Chem. Rev.*, **1965**, *65*, 491. https://doi.org/10.1021/cr60237a001

[21]Lu, Z. H., Liu, G. J., Duncan, S., *J. Membrane Sci.*, **2003**, *221*, 113. https://doi.org/10.1016/S0376-7388(03)00251-5

[22]Chiang, P. C., Whang, W. T., Tsai, M. H., Wu, S. C., *Thin Solid Films*, **2004**, *447/448* 359. https://doi.org/10.1016/S0040-6090(03)01081-2

[23]Taniguchi, A., Cakmak, M., *Polymer*, **2004**, *45*, 6647. https://doi.org/10.1016/j.polymer.2004.06.056

[24]Neelakandan, C., Pugazhenthi, G., Kumar, A., *Eur. Poly. J.*, **2003**, *39*, 2383. https://doi.org/10.1016/S0014-3057(03)00183-6

[25]Pusch, W., *Pure Appl. Chem.*, **1986**, *58*, 1669. https://doi.org/10.1351/pac198658121669

[26]Dar, A. M., Shamsuzzaman, Khan. S., *J. Fluoresc.*, **2016**, *26, 639* https://doi.org/10.1007/s10895-015-1750-7

[27]Liu, J., Xu, T., Gong, M., Yu, F., Fu, Y., *J. Membrane Sci.*, **2006**, *283*, 190. https://doi.org/10.1016/j.memsci.2006.06.027

[28]Silva, V. S., Ruffmann, B., Vetter, S., Mendes, A., Madeira, L. M., Nunes, S. P., *Catal. Today*, **2005**, *104*, 205. https://doi.org/10.1016/j.cattod.2005.03.051

[29]Titiloye, J. O., Hussain, I., *J. Colloid Interf. Sci.*, **2008**, *318*, 50. https://doi.org/10.1016/j.jcis.2007.10.025

[30]Resina, M., Macanas, J., Gyves, J. D., Munoz, M., *J. Membrane Sci.*, **2007**, *289*, 150. https://doi.org/10.1016/j.memsci.2006.11.049

[31] Monroy-Guzman, F., Romero, O. C., Velázquez, H. D., *J. Nucl. Radiochem. Sci*., **2007**, *8*, 11. https://doi.org/10.14494/jnrs2000.8.11

[32]Bratescu, M. A., Suda, Y., Sakai, Y., Saito, N., Takai, O., *Thin Solid Films*, **2006**, *515*, 1314. https://doi.org/10.1016/j.tsf.2006.03.022

[33]Chalmer, J., Griffths, P., *Handbook of Vibrational Spectroscopy*, Wiley, **2001** https://doi.org/10.1002/0470027320

[34]Saleem, S. S., Aruldhas, G., *Polyhedron*, **1982**, *1*, 331. https://doi.org/10.1016/S0277-5387(00)80814-1

[35]Erb, U., *Nanostruct. Mat.*, **1995**, *6*, 533. https://doi.org/10.1016/0965-9773(95)00114-X

Received: 26.12.2016.
Accepted: 19.02.2017.

EXPERIMENTAL AND THEORETICAL STUDIES ON MILD STEEL CORROSION INHIBITION BY THE GRIESEOFULVIN IN 1 M HCl

Dakeshwar Kumar Verma[a], Fahmida Khan[b], Chandrabhan Verma[c], Rajendran Susai[d,e] and M. A. Quraishi[c]

Keywords: adsorption; mild steel; corrosion inhibitor; grieseofulvin

The inhibition effect of grieseofulvin against the mild steel corrosion in 1 M HCl solution has been investigated by potentiodynamic polarization measurements, electrochemical impedance spectroscopy (EIS) and quantum chemical methods. It was found thatgrieseofulvin acts as a good mild steel corrosion inhibitor in the acid solution at temperature ranging from 298-328 K. The potentiodynamic polarization study reveals that grieseofulvin acts as mixed type inhibitor. The adsorption of grieseofulvin on mild steel follows the Langmuir adsorption isotherm. Scanning electron microscopy equipped with energy dispersive spectroscopy (SEM-EDS) studies established that grieseofulvin formed a protective layer on the surface of mild steel.

* Corresponding Authors
Tel: +91-9307025126
Fax: +91-542-2368428
E-Mail:maquraishi.apc@itbhu.ac.in;
[a] Department of Chemistry, VEC Lakhanpur, Sarguja University, Ambikapur, Chhattisgarh, India, 497116
[b] Department of Chemistry, National Institute of Technology Raipur, Raipur, Chhattisgarh, India, 492010
[c] Department of Applied Chemistry, Indian Institute of Technology, Banaras Hindu University, Varanasi-221005,
[d] Servite College of Education for Women, Thogaimalai-621313, Tamil Nadu, India
[e] Corrosion Research Centre, Post Graduate and Research Department of Chemistry, GTN Arts College, Dindigul-624005, India

Introduction

Mild steel corrosion inhibition is a matter of theoretical as well as practical importance which is an engineering material widely used in process industries, boilers, oil and gas, water pipelines, cooling water systems and refining and extraction etc. several acidic solutions are widely used in many industrial process such as acid cleaning, acid pickling, oil well acidizing and acid descaling.[1-3] These process generally leads to serious metallic corrosion. Use of an inhibitors is the sensible and most effective approach to protect the metal from corrosion.[4] Electronic characteristics and molecular structure of inhibitors molecules are the main factors in establishing the adsorption capability of inhibitors on metal surfaces.[5] The greater efficiency of these inhibitors is associated to the presence of various polar elements such as N, O, S and P in the organic molecules as well as pi electrons.[6-8] The presence of such hetero atoms with lone pair(s) of electrons and π electrons in the molecular structure increase the adsorption ability of inhibitor molecules on the metal surface.[9] The inhibitive effect of some antibacterial drugs namely cloxacillin, amoxicillin, ampicillin and flucloxacillin was studied. The corrosion inhibition mechanism of these drugs was attributed to blocking the metal surface by the formation of protective film.[10]

Nowadays, various experimental and theoretical techniques have been developed to study the structural properties of inhibitor molecules and their activity towards metal surfaces, but quantum chemical calculations based on density functional theory (DFT) have led to an attractive theoretical method because it gives several vital parameters. A quantum chemical approach is adequately sufficient to forecast the inhibitor effectiveness.

The aim of the present study is to investigate the mild steel corrosion behaviour in 1 M HCl in the presence and absence of antifungal drug namely, Grieseofulvin which is the commercial name of 7-chloro-2',4,6-trimethoxy-6'-methyl-3*H*,4'*H*-spiro[1-benzofuran-2,1'-cyclohex[2]ene]-3,4'-dione.[11] The present study is carried out using the weight loss measurements, DFT, Tafel polarization, and electrochemical impedance techniques. Protective film formation against acid attack on metal surface was confirmed by Scanning electron microscopy equipped with energy dispersive spectroscopy (SEM-EDS). The activation energy and thermodynamic parameters (ΔH^* and ΔS^*) of the inhibitor were investigated. Several commonly used adsorptions were also tested for their significance in defining the adsorption behaviour of the inhibitor. The chemical structure of the investigated inhibition is given in Fig.1.

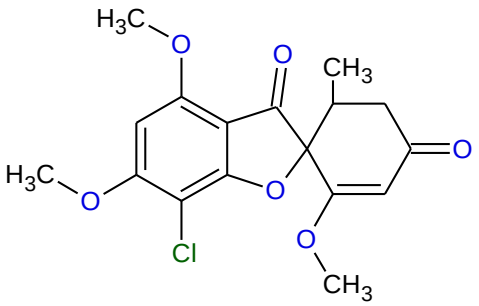

Figure 1. Molecular structure of grieseofulvin

Experimental

Materials preparation

Mild steel specimenshaving chemical composition(%wt): Fe (98.67), C (0.22), O (0.06), Mn (0.51), P (0.03), S (0.02) and Cr (0.49) were used for electrochemical, weight loss and surface measurements. Before performing the experiments, the metallic specimens were cleaned with the help of emery papers of different grades, washed with distilled water, degreased with acetone and stored in moister free desiccators. The test solution of 1 M HCl was prepared by dilution of analytical grade HCl (Merck) with purified water obtained from Elix essential 10 millipore water purifier. During course of weight loss and electrochemical experiments, the concentration range of inhibitor was allowed to varied from 100-400 ppm.

Electrochemical measurements

Gamry Potentiostat/Galvanostat electrochemical workstation (ESA300 USA) with three electrode cell assembly was used for impedance measurements. In cell assembly, saturated calomel electrode (SCE) served as reference electrode, and a bare mild steel electrode and platinum electrode were used as working and counter electrodes, respectively. The working electrode with exposed area 1cm^2 was kept in test solution for 30 minutes for attainment of steady open circuit potential (OCP) before electrochemical tests. The impedance measurements were performed in the frequency range from 100 kHz to 10 MHz with a.c. ± 10 mV and Nyquist plots were obtained. The potential range of ± 250 mV vs. corrosion potential at a scan rate of 1 mV s^{-1} was applied for polarization experiment in the same cell assembly.

Weight loss measurements

Weight loss measurements were performed at temperature ranging from 298-328 K with different concentration of inhibitor at the immersion period of 6h. After the 6h of immersion time the mild steel strips were picked out, cleaned and dried. Electronic balance (METTLER TOLEDO sensitivity up to 0.0001gm) was used for weigh the mild steel specimens. The corrosion rate (C_R) in terms of weight loss was calculated according to equation (1):[12]

$$C_R = \frac{W}{At}) \quad (1)$$

where

A is the total area of metal specimen in cm^2,
W is the average weight loss in mg, and
t is the exposure time (6h).

The % inhibition efficiency (η%) was calculated as given:[12]

$$\eta\% = \frac{C_R - C_{R(i)}}{C_R} \times 100 \quad (2)$$

where C_R and $C_{R(i)}$ are the corrosion rates of the test specimens without and with the inhibitor respectively.

Surface analysis

Scanning electron microscope and energy dispersion x-ray spectroscopy (SEM-EDS ZEISS EVO SEM 18 model 20mm Detector equipped with INCA 250 EDS X-MAX 20 Detector Oxford) were used to study the surface morphology and surface composition of mild steel in 1 M HCl in the presence and absence of inhibitor respectively.

Quantum chemical study

Gaussian 09 (G 09) software package is used for quantum chemical calculation of grieseofulvin with geometrically optimised structure.[32] The backe's three parameters hybrid exchange functional and Lee-Yang-Parr non-local correlation function (B3LYP) as well as 3-21G basic set were employed for calculations. The theoretical parameters such as lowest unoccupied molecular orbital (LUMO) energies, highest occupied molecular orbital (HOMO) energies, energy gap ΔE (E_{HOMO}-E_{LUMO}) and dipole moment (μ) were calculated.

Result and discussion

Potentiodynamic polarization measurements

Potentiodynamic polarization curves for grieseofulvin in 1 M HCl solution with and without inhibitor at room temperature represented in Fig. 2.

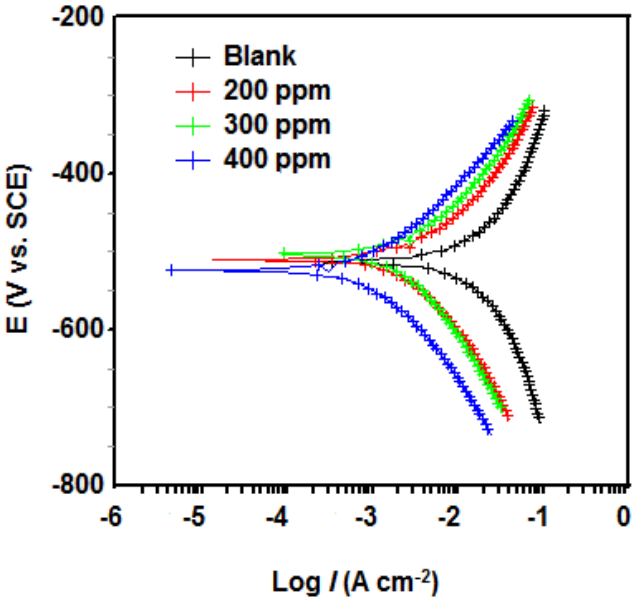

Fig. 2. Tafel polarization curves of mild steel in 1 M HCl with and without grieseofulvin.

Table 1. Potentiodynamic polarization parameters of mild steel in 1 M HCl at room temperature containing different concentration of grieseofulvin.

Conc., ppm	$i_{corr,}$, mA/cm^2)	$E_{corr,}$ (mV/SCE)	$\beta_{a,}$ (mV/dec)	$\beta_{c,}$ (mV/dec)	ϑ	η%
Blank	85.10	-514	665.2	1219	-	-
200	21.68	-511	109.3	193	0.745	74.52
300	14.31	-506	127.0	221.4	0.831	83.18
400	4.777	-525	108.6	129.2	0.943	94.38

Table 2. Impedance data of mild steel in 1 M HCl in the presence and absence of inhibitor at room temperature.

Conc., ppm	$R_{s.,}$ Ω cm^2	$R_{ct,}$ Ω cm^2	$C_{dl,}$ µF cm^{-2}	ϑ	η%
Blank	0.160	1.952	120.77	-	
200	1.407	5.791	82.57	0.662	66.29
300	2.273	19.77	81.43	0.901	90.12
400	1.194	25.27	68.19	0.922	92.22

Important kinetic parameters including corrosion potential (E_{corr}), corrosion current density (i_{corr}), and percentage inhibition efficiency (η%) from Tafel plots were calculated and given in Table 1. The inhibition efficiency was calculated from the values of corrosion current density (i_{corr}) which itself derived by extrapolating the linear segments of anodic and cathodic Tafel slopes, using the following relation:[13]

$$\eta\% = \frac{i^0_{corr} - i^i_{corr}}{i^0_{corr}} \times 100 \qquad (3)$$

where i_{corr} and i^i_{corr} are the corrosion current densities without and with inhibitor, respectively.

Table 1 shown that corrosion current density (i_{corr}) of cathodic and anodic curves decreasesand inhibition efficiency increases as the inhibitor concentration increases in compared to blank 1 M HCl solution. The decrease in corrosion current density and increased inhibition efficiency suggests the adsorption of grieseofulvin molecules on the mild steel surface at the metal/solution interface. Adsorption of inhibitor molecules mitigates the corrosion process by forming the protective layer on the mild steel surface where direct corrosive attack occurs.[14] From the results depicted in Table 1 it can be seen that presence of inhibitor did not causes any significant change in the value of corrosion potential (E_{corr}) suggesting that investigated inhibitor behaves as mixed type.

Electrochemical impedance spectroscopy (EIS)

EIS analysis is an important and complementary tool undertaken for the determination of corrosion rates. Nyquist and bode plots were represented in Figs. 3 and 4 with and without the inhibitor at temperature 298 K.It is concluded from Nyquist plots (Fig. 3) shows that the curves approximated by a single capacitive depressed semi-circles.

This displaying that the corrosion process in mild steel is controlled by charge transfer process.[15] Also, these impedance diagrams are not perfect, this features is related to inhomogeneity and frequency dispersion of metal as a result of surface roughness.[16] Fig. 5 represents the equivalent circuit model which is used to explain the impedance spectra for Nyquist plots in steel/acid solution interface.[17] In this equivalent circuit modal, R_{ct} is charge transfer resistance, R_s is the solution resistance and *CPE* is a constant phase element. A constant phase element (CPE) is used instead of double layer capacitance (C_{dl}) for the description of a frequency phase shift between an applied potential and its current response. The double layer capacitance was replaced by the constant phase element (CPE), in order to obtain the representative fit.

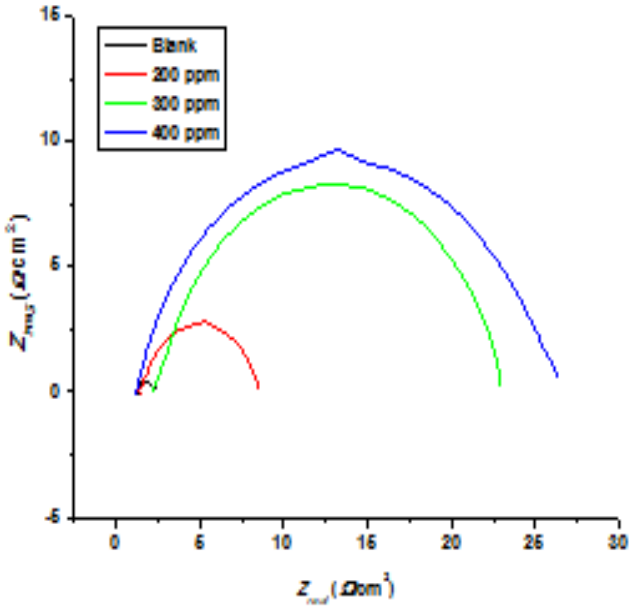

Figure 3. Nyquist plot for mild steel in 1 M HCl solution at different concentrations of inhibitor at 298 K.

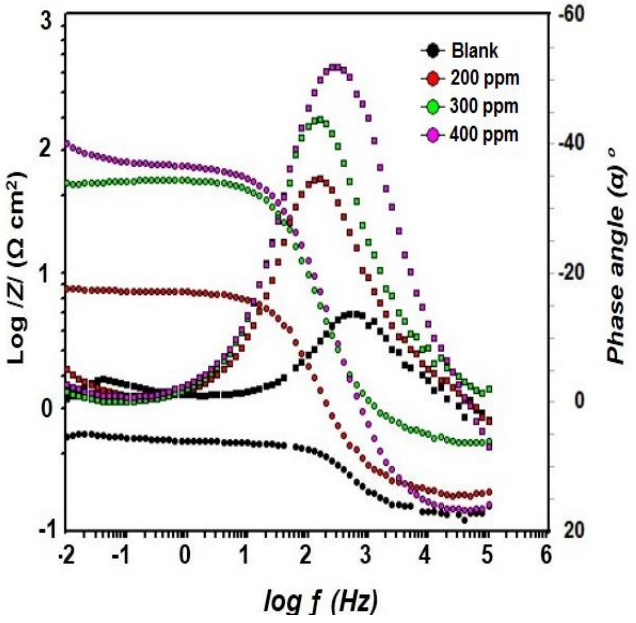

Figure 4. Bode plots of impedance spectra for mild steel in 1 M HCl solution with and without the inhibitor at 298 K.

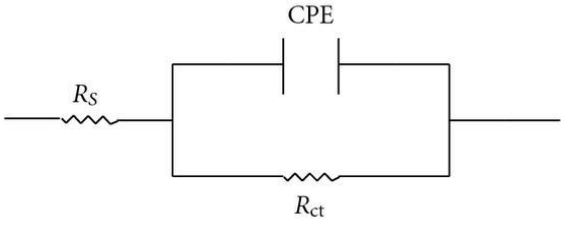

Figure 5. Equivalent circuit model used to fit the impedance spectra.

The double layer capacitance *(C_{dl})* is defined by the mathematical expression.[18]

$$C_{dl} = Y_0 (\omega_{max})^{n-1} \quad (4)$$

where

n is *CPE* exponent (phase shift),

Y_0 is *CPE* coefficient,

ω is the angular frequency and

ω_{max} shows the frequency at which the imaginary component reaches the maximum.

Value of *n* can be associated with non-uniform current distribution, a distribution of reaction rates and roughness of electrode surface etc.[19] Depending on the value of *n*, *CPE* can represent capacitance (n = 1, Y_0 =*C*), represent resistance (n=0, Y_0 = *R*), Warburg impedance (n = 0.5, Y_0 = W) or inductance (n=-1, Y_0=*L*). Various electrochemical impedance parameters such as CPE, R_{ct}, R_s, and *n* calculated using the nyquist plot. By using charge transfer resistance (R_{ct}) values the %η were calculated following the equation below.[20]

$$\%\,\eta = \frac{R_{ct(inh)} - R_{ct}}{R_{ct(inh)}} \text{x } 100 \quad (5)$$

where $R_{ct\,(inh)}$ and R_{ct} are the charge transfer resistances with and without inhibitor respectively. Corresponding values of EIS measurements shown in Table 2. It is clear from Table 2 that grieseofulvin exhibits the highest inhibition efficiency of 92.22 % at the 400 ppm concentration of inhibitor.

Weight loss measurements

Variouscorrosion parameters such as corrosion rate (ρ), inhibition efficiency (% *IE*) and surface coverage (θ) were determined from gravimetric analysis data for mild steel in 1 M HCl solution with and without inhibitor of different concentrations (100-400 ppm). For the mild steel, the mean value of corrosion rate (mg cm^{-2} h^{-1}) was determined for every concentration and inhibition efficiency was calculated using equations (1) and (2) respectively. Measurement performed in temperature ranging from 298-328 K after 6h of immersion period. The variation of corrosion rates and inhibition efficiency with temperature and inhibitor concentration for grieseofulvin is listed in Table 3. From Table 3 it is observed that grieseofulvin exhibits its higher inhibition efficiency (94.35 %) at optimum concentration (400 ppm) of inhibitor. Better inhibition efficiency at optimum concentration of grieseofulvin may be attributed to more coverage of mild steel by inhibitor molecules.[21] Based on the above result grieseofulvin can be considered as a good corrosion inhibitor for mild steel in 1 M HCl solution.

Adsorption and thermodynamic consideration

The efficiency of inhibitor molecules as corrosion inhibitor can be considered as the adsorption of these molecules on the mild steel surface through their hetero polar atoms viz. P, O, N and S.[22] The experimental data have been tested with several adsorption isotherms namely Langmuir, Frumkin and Temkin to obtain information regarding the type and mode of adsorption of grieseofulvin. In present study the Langmuir adsorption isotherm fitted well and the isotherm is expressed by the mathematical equation given below:[23]

$$\frac{C}{\theta} = \frac{1}{K_{ads}} + C \quad (6)$$

where

θ is the surface coverage,

C is the inhibitor concentration in electrolyte and

K_{ads} is equilibrium constant of the adsorption process which is related to the Gibbs energy of adsorption (ΔG_{ads})according to given equation. [23]

$$\Delta G_{ads} = -RT \ln (55.5\, K_{ads}) \quad (7)$$

Table 3. Various corrosion parameters obtained from weight loss measurements for mild steel in 1 M HCl with and without inhibitor at studied temperatures.

Temperature, *K*	Concentration, ppm	C_R, mgcm^{-2} h^{-1}	(η%)	ϑ
298	0.0	0.984	-	-
	100	0.146	85.16	0.851
	200	0.119	87.90	0.879
	300	0.097	90.14	0.901
	400	0.075	92.37	0.923
308	0.0	1.931	-	-
	100	0.183	90.52	0.905
	200	0.161	91.66	0.916
	300	0.147	92.38	0.923
	400	0.109	94.35	0.943
318	0.0	3.998	-	-
	100	0.689	82.76	0.827
	200	0.463	88.41	0.884
	300	0.409	89.76	0.897
	400	0.327	91.82	0.918
328	0.0	5.497	-	-
	100	1.189	78.37	0.783
	200	1.022	81.40	0.814
	300	0.810	85.26	0.852
	400	0.687	87.50	0.875

where

T is the thermodynamic temperature,

K is the binding constant and

R is gas constant.

Fig. 6 represents the relationship between C/θ and inhibitor concentration (C_{inh}) which represents typical Langmuir adsorption isotherm. A very good linear plot was observed with regression coefficient up to 0.999 and slope of unity. The value of K_{ads} value can be calculated from the intercept of straight line and average values of K_{ads}-21.67 kJ mol $^{-1}$was obtained and are given in Table 4. The higher negative values of ΔG_{ads} suggests the spontaneity of the stability of the adsorbed film and adsorption process on the mild steel surface, [24] as well as strong interaction.

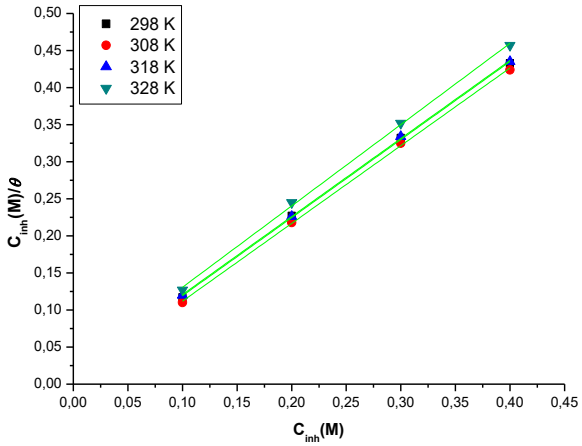

Figure 6. Langmuir adsorption linear fitting curves for mild steel in 1 M HCl at different temperatures and concentrations of inhibitor.

Effect of temperatures

Temperature has a great effect on the mild steel electrochemical corrosion rate in 1 M HCl. Many changes such as decomposition of the inhibitor, desorption of inhibitor and rapid etching may occur on the metal surface in different temperatures in the inhibitor solution. In case of metal corrosion in 1 M HCl solution, the rate of corrosion increases exponentially with temperature increases because the hydrogen evolution overpotential decreases.[25] Apparent activation energy (E_a), can be calculated from the values of corrosion rate obtained from weight loss measurement and applying the Arrhenius equation. [26]

$$C_R = A \exp\left(\frac{-E_a}{RT}\right) \quad (8)$$

where

C_R is the corrosion rate,

*E*a is the activation energy,

A is the frequency factor,

R is the gas constant (8.314 J K^{-1} mol $^{-1}$) and

T is the absolute temperature.

The slope of log ρ versus 1/*T* K^{-1} (K) plots for mild steel with and without inhibitor is presented in Fig. 7 and corresponding parameters were given in Table 5. Usually *E*a values with inhibitor (100-400 ppm) are higher than that of without inhibitor. These increased values of *E*a indicating a strong inhibitive action of grieseofulvin by increasing the energy barrier for the metal corrosion process.[27]

The enthalpy of activation (ΔH^*) and entropy of activation (ΔS^*) in 1 M HCl solution for the mild steel corrosion were obtained by applying the transition-state equation: [12]

$$C_R = \frac{RT}{Nh}\exp\left(\frac{\Delta S_a}{R}\right)\exp\left(-\frac{H_a}{RT}\right) \qquad (9)$$

where

ΔH^* is the enthalpy of activation,

ΔS^* is the entropy of activation,

ρ is the corrosion rate,

h is plank's constant (6.626176 x 10^{-34}),

R is gas constant and

N is the Avogadro's number.

Fig. 8 represents the linear plot of log ρ/T vs. $1/T$ K^{-1} gave an intercept of log (R/Nh) + (ΔS^* /2.303) and a straight line with a slope of ΔH^* /2.303R.The values of ΔH^* and ΔS^* were calculated and summarised in Table 5.

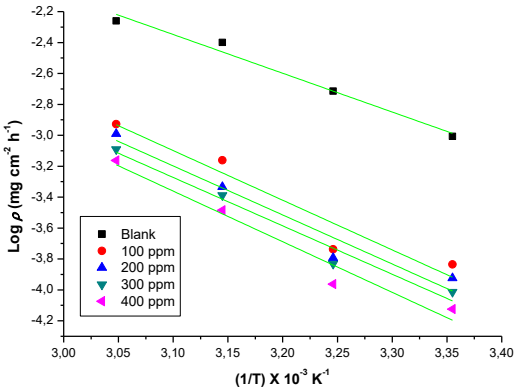

Figure 7. Arrhenius plots for the mild steel corrosion in 1 M hydrochloric solution in the presence and absence of inhibitor at studied temperatures.

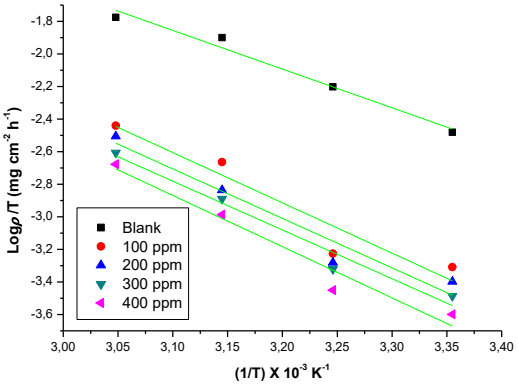

Figure 8. Transition state plots of Log $C_R(\rho)/T$ vs. $1/T$ in the presence and absence of inhibitor for mild steel corrosion in 1 M HCl solution.

The enthalpy of activation ΔH^* showed similar trend like the apparent activation energy values i.e. values increases as inhibitor concentration increases. The entropy of activation energy ΔS^* values is more negative in the absence of inhibitor than the presence of inhibitor, indicates the activated complex is more ordered in uninhibited solution. The less negative values of ΔS^* suggest the driving force for the adsorption process on metal/solution interface. [28]

Surface (SEM-EDX) analyses

The formation of protective layer by inhibitor and elements present on the mild steel surface were confirmed by SEM and EDX analysis. These analyses were performed before and after the exposure to the acidic solution in the absence and presence of inhibitor and represented in Figs. 9 and 10 respectively.

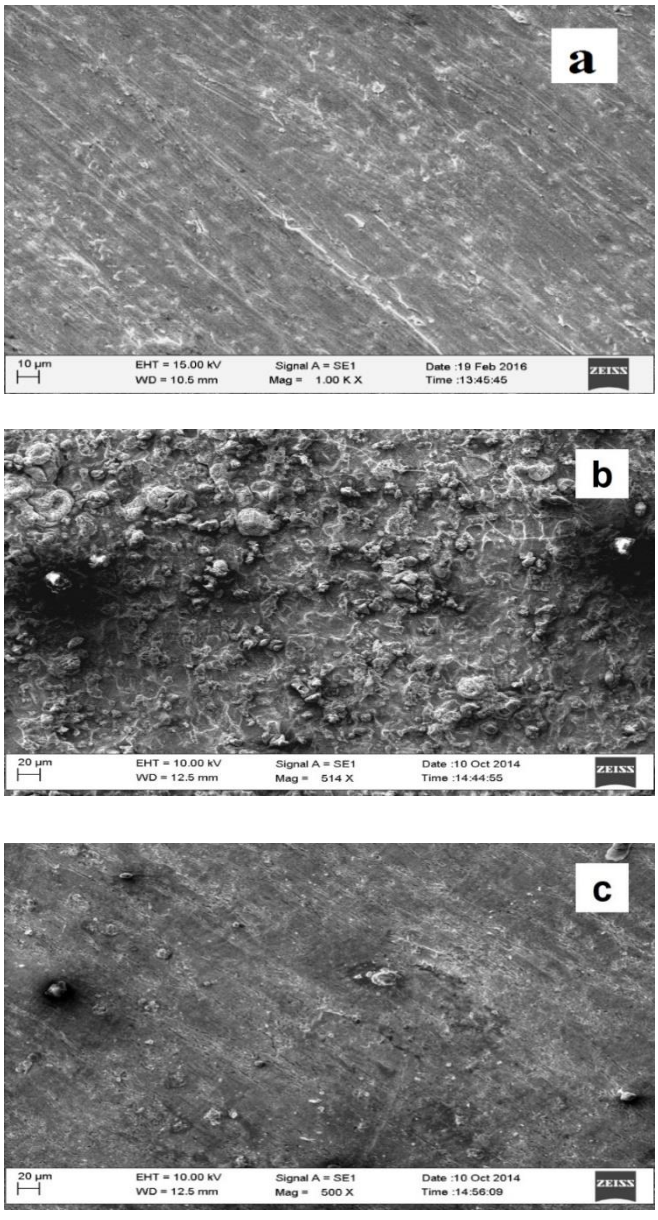

Figure 9. SEM microphotographs of the mild steel surface: (a) polished metal surface, (b) metal immersed in 1 M HCl solution without and (c) with the inhibitor.

Table 4. Langmuir parameters for the adsorption of grieseofulvin on the mild steel surface in 1 M HCl solution.

T (K)	R^2	Slope	K_{ads}, L mol $^{-1}$	ΔG_{ads}, kJ mol $^{-1}$
298	0.999	1.053	71.42	-20.52
308	0.999	1.049	142.8	-22.99
318	0.999	1.053	66.66	-21.72
328	0.998	1.097	47.61	-21.48

Table 5. Activation parameters mild steel dissolution in 1 M HCl with and without the inhibitor at studied temperatures.

Conc., ppm	*A*, mg cm^{-2} h^{-1}	*E*a, kJ mol^{-1}	ΔH^*, kJ mol^{-1}	ΔS^*, kJ mol^{-1}
0.0	2.65 x 10^5	48.00	45.45	-11.08
100	7.26 x 10^6	61.50	58.97	-07.72
200	4.30 x 10^6	60.71	58.14	-08.30
300	2.69 x 10^6	59.93	57.32	-08.79
400	6.15 x 10^6	62.68	60.19	-07.92

Table 6. Percentage elemental contents (wt %) recorded from EDX spectra of mild steel in the absence and presence (400 ppm) of grieseofulvin in 1 M HCl.

Medium	Composition (wt %)							
	Fe	C	O	P	S	Cr	Mn	Cl
Mild steel (MS)	98.24	0.213	0.106	0.048	0.512	0.481	0.392	-
MS in 1 M HCl	89.13	1.422	3.698	0.029	0.312	0.325	0.289	4.786
MS in grieseofulvin	93.55	2.159	2.361	0.025	0.119	0.311	0.254	1.211

Table 7. Quantum chemical parameters for the grieseofulvin

Inhibitor	E_{HOMO}, eV	E_{LUMO}, eV	ΔE,eV	μ,eV	Υ
Grieseofulvin	-0.0423	-0.0059	0.0364	3.2396	0.0182

Figure 9a represents the surface morphology of polished mild steel coupon exhibit smooth and homogeneous surface. Whereas Fig. 9b and 9c reveals the mild steel samples in the absence and presence of inhibitor respectively.

Specimen in the uninhibited solution is highly damaged due to direct acid attack (Fig. 9b) and mild steel surface is not as damaged as in the case of uninhibited acidic solution shown in Fig. 9c. This reveals the protective layer formation of inhibitor on mild steel surface thus protecting it from direct corrosive attack. [29]

EDX analysis was performed in order to get information regarding the elemental composition of mild steel surface in the presence and absence of grieseofulvin in 1 M HCl solution. The EDX spectra and corresponding values of elementals composition (wt%) shown in Fig. 10 and Table 6 respectively. The EDX data in Table 6 shows that the mild steel surface in the absence of inhibitor show a higher chloride content of due to corrosive attack of hydrochloric acid (Fig. 10b) whereas metal in inhibited solution shows the lower chloride content of (Fig. 10c). SEM-EDS analysis further conform the adsorption of grieseofulvin molecules on the mild steel surface and decrease the corrosion rate. [30].

Quantum chemical analysis

Quantum chemical calculations were performed in order to study the molecular structure of grieseofulvin on the inhibition efficiency by using density functional theory (DFT). Various electronic properties such as the energy of lowest unoccupied molecular orbital (ELUMO), energy of highest occupied molecular orbital (EHOMO), and energy gap (ΔE) between the LUMO and HOMO, global hardness (ϒ), softness (σ), and dipole moment (μ) were determined by optimizing the structure. The optimized structure, lowest unoccupied molecular orbital (LUMO) and highest occupied molecular orbital (HOMO)of grieseofulvin are shown in Fig.11 (a, b & c).

Corresponding values of parameters are given in Table 7. For the calculation of global hardness (ϒ) the equation used is given as: [31]

$$\Upsilon = \frac{E_{LUMO} - E_{HOMO}}{2} \qquad (10)$$

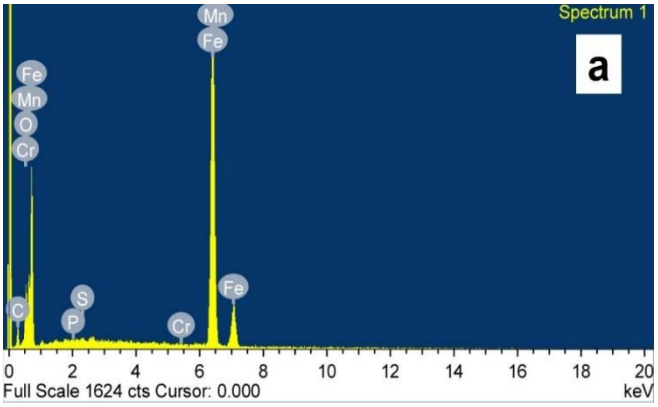

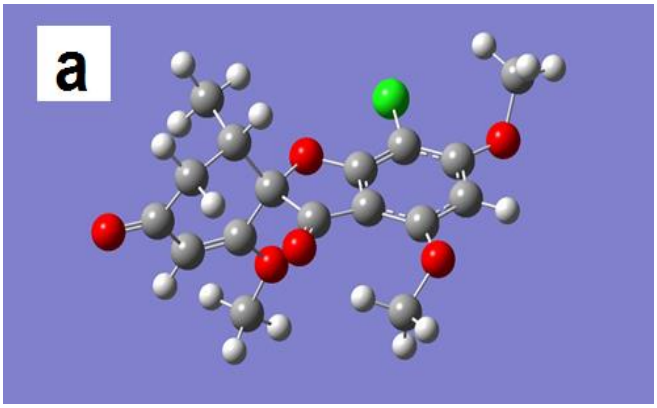

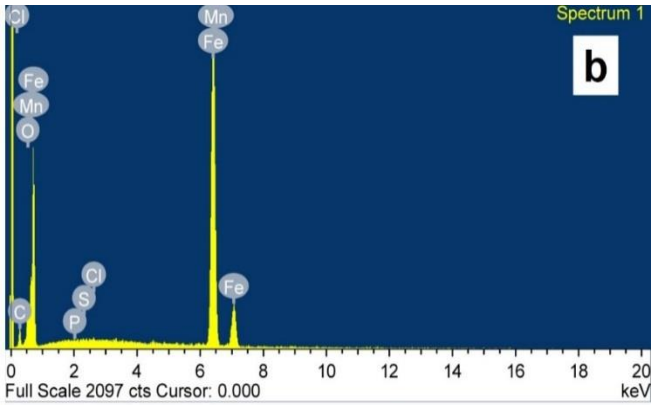

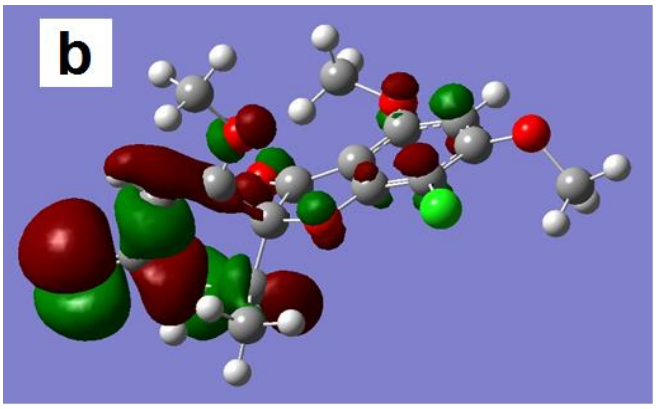

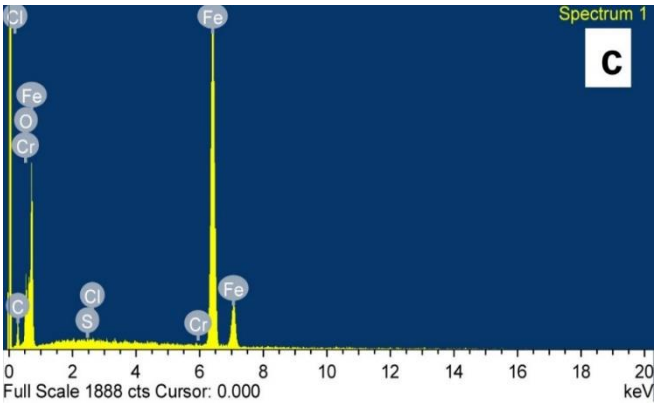

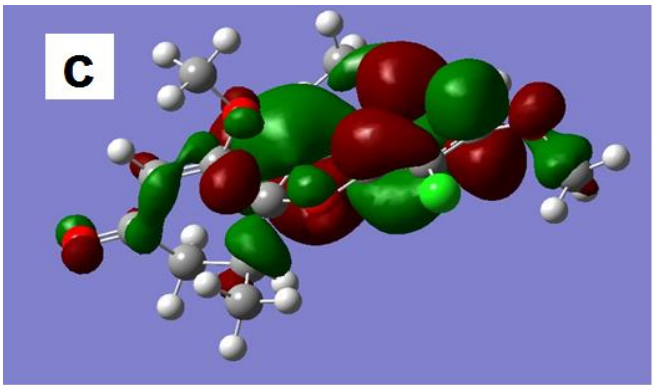

Figure 10. EDX spectra of (a) polished mild steel surface, (b) mild steel immersed in 1 M HCl and (c) mild steel in the inhibited solution.

Figure 11. (a) The optimized structure, (b) LUMO and (c) HOMO for the grieseofulvin.

The calculated frontier molecular orbital (FMO) properties for grieseofulvin is given in Table 7. Higher value of $E_{HOMO}$of molecule indicates the higher electron donating ability of inhibiting molecule to appropriate acceptor molecules. Consequently, an increased E_{HOMO}value reveal good adsorption ability of inhibitor on the metal surface. Lower E_{LUMO}value of molecule measures its greater ability to accept the electrons.[33]

Conclusion

Grieseofulvin exhibits good anticorrosive property towards the mild steel in 1 M HCl solution at studied temperatures (298-328K). Potentiodynamic polarization measurements reveals the mixed type inhibition property of grieseofulvin. Impedance analysis shows that grieseofulvin reducing the rate of charge transfer process by forming

protective layer on the mild steel surface. Weight loss measurements exhibits the increased inhibition efficiency (IE%) with increasing inhibitor concentration and the maximum IE% was found to be 94.35 at 400 ppm inhibitor concentration. The adsorption of the inhibitor obeys the Langmuir adsorption isotherm at studied temperatures. The values of free energy of adsorption shows that the spontaneous adsorption process of inhibitor on mild steel surface. SEM-EDX analysis also show that inhibitor molecules inhibits the mild steel corrosion by formation of protective layer on mild steel surface. The results of quantum chemical analysis revealed good correlation with the studied experimental results.

References

[1]Shukla, S. K., Quraishi, M. A., Ceftriaxone: a novel corrosion inhibitor for mild steel in hydrochloric acid, *J. Appl. Elecrochem*., **2009**, *39*, 1517-1523. https://doi.org/10.1007/s10800-009-9834-1

[2]Gobara, M., Baraka, A., Zaghloul, B., Inhibition of mild steel corrosion in sulphuric acid solution using collagen, *Res. Chem. Tntermed*., **2014**, doi: 10.1007/s11164-014-1809-0. https://doi.org/10.1007/s11164-014-1809-0

[3]Pavithra, M. K., Venkatesha, T. V., Kumar M. K. P., Manjunatha, K., Investigation of the inhibition effect of ibuprofen triazole against mild steel corrosion in an acidic environment, *Res. Chem. Intermed*., **2014**, https://doi.org/10.1007/s11164-014-1804-5.

[4]Saha, S.K., Dutta, A., Ghosh, P., Sukul, D., Banerjee, P., Adsorption and corrosion inhibition effect of Schiff base molecules on the mild steel surface in 1 M HCl medium: a combined experimental and theoretical approach, *Phys. Chem. Chem. Phys*., **2015,** *17*, 5679-5690. https://doi.org/10.1039/C4CP05614K, PMid:25623363

[5]Fiori-Bimbi, M. V., Alvarez, P. E., Vaca H., Gervasi, C. A., corrosion inhibition of mild steel in HCl solution by pectin, *Corros. Sci*., **2015**, *92*, 192-199. https://doi.org/10.1016/j.corsci.2014.12.002

[6]Singh, P., Singh, D. P., Tiwari, K., Mishra, M., Singh, A. K., V. P. Singh, Synthesis, structural investigation and corrosion inhibition studies on Mn(II), Co (II), Cu (II) and Zn (II) complex with 2-amino-benzoic acid (phenyl-pyridin-2-yl-methylene)-hydrazide, *RSC Adv*., **2015**, *5*, 45217-45230. https://doi.org/10.1039/C4RA11929K

[7]Bai, L., Feng, L., Wang. H. Y., Lu Y. B., Lei, X. W., Bai, F. L., comparison of the synergistic effect of counterions on the inhibition of mild steel corrosion in acid solution: electrochemical, gravimetric and thermodynamic studies, *RSC Adv*., **2015**, *5*, 4716-4726. https://doi.org/10.1016/j.electacta.2015.10.100

[8]Souza, F. S. D., Spinelli, A., Caffic acid as a green corrosion inhibitor for mild steel, *Corros. Sci*., **2009**, *51*, 642-649. https://doi.org/10.1016/j.corsci.2008.12.013

[9]Solmazm, R., Investigation of corrosion inhibition mechanism and stability of vitamin B1 on mild steel in 0.5 M HCl solution, *Corros. Sci*., **2014,***81*, 75-84. https://doi.org/10.1016/j.corsci.2013.12.006

[10]Abdallah, M., Antibacterial drugs as corrosion inhibitors for corrosion of aluminium in hydrochloric solution, *Corros. Sci*., **2004**, *46*, 1981-1996. https://doi.org/10.1016/j.corsci.2003.09.031

[11]Stuart, M. C., Kouimtzi, M., Hill, S. R., WHO model formulary, **2008**, p.no. 149.

[12]Verma, D. K., Khan, F., Corrosion inhibition of mild steel in hydrochloric acid using extract of glycine max leaves, *Res. Chem. Intermed*., **2016**, *42* ,3489–3506. https://doi.org/10.1007/s11164-015-2227-7

[13]Sudheer, Quraishi, M. A., The corrosion inhibition effect of aryl pyrazolo pyridines on copper in hydrochloric acid system: computational and electrochemical studies, *RSC Adv*., **2015**, *5*, 41923-41933. https://doi.org/10.1039/C5RA03966E

[14]Alkhathlan, H. Z., Khan, M., Abdullah, M. M. S., Aimayouf, A. M., Ahmed, A. Y. B. H., Alothman, Z. A., Mousa, A. A., Anticorrosive assay-guided isolation of active phytoconstituents from Anthemis pseudocotula extract and a detailed study of their effect on the corrosion of mild steel in acidic media, *RSC Adv*., **2015**, 5, 54283-54292. https://doi.org/10.1039/C5RA09154C

[15]Ostovari, A., Hoseinieh, S. M., Peikari, M., Shadizadeh, S. R., Hashemi, S. J., Corrosion inhibition of mild steel in 1 M HCl solution by henna extract: A comparative study of the inhibition by henna and its constituents (Lawsone, Gallic acid, a-D-Glucose and Tannic acid), *Corros. Sci*., **2009**, *51*, 1935–1949. https://doi.org/10.1016/j.corsci.2009.05.024

[16]Li, X. H., Deng, S., Fu, H., Inhibition by Jasminum nudiflorum Lindl. leaves extract of the corrosion of cold rolled steel in hydrochloric acid solution, *J. Appl. Electrochem*. **2010,** *40*, 1641–1649. https://doi.org/10.1007/s10800-010-0151-5

[17]Quraishi, M.A., Singh, A., Singh, V. K., Yadav, D. K., Singh, A. K., Green approach to corrosion inhibition of mild steel in hydrochloric acid and sulphuric acid solutions by the extract of Murraya koenigii leaves, *Mater. Chem. Phy*., **2010**, *122*, 114–122. http://dx.doi.org/10.1016/j.matchemphys.2010.02.066

[18]Shahi, G., Verma, C. B., Ebenso, E. E., Quraishi, M. A., Thermodynamic and Electrochemical investigation of (9-[(R) 2[[bis [[(isopropoxycarbonyl)oxy]methoxy] phosphinyl] methoxy] propyl] adenine fumarate) as Green Corrosion Inhibitor for Mild Steel in 1M HCl, *Int. J. Electrochem. Sci*., **2015**, *10*, 1102 – 1116.

[19]Soltani, N., Tavakkoli, N., Khayatkashani, M., Jalali, M. R., Mosavizade, A., Green approach to corrosion inhibition of 304 stainless steel in hydrochloric acid solution by the extract of Salvia officinalis leaves, *Corros. Sci*., **2012**, *62*, 122–135. https://doi.org/10.1016/j.corsci.2012.05.003

[20]Korde, R., Verma, C. B., Ebenso, E.E., Quraishi, M.A., Electrochemical and Thermo Dynamical Investigation of 5-ethyl 4-(4-methoxyphenyl)-6-methyl-2-thioxo-1, 2, 3, 4 tetrahydropyrimidine-5-carboxylate on Corrosion Inhibition Behavior of Aluminium in 1M Hydrochloric Acid Medium, *Int. J. Electrochem. Sci*., **2015**, *10*, 1081 – 1093.

[21]Singh, A. K., Khan, S., Singh, A., Quraishi, S. M., Quraishi, M. A., Ebenso, E. E., Inhibitive effect of chloroquine towards corrosion of mild steel in hydrochloric acid solution, *Res. Chem. Intermed*., **2013**, *39*, 1191–1208. https://doi.org/10.1007/s11164-012-0677-8

[22]Khadraoui, A., Khelifa, A., Hamitouche, H., Mehdaoui, R., Inhibitive effect by extract of Mentha rotundifolia leaves on the corrosion of steel in 1 M HCl solution, *Res. Chem. Intermed*., **2014**, *40*, 961–972. https://doi.org/10.1007/s11164-012-1014-y

[23]Verma, D. K., Khan, F., Green approach to corrosion inhibition of mild steel in hydrochloric acid medium using extract of spirogyra algae, *Green chem lett rev*, **2016**, *9(1)*, 52–60. https://doi.org/10.1080/17518253.2015.1137976

[24]Nazeer, A. A., Shalabi, K., Fouda, A. S., Corrosion inhibition of carbon steel by Roselle extract in

hydrochloric acid solution: electrochemical and surface study, *Res. Chem. Intermed*., **2014**, DOI 10.1007/s11164-014-1570-4. https://doi.org/10.1007/s11164-014-1570-4

[25]Hussin, M. H., Kassim, M. J., Inhibitive properties, thermodynamic and quantum chemical studies of alloxazine on mild steel corrosion in H2SO4, *Corros. Sci*., **2011**, *53*, 263–275. https://doi.org/10.1016/j.corsci.2010.09.020

[26]Obi-Egbedi, N.O., Obot, I.B., Inhibitive properties, thermodynamic and quantum chemical studies of alloxazine on mild steel corrosion in H2SO4, *Corros. Sci*., **2011**, *53*, 263–275.

[27]Noor, E. A., Al-Moubaraki, A. H., Thermodynamic study of metal corrosion and inhibitor adsorption processes in mild steel/1-methyl-4[4_(-X)-styryl pyridinium iodides/hydrochloric acid systems, *Mater. Chem. Phys*., **2008**, 110:145–154.

[28]Vishwakarma, S., Mourya, P., Chaubey, N., Kumar, S., Singh, V. K., Singh, M. M., Strychnos nuxvomica, Piper longum and Mucuna pruriens seed extracts as eco-friendly corrosion inhibitors for copper in nitric acid, *RSC Adv*., **2016**, https://doi.org/10.1039/C6RA16481A

[29]Ramaganthan, B., Gopiraman, M., Olasunkanmi, L. O., Kabanda, M. M., Yesudass, S., Bahadur, I., Adekunle, A. S., Obote, I. B., Ebenso, E. E., Synthesized photo-cross-linking chalcones as novel corrosion inhibitors for mild steel in acidic medium: experimental, quantum chemical and Monte Carlo simulation studies, *RSC Adv*., **2015**, *5*,76675-76688. https://doi.org/10.1039/C5RA12097G

[30]Tamilarasan, R., Sreekanth, A., Spectroscopic and DFT investigations on the corrosion inhibition behavior of tris(5-methyl-2-thioxo-1,3,4- thiadiazole)borate on high carbon steel and aluminium in HCl media, *RSC Adv*., **2013**, *3*, 23681-23691. https://doi.org/10.1039/c3ra43681k

[31]Yadav, M., Sinha, R. R., Kumar, S., Sarkar, T. K., Corrosion inhibition effect of spiropyrimidinethiones on mild steel in 15% HCl solution: insight from electrochemical and quantum studies, *RSC Adv*., **2015**, *5*, 70832-70848. https://doi.org/10.1039/C5RA14406J

[32]Gaussian 09, Revision A.02, M. J. Frisch, G. W. Trucks, H. B. Schlegel, G. E. Scuseria, M. A. Robb, J. R. Cheeseman, G. Scalmani, V. Barone, B. Mennucci, G. A. Petersson, H. Nakatsuji, M. Caricato, X. Li, H. P. Hratchian, A. F. Izmaylov, J. Bloino, G. Zheng, J. L. Sonnenberg, M. Hada, M. Ehara, K. Toyota, R. Fukuda, J. Hasegawa, M. Ishida, T. Nakajima, Y. Honda, O. Kitao, H. Nakai, T. Vreven, J. A. Montgomery, Jr., J. E. Peralta, F. Ogliaro, M. Bearpark, J. J. Heyd, E. Brothers, K. N. Kudin, V. N. Staroverov, R. Kobayashi, J. Normand, K. Raghavachari, A. Rendell, J. C. Burant, S. S. Iyengar, J. Tomasi, M. Cossi, N. Rega, J. M. Millam, M. Klene, J. E. Knox, J. B. Cross, V. Bakken, C. Adamo, J. Jaramillo, R. Gomperts, R. E. Stratmann, O. Yazyev, A. J. Austin, R. Cammi, C. Pomelli, J. W. Ochterski, R. L. Martin, K. Morokuma, V. G. Zakrzewski, G. A. Voth, P. Salvador, J. J. Dannenberg, S. Dapprich, A. D. Daniels, O. Farkas, J. B. Foresman, J. V. Ortiz, J. Cioslowski, and D. J. Fox, Gaussian, Inc., Wallingford CT, 2009.

[33]Soltani, N., Behpour, M., Oguzie, E. E., Mahluji, M.,Ghasemzadeh, M. A., Pyrimidine-2-thione derivatives as corrosion inhibitors for mild steel in acidic environments, *RSC Adv*., **2015**, *5*, 11145-11162. https://doi.org./10.1039/C4RA11642A

Received: 02.02.2017.
Accepted: 25.02.2017.

CRYSTAL STRUCTURE OF 1,8-BIS(4-FLUOROBENZOYL)NAPHTHALENE-2,7-DIYL DIBENZOATE: ROLE OF (SP^2)C–H…F HYDROGEN BONDING AS DISTINCTLY STRONG INTERACTION AMONG NON-CLASSICAL HYDROGEN BONDS CONTRIBUTING STABILITY OF THE CRYSTAL

Genta Takahara,[a] Rei Sakamoto, [a] Kazuki Ogata, [a] Shinji Ohisa, [a] Takahiro Mido, [a] Takeshi Yokoyama, [a] Noriyuki Yonezawa, [a] and Akiko Okamoto[a]*

Keywords: non-coplanarly accumulated aromatic rings; non-classical hydrogen bonds; C–H···F hydrogen bonds; C–H···O=C hydrogen bonds.

In crystal of 1,8-bis(4-fluorobenzoyl)naphthalene-2,7-diyl dibenzoate, $C_{38}H_{22}O_6F_2$, the phenyl rings of benzoyloxy groups and the naphthalene ring demonstrate largely disproportionate interplanar angles [38.97(7)° and 52.62(6)°] different from those between 4-fluorobenzoyl group and the naphthalene ring core [71.24(5)° and 78.85(6)°]. One of two benzoyloxy groups has three effective *intra*molecular interactions [(benzoyloxy)C–$H_{(o-)}$···O(benzoyloxy), (naphthalene)C–$H_{(6-)}$···O=C(benzoyloxy), and (benzoyloxy)C–$H_{(o-)}$···π(4-fluorobenzoyl) hydrogen bonds] and the other has no *intra*molecular interactions. In crystal, the molecules of identical enantiomeric isomer are unidirectionarly arranged along the *b* axis through (4-fluorobenzoyl)C–$H_{(m-)}$···O=C(4-fluorobenzoyl) hydrogen bonding interactions forming columnar structure. Moreover, a column is connected with the mirror imaged column composed of the opposite enantiomeric isomers into centrosymmetric dimer aggregates by three types of complementary interactions, *i.e.*, (benzoyloxy)C–$H_{(m-)}$···F, (4-fluorobenzoyl)C–$H_{(m-)}$···π(4-fluorobenzoyl), and (4-fluorobenzoyl)C–$H_{(m-)}$···π(benzoyloxy) hydrogen bondings. The tubular structures thus formed are stacked parallel to the *ac* plane *via* (benzoyloxy)C–$H_{(p-)}$…F, (benzoyloxy)C–$H_{(m-)}$…π(benzoyloxy), (naphthalene)C–$H_{(6-)}$…O=C(4-fluorobenzoyl), and (4-fluorobenzoyl)C–$H_{(o-)}$…O=C(benzoyloxy) hydrogen bonds. In homologous compound, a fluoro group-free derivative for title compound, the enantiomeric isomer and the opposite enantiomeric counterpart isomer are alternately arranged in a head-to-tail fashion through (benzoyl)C–$H_{(p-)}$…O=C(benzoyl) hydrogen bonds along *b*-axis. The zigzagged columns are aligned along *a*-axis with inversion center to form a sheet structure. However, there are no effective non-covalent bonding interactions between the zigzagged columns. In other words, the molecular packing structure of the homologous compound is governed by solely one strong (benzoyl)C–$H_{(p-)}$…O=C(benzoyl) hydrogen bonds, contrary to the organization of supramolecular architecture in title compound ascribed to cooperative unidirectional (4-fluorobenzoyl)C–$H_{(m-)}$…O=C(4-fluorobenzoyl) hydrogen bonds and bidirectional (benzoyloxy)C–$H_{(m-/p-)}$…F hydrogen bonds.

* Corresponding Authors
Fax: +81-42-388-7291
E-Mail: aokamoto@cc.tuat.ac.jp
[a] Department of Organic and Polymer Materials Chemistry, Tokyo University of Agriculture and Technology, 2-24-16 Naka-machi, Koganei, Tokyo 184–8588, Japan

Introduction

Supramolecular architecture[1-3] along with supramolecular chemistry[4-9] has become of interest in recent years from the viewpoint of green chemistry and novel phase of functional device material development. Various building blocks bearing unique functions might be tailored to supramolecular structure exhibiting desired chemical and physical properties without formation of covalent bonds. The research primarily relies on knowledge of the characteristics of non-covalent bonding interactions including atomic geometrical and molecular orientation features.[10-13] Attempts of formation of tough hydrogen bonds involving $CONR_2$ group and OH group, and COOH group and NH_2 group were undertaken both experimentally and theoretically.[14-16] These have been successfully employed for the preparation of numerous molecular assemblies. However, to grasp nature of weak hydrogen bonds including "non-classical" hydrogen bonds where C–H group acts as hydrogen donor, for example, has scarcely achieved probably because they are often hidden by strong hydrogen bonds. The authors have reported single molecular structure and the structural features of the molecular packing for roughly eighty compounds having 1,8-diaroylated naphthalene skeleton or the homologous/analogous structure *via* the Cambridge Structure Database (CSD).[17, 18] Molecular structures of 1,8-diaroylated 2,7-dialkoxynaphthalene compounds in crystals have common features that two aroyl groups are non-coplanarly located to the 2,7-dialkoxynaphthalene core and oriented in an opposite direction[19] with a few exceptional compounds bearing unidirectional-alignment of aroyl groups.[20-22] The molecular packing of 1,8-diaroylated 2,7-dialkoxynaphthalene compounds are mainly stabilized by weak hydrogen bonds. Four kinds of noncovalent-bonding interactions, (sp^2)C–H···O=C hydrogen bond, (sp^3)C–H···O hydrogen bond, C–H···π hydrogen-bonding interaction, and π···π stacking interaction are observed in decreasing order

of frequency. The features can be interpreted that the non-coplanarly accumulated aromatic rings structure disturbs formation of strong π…π stacking interactions. Therefore, the authors planned to elucidate systematically non-classical hydrogen bonds, weak hydrogen bonds between C–H group and electron rich atom/group, by the aid of structure analysis of 1,8-diaroylated naphthalene compounds. Herein, crystal structure of 1,8-bis(4-fluorobenzoyl)naphthalene-2,7-diyl dibenzoate[23] is demonstrated. The compound has characteristic molecular structure of four aromatic ring containing groups located at one long edge of naphthalene ring in serial order (1,2,7,8-positions) with other positions of another long edge free of substituent. The crystal structure is discussed from the standpoint of clarification of the correlation among single molecular structure, non-covalent bonding interactions, and molecular packing structure through comparison with the fluoro group-free homologous compound, 1,8-dibenzoylnaphthalene-2,7-diyl dibenzoate.[24]

Experimental

Materials and methods

All reagents were of commercial quality and were used as received. Solvents were dried and purified using standard procedures.[25] Synthetic methods and spectral data for the precursor, 2,7-diethoxy-1,8-bis(4-fluorobenzoyl)naphthalene, have been reported in literature.[26]

Measurements

^{1}H NMR spectra were recorded on a JEOL JNM-AL300 spectrometer (300 MHz) and a JEOL ECX400 spectrometer (400 MHz). Chemical shifts are expressed in ppm relative to internal standard of Me_4Si (δ 0.00). ^{13}C NMR spectra were recorded on a JEOL JNM-AL300 spectrometer (75 MHz) and a JEOL ECX400 spectrometer (100 MHz). Chemical shifts are expressed in ppm relative to internal standard of $CDCl_3$ (δ 77.0). IR spectra were recorded on a JASCO FT/IR-4100 spectrometer (KBr tablet). High-resolution FAB mass spectra were recorded on a JEOL MStation (MS700) ion trap mass spectrometer in positive ion mode.

X-ray crystallography

For the crystal structure determination, the single-crystal of title compound was used for data collection on a four-circle Rigaku RAXIS RAPID diffractometer (equipped with a two-dimensional area IP detector). The graphite-monochromated Cu Kα radiation (λ = 1.54187 Å) was used for data collection. The lattice parameters were determined by the least-squares methods on the basis of all reflections with F2>2σ (F2).

Crystal data, data collection and structure refinement details are summarized in Table 1. All H atoms could be located in difference Fourier maps, but were subsequently refined in optimized positions as riding atoms, with C–H = 0.95 (aromatic) and 0.98 (methyl) and with U_{iso}(H) = 1.2 U_{eq}(C). For data collection: *PROCESS-AUTO*[27]; cell refinement: *PROCESS-AUTO;*[27] data reduction: *CrystalStructure*,[28] program(s) used to solve structure: *SIR2004*,[29] program(s) used to refine structure: *SHELXL97*,[30] molecular graphics: *ORTEPIII*.[31] The hydrogen bond geometries of title compound are listed in Table 2.

Synthetic procedures

Synthesis of 1,8-bis(4-fluorobenzoyl)-2,7-dihydroxynaphthalene

To a 100 mL flask, 1,8-bis(4-fluorobenzoyl)-2,7-diethoxynaphthalene (5.0 mmol, 2.3 g) and toluene (40 mL) were placed and stirred at 90 °C. To the reaction mixture thus obtained, $AlCl_3$ (30.0 mmol, 3.9 g) was added. After the reaction mixture was stirred at 90 °C for 1 h, it was poured into 2*M* aqueous HCl and the mixture was extracted with $CHCl_3$. The combined extracts were washed with brine. The organic layers thus obtained were dried over anhydrous $MgSO_4$. The solvent was removed under reduced pressure to give cake. The crude product was purified by recrystallization from AcOEt (62 % isolated yield).

^{1}H NMR δ (400 MHz, DMSO-d_6) :7.02 (2H, d, J = 9.1 Hz), 7.18 (4H, t, J = 8.7 Hz), 7.59 (4H, t, J = 8.5, 5.5 Hz), 7.88 (2H, d, J = 9.1 Hz), 10.04 (2H, s) ppm; ^{13}C NMR δ (100 MHz, DMSO-d_6) : 114.87, 115.00 (d, $^2J_{C\text{-}F}$ = 22.0 Hz), 117.35, 123.21, 130.48, 131.62 (d, $^3J_{C\text{-}F}$ = 9.5 Hz), 131.99, 135.20 (d, $^4J_{C\text{-}F}$ = 2.8 Hz), 154.28, 164.62 (d, $^1J_{C\text{-}F}$ = 250.1 Hz) 195.41 ppm; IR (KBr) : 1642 (C=O), 1588, 1510, 1487 (Ar, naphthalene) cm^{-1}. HRMS (m/z): $[M+H]^+$ calcd for $C_{36}H_{23}F_2O_4$, 405.0938 found, 405.0986. m.p. = 298℃.

Synthesis of 1,8-bis(4-fluorobenzoyl)naphthalene-2,7-diyl dibenzoate

The title compound was prepared by reaction of 1,8-bis(4-fluorobenzoyl)-2,7-dihydroxynaphthalene (0.2 mmol, 80.9 mg) obtained via ethyl ether cleavage reaction of 1,8-bis(4-fluorobenzoyl)-2,7-diethoxynaphthalene, benzoyl chloride (0.4 mmol, 56.2 mg), and triethylamine (0.2 mmol, 20.2 mg) in dichloromethane (0.5 mL). After the reaction mixture was stirred at room temperature for 3 h, it was poured into water (30 mL) and the mixture was extracted with $CHCl_3$ (10 mL × 3). The combined extracts were washed with brine. The organic layers thus obtained were dried over anhydrous $MgSO_4$. The solvent was removed under reduced pressure to give the crude product followed by recrystallization purification from ethyl acetate–hexane affording colourless block single crystals suitable for X-ray diffraction measurement (isolated yield 72%).

^{1}H NMR δ (400 MHz, $CDCl_3$); 6.93 (4H, t, J = 8.8 Hz), 7.28 (4H, t, J = 8.0 Hz), 7.49 (2H, t, J = 7.6 Hz), 7.53 (2H, d, J = 9.2 Hz), 7.60 (4H, d, J = 7.2 Hz), 7.74 (4H, t, J = 7.2 Hz), 8.15 (2H, d, J = 8.8 Hz) ppm; ^{13}C NMR δ (75 MHz, $CDCl_3$); 115.48 (d, $^2J_{C—F}$ = 22.4 Hz), 122.36, 127.63, 128.17, 128.43, 129.93, 130.94, 131.97, 133.95, 134.81, 148.00, 164.05, 165.94 (d, $^1J_{C—F}$ = 255.0 Hz), 194.03 ppm; IR ν (KBr): 1743, 1670 (C=O), 1596, 1504, 1451 (Ar, naphthalene), 1255 (C—O—C) cm^{-1}; HRMS (m/z) : $[M+H]^+$ calcd for $C_{38}H_{22}O_6F_2$, 613.1463. found, 613.1447; m.p. = 186.1–186.7℃.

Table 1. Crystallographic data and structure refinement parameters of title compound.

Crystal data	
Chemical formula	$C_{38}H_{22}F_2O_6$
Mw.	612.58
Crystal system, space group	Monoclinic, P21/n
Temperature (K)	193
a, (Å)	16.1624 (3),
b (Å)	7.53034 (14),
c (Å)	24.3392 (5)
β (˚)	92.012 (1)
V (Å ^{3})	2960.47 (10)
Z	4
Radiation type	Cu *K*α
μ (mm^{-1})	0.85
Crystal size (mm)	0.60 × 0.10 × 0.10
Data collection	
Diffractometer	Rigaku R-AXIS RAPID
Absorption correction	Numerical (NUMABS; Higashi, 1999)
T_{min}, T_{max}	0.631, 0.920
No. of measured, independent and observed [$I > 2\sigma(I)$] reflections	37661, 5405, 4956
R_{int}	0.049
(sin θ/λ)max (Å $^{-1}$)	0.602
Refinement	
$R[F^2 > 2\sigma(F^2)]$, $wR(F^2)$, S	0.035, 0.094, 1.06
No. of reflections	5405
No. of parameters	416
H-atom treatment	H-atom parameters constrained
$\Delta\rho_{max}$,(eÅ^{-3})	0.25,
$\Delta\rho_{min}$ (eÅ $^{-3}$)	−0.15

Computer programs: *PROCESS-AUTO* (Rigaku, 1998), *PROCESS-AUTO* (Rigaku, 1998, *CrystalStructure* (Rigaku, 2007), *SIR2004* (Burla *et al.*, 2007), *SHELXL97* (Sheldrick, 2008), ORTEPIII (Burnett & Johnson, 1996).

Table 2. Hydrogen-bond geometry (Å, ˚)

D—H…*A*	*D*-H	H…*A*	D..A	*D*-H..*A*
C23—H23…O2^{i}	0.95	2.22	3.1552(15)	169
C34—H34…O4	0.95	2.36	2.6943(17)	100
C7—H7…O2^{ii}	0.95	2.46	3.3012(16)	147
C7—H7…O6	0.95	2.48	2.8739(16)	105
C28—H28…F2^{iii}	0.95	2.48	3.3026(16)	145
C24—H24…O6^{ii}	0.95	2.52	3.4514(16)	166
C29—H29…F2^{iv}	0.95	2.67	3.2914(17)	113
C14—H14…Cg1^{iii}	0.95	2.80	3.5679(16)	139
C35—H35…Cg2^{iv}	0.95	2.81	3.528(2)	133
C21—H21…Cg2^{iii}	0.95	2.86	3.7592(14)	157
C34—H34…Cg1	0.95	2.88	3.8050(16)	164

Symmetry codes: (i) x, y, z; (ii) 1/2-x, 1/2+y, 1/2-z; (iii) -x, -y, -z; (iv) 1/2+x, 1/2-y, 1/2+z. Cg1 and Cg2 are the centroids of the C19—C24 and C26—C31 rings, respectively.

Results and discussion

Single molecular structure of title compound is illustrated in Figure 1. The benzene rings of 4-fluorobenzoyl groups and those of benzoyloxy groups are situated out of the plane of the naphthalene ring core. The two benzene rings of 4-fluorobenzoyl groups at the 1,8-positions of the naphthalene ring are leant symmetrically, whereas the two benzene rings of the benzoyloxy groups at the 2,7-positions of the naphthalene ring are tilted unsymmetrically. The two interplanar angles between the benzene rings of the 4-fluorobenzoyl groups (C12—C17 and C19—C24) and the naphthalene ring system are 71.24 (5)° [C10—C1—C11—O1 torsion angle = 61.37 (17) °] and 78.85 (6)° [C10—C9—C18—O2 torsion angle = 71.43 (15) °], respectively. The interplanar angle between the two benzene rings of the 4-fluorobenzoyl groups is 45.02 (7)°. The two interplanar angles between the benzene rings of the benzoyloxy groups and the naphthalene ring are 38.97 (7)° and 52.62 (6)°, respectively. The benzene rings and the carbonyloxy moieties situate almost coplanarly [O6—C32—C33—C38 torsion angle = 0.0 (2)° and O5—C25—C26—C31 torsion angle = -5.5 (2)°]. One of two benzoyloxy groups forms three kinds of effective *intra*molecular hydrogen bonding interactions, (benzoyloxy)C–H$_{(o\text{-})}$···O (benzoyloxy)hydrogen bond (C34–H34···O4 = 2.36 Å), (naphthalene)C–H$_{(6\text{-})}$···O=C(benzoyloxy) hydrogen bond (C17–H17···O6 = 2.48 Å), and (benzoyloxy)C–H$_{(o\text{-})}$···π(4-fluorobenzoyl) hydrogen bond (C34–H34···Cg4 = 2.88 Å). Contrarily, the other benzoyloxy group has no *intra*molecular hydrogen bonds.

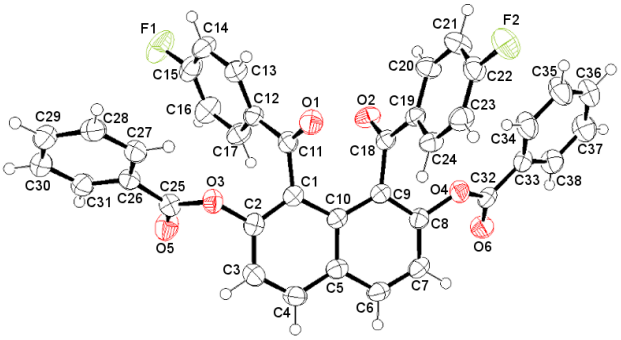

Figure 1. Molecular structure of 1,8-bis(4-fluorobenzoyl)-naphthalene-2,7-diyl dibenzoate, with the atom-labeling scheme and displacement ellipsoids drawn at the 50% probability level.

Observed non-covalent bonding interactions are listed in the order of distance in Table 2. In the molecular packing, (4-fluorobenzoyl)C–H$_{(m\text{-})}$···O=C(4-fluorobenzoyl) hydrogen bonds link the molecules unidirectionarly along the *b* axis forming a column structure (Figure 2).

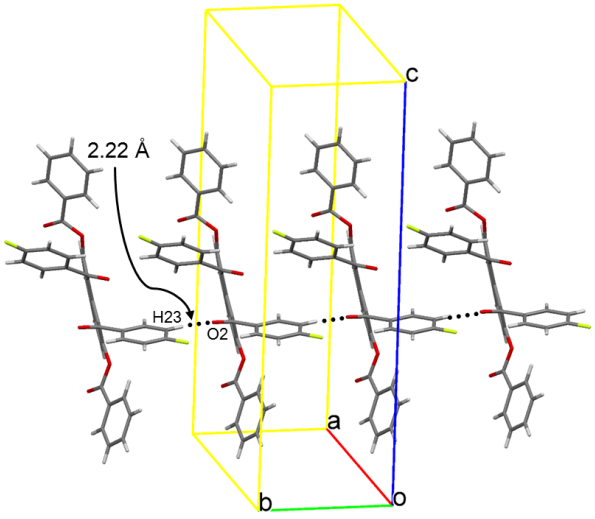

Figure 2. (4-Fluorobenzoyl)C—H$_{(m\text{-})}$···O=C(4-fluorobenzoyl) hydrogen bonds link the molecules unidirectionarly along the *b* axis is shown as black broken lines. [Symmetry codes: (i) x, y, z.]

The columns are connected by three types of complementary intermolecular interactions between 4-fluorobenzoyl groups and between 4-fluorobenzoyl group and benzoyloxy group forming face-to-face type dimeric aggregates, *i.e.*, (benzoyloxy)C–$H_{(m-)}$···F hydrogen bonds (2.48 Å), (4-fluorobenzoyl)C–$H_{(m-)}$···π(4-fluorobenzoyl) hydrogen bonds (2.80 Å), and (4-fluorobenzoyl)C–$H_{(m-)}$···π(benzoyloxy) hydrogen bonds (2.86 Å) (Figure 3).

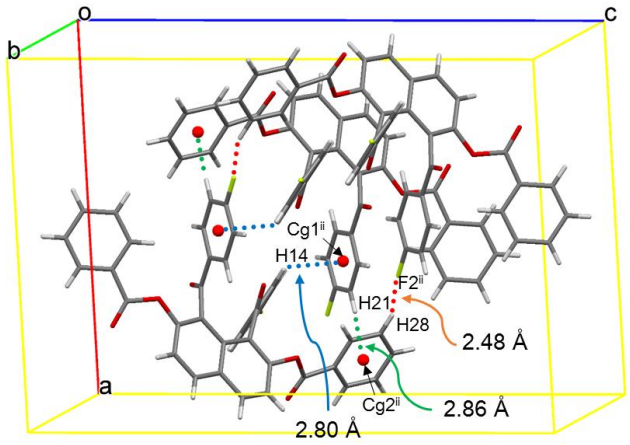

Figure 3. The columns are connected by three types of complementary intermolecular interactions. [Symmetry code: (iii) -x, -y, -z.]

The tubular structures thus formed are connected to each other through four kinds of hydrogen bonds. In this aggregation, disproportional contribution of two benzoyloxy groups is also observed. That is, three of four kinds of hydrogen bonds (benzoyloxy)C–$H_{(p-)}$…F hydrogen bonds (2.67 Å), (benzoyloxy)C–$H_{(m-)}$…π(benzoyloxy) hydrogen bonds (2.81 Å), and (4-fluorobenzoyl)C–$H_{(o-)}$…O=C(benzoyloxy) hydrogen bonds (2.52 Å)] are concerned with just the benzoyloxy group that makes three *intra*molecular hydrogen bonds described above and the remaining hydrogen bond is (naphthalene)C–$H_{(6-)}$…O=C(4-fluorobenzoyl) hydrogen bonds (2.46 Å) located between the 4-fluorobenzoyl group, which also acts a role of *intra*molecular hydrogen bond acceptors, and the naphthalene ring (Figure 4).

The authors' group has reported crystal structure of homologous compound, 1,8-dibenzoylnaphthalene-2,7-diyl dibenzoate.[24] The molecular structure of the homologous compound corresponds to fluoro group-free derivative for the title compound. Single molecular structure of the homologue is shown in Figure 5. Four benzene rings are situated out of the plane of the naphthalene ring core as well as title compound. However, correlation between kinds of benzene rings and the symmetric nature is inverse to title compound, *i.e.*, the two benzene rings of the benzoyloxy groups at 2,7-positions of the naphthalene ring are tilted symmetrically, whereas the two benzene rings of benzoyl groups at 1,8-positions of the naphthalene ring lean unsymmetrically. The interplanar angles between the benzene rings of benzoyl groups and the naphthalene ring system are 67.12 (5)° and 85.15 (5)°, respectively. The two interplanar angles between the best planes of the benzoyloxy groups and the naphthalene ring are 71.47 (5)° and 76.41 (5)°, respectively. The interplanar angle between the two benzene rings of the benzoyl groups is 59.81 (6)°. Furthermore, the homologous molecule has no *intra*molecular hydrogen bondings differently from the title compound. In the crystal packing, (benzoyl)C–$H_{(p-)}$…O=C(benzoyl) hydrogen bonds (2.41 Å) and two types of (benzoyloxy)C–$H_{(m-/o-)}$…π(naphthalene) hydrogen bonds (2.65 Å and 2.96 Å) link the homologous molecules in face-to-back fashion forming a zigzagged column structure along *b*-axis (Figure 6). The zigzagged columns are aligned with inversion center into a sheet structure along *a*-axis. However, there are no effective non-covalent bonding interactions between the zigzagged columns. (benzoyl)C–$H_{(p-)}$…π(benzoyl) Hydrogen bonds are also observed along *c*-axis (2.94 Å) (Figure 7).

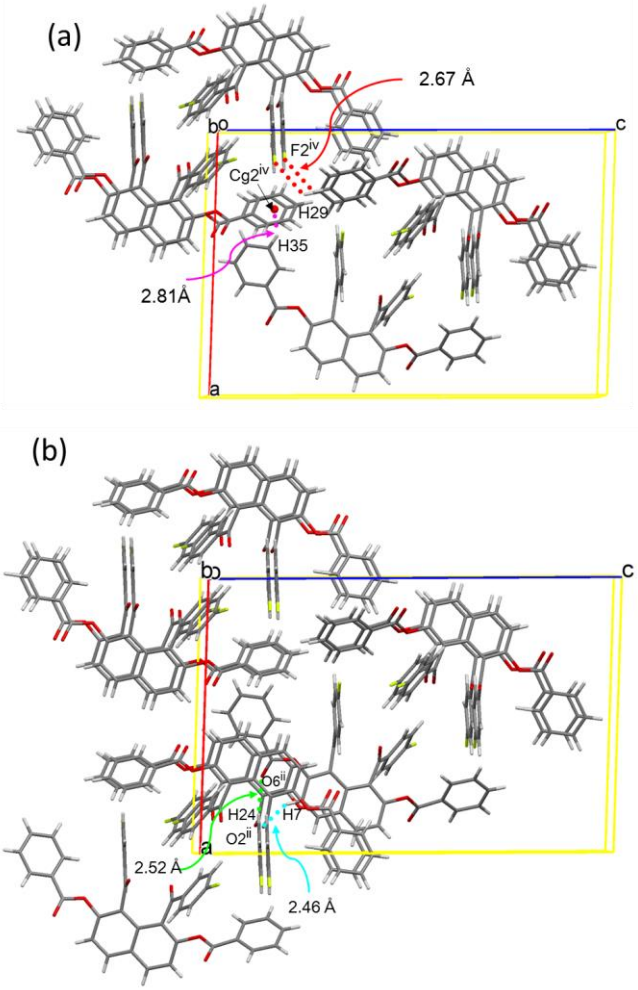

Figure 4. The tubular structures are connected to each other through four kinds of hydrogen bonds. (a) (benzoyloxy)C–$H_{(p-)}$…F hydrogen bonds and (benzoyloxy)C–$H_{(m-)}$…π(benzoyloxy) hydrogen bonds; (b) (4-fluorobenzoyl)C–$H_{(o-)}$…O=C(benzoyloxy) hydrogen bonds and (naphthalene)C–$H_{(6-)}$…O=C(4-fluorobenzoyl) hydrogen bonds. [Symmetry codes: (ii) 1/2-x, 1/2+y, 1/2-z, (iv) 1/2+x, 1/2-y, 1/2+z.]

In the crystal packings of title compound and the homologous compound, the molecules exhibit axial chirality, with either *R,R*- or *S,S*- stereogenic axis.

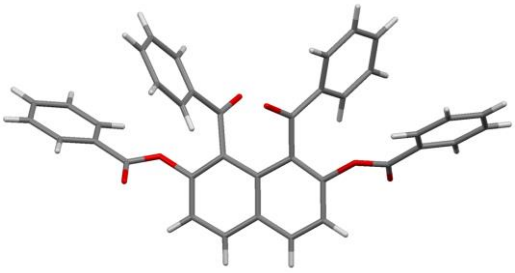

Figure 5. Single molecular structure of homologous compound.

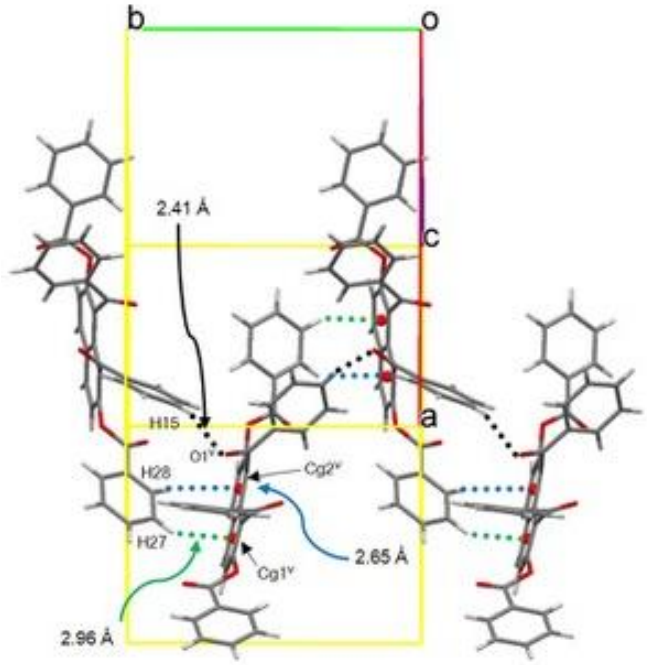

Figure 6. (benzoyl)C–H$_{(p\text{-})}$…O=C(benzoyl) hydrogen bonds and two types of (benzoyloxy)C–H$_{(m\text{-/}o\text{-})}$…π(naphthalene) hydrogen bonds link the homologous molecules into zigzagged column structure along *b*-axis. [Symmetry codes: (v) 1/2-x, -1/2+y, z.]

Table 3 summarizes correlation between absolute configuration of molecule and non-covalent bonding hydrogen bonds in title compound and the homologous compound. As a common feature about non-covalent bonding interactions, both of title compound and the homologous one have (aroyl)C–H$_{(p\text{- or }m\text{-})}$…O=C(aroyl) hydrogen bonds. However, they are observed between *R,R*- and *S,S*-enantiomeric isomers in the molecules of the homologous compound (2.41 Å), whereas those interactions are found between identically enantiomeric isomers in title compound (2.22 Å). In the homologous compound, two kinds of (benzoyloxy)C–H$_{(m\text{-/}o\text{-})}$…π hydrogen bonds are also formed effectively between opposite enantiomeric isomers (2.65 Å and 2.96 Å). In title compound, (4-fluorobenzoyl/benzoyloxy)C–H$_{(m\text{-})}$…π hydrogen bonds are observed between opposite enantiomeric isomers as well as homologous compound (2.80 Å, 2.81 Å, and 2.86 Å). Non-classical hydrogen bonds involving fluoro groups link opposite enantiomeric isomers (2.48 Å and 2.67 Å). These observation can be explained as follows: (aroyl)C–H$_{(m\text{- or }p\text{-})}$…O=C(aroyl) hydrogen bonds potentially connect either of opposite enantiomeric isomers or identical enantiomers.

However, the role of (aroyl)C–H$_{(p\text{-})}$…O=C(aroyl) hydrogen bonds in the homologous compound for connection of identical enantiomers is severely hidden.

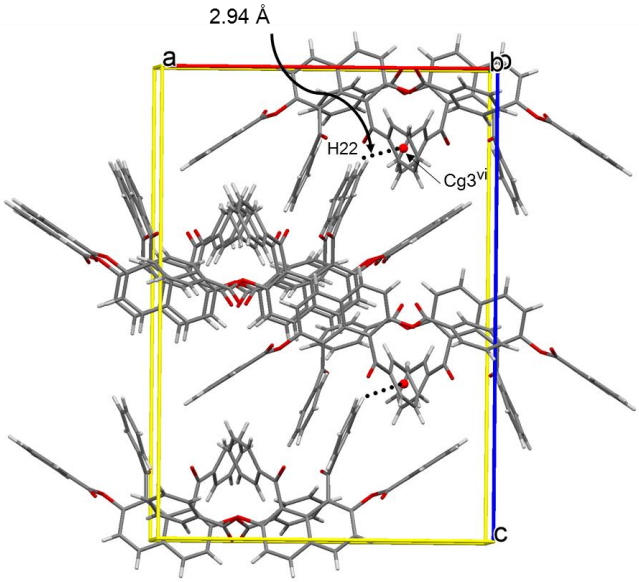

Figure 7. (benzoyl)C–H$_{(p\text{-})}$…π(benzoyl) Hydrogen bonds are also observed along *c*-axis. [Symmetry codes: (vi) -x, 1/2+y, 1/2-z.]

Table 3. Non-covalent bonding interactions in title compound and the homologous compound (Å).

	Title compound	**Homologue**
***intra*molecular hydrogen bondings**		
C34—H34…O4	2.36	
C7—H7…O6	2.48	
C34—H34…Cg1	2.88	
intermolecular hydrogen bondings		
(4-fluorobenzoyl)C23—H23…O2(4-fluorobenzoyl)	2.22^{i}	
(benzoyl)C15—H15…O1(benzoyl)		2.41^{v}
(naphthalene)C7—H7…O2(benzoyloxy)	2.46^{ii}	
(benzoyloxy)C28—H28…F2	2.48^{iii}	
(4-fluorobenzoyl)C24—H24…O6(benzoyloxy)	2.52^{ii}	
(benzoyloxy)C28—H28…Cg2(naphthalene)		2.65^{v}
(benzoyloxy)C29—H29…F2	2.67^{iv}	
(4-fluorobenzoyl)C14—H14…Cg1(4-fluorobenzoyl)	2.80^{iii}	
(benzoyloxy)C35—H35…Cg2(benzoyloxy)	2.81^{iv}	
(4-fluorobenzoyl)C21—H21…Cg2(benzoyloxy)	2.86^{iii}	
(benzoyl)C22—H22…Cg3(benzoyl)		2.94^{vi}
(benzoyloxy)C27—H27…Cg1(naphthalene)		2.96^{v}

Symmetry codes: (i) x, y, z; (ii)1/2-x, 1/2+y, 1/2-z; (iii) -x, -y, -z; (iv) 1/2+x, 1/2-y, 1/2+z; (v) 1/2-x, -1/2+y, z; (vi) -x, 1/2+y, 1/2-z.

Red characters = non-covalent bonding distances between same enantiomeric molecules; blue characters = non-covalent bonding distances between opposite enantiomeric molecules.

By formation of fluoro group concerning hydrogen bonds, (aroyl)C–$H_{(m-)}$…O=C(aroyl) hydrogen bonds cannot play the role for linking opposite enantiomeric isomers, *viz.*, (aroyl)C–$H_{(m-)}$…O=C(aroyl) hydrogen bonds can connect solely identically enantiomeric molecules. This can be restated that (aroyl)C–$H_{(m-)}$…O=C(aroyl) non-classical hydrogen bonds between identical enatiomers and (benzoyloxy)C–$H_{(m-/p-)}$…F non-classical hydrogen bonds between opposite enantiomeric isomers work cooperatively to organization of supramolecular structure.

Conclusively, crystal structure of 1,8-bis(4-fluorobenzoyl)naphthalene-2,7-diyl dibenzoate was determined and the structural features of single molecule and molecular aggregation are discussed by comparison with the fluoro group-free homologue.

Generally, C_2 symmetrical molecules in crystal are considered to be best stabilized by formation of pairs of identical effective intermolecular interactions on condition that satisfactory room is present for conformation perturbation free from specific regulations. To realize such crystalline structure, the molecules in crystal should take either complimentary face-to-face interactions or unidirectional stacking by a face-to-back mode. Presumably, the mode of face-to-face or face-to-back is determined according to the stabilization energy afforded in respective aggregation modes. As the interactions that perform the largest stabilization energy are considered to be aligned with a higher symmetric feature, the nearly identical spatial structure should be constructed as face-to-face mode for dimer formation or face-to-back mode for unidirectional alignment. The secondly or less effective interactions should be arranged to obtain totally the largest stabilization energy.

In title compound, the strong (benzoyloxy)C–$H_{(m-/p-)}$…F non-classical hydrogen-bonding interaction between opposite enantiomers is considered to predominate possible interactions between identical enantiomers. This brings about the restriction of the formation of comparatively effective non-covalent bonding interactions at the backside position of the molecules. For the compensation of rather poor effect of intermolecular interaction stabilization, the larger *intra*molecular stabilization is achieved along with reinforcement of the disproportionation of molecular spatial organization. Furthermore, the stabilization should be best achieved when strongest interactions functions complementally, *i.e.*, these interactions require a highly symmetric spatial arrangement. To consistent rather contracted molecular structural requisites, one pair of the aroyl groups showing stronger intermolecular interaction take the positions in a highly symmetrical manner and the other pairs of aroyl groups arrange themselves dissymmetrically to attain the largest intramolecular stabilization. In this consequence, the characteristic disproportionation of spatial organization bearing highly symmetric alignment part for such molecule of symmetric molecular structure is generated. Under such characteristic structural regulation, the spatial organization of molecules should be performed to maximize the total stabilization by various weak interaction.

On the other hand, absence of superior intermolecular interaction in the crystal of the homologous compound presumably performs the largest stabilization when largest number of moderate and weak non-covalent bonding interactions among neighbouring molecules contributes effectively. To realize such spatial circumstance, disproportion of single molecular spatial alignment should affect unfavourably. Then, the accumulation of molecules with rather isotropic spatial alignment is advantageous.

On the basis of above interpretation, presence or absence of (benzoyloxy)C–$H_{(m-/p-)}$…F non-classical hydrogen bond is strongly suggested to determine both the molecular proportional properties and stabilization fashion between enantiomeric isomers or between identically configurated molecules of apparently C_2 symmetrical molecules in crystal.

Acknowledgements

The authors would express their gratitude to Professor Keiichi Noguchi, Instrumentation Analysis Center, Tokyo University of Agriculture and Technology, for his technical advice. This work was partially supported by the Ogasawara Foundation for the Promotion of Science & Engineering, Tokyo, Japan.

References

[1]Janczak, J. *Cryst. Growth Des.*, **2015**, *15*(10), 5097. https://doi.org/10.1021/acs.cgd.5b01049

[2]Macháček, V., Bertolasi, V., Šimůnek, P., Svobodová, M., Svoboda, J. and černošková, E. *Cryst. Growth Des.*, **2010**, *10*(1), 85. https://doi.org/10.1021/cg900295n

[3]Shimpi, M. R., SeethaLekshmi, N.and Pedireddi, V. R. *Cryst. Growth Des.*, **2007**, *7*(10), 1958. https://doi.org/10.1021/cg060863p

[4]Lehn, J.-M. *Supramolecular Chemistry*: *Concepts and Perspectives*; VCH: New York, 1995. https://doi.org/10.1002/3527607439

[5]Atwood, J. L., Davies, J. E. D., MacNicol, D. D. and Vogtle, F., *In Comprehensive Supramolecular Chemistry*; Pergamon, Oxford, UK, 1996; Vols. 1-11.

[6]Jeffrey, G. A. and Saenger, W. *Hydrogen Bonding in Biological Structures*; Springer: Berlin, 1991. https://doi.org/10.1007/978-3-642-85135-3

[7]Desiraju, G. R. *Crystal Engineering*: *The Design of Organic Solids*; Elsevier: Amsterdam, 1989.

[8]MacDonald, J. C.; Whitesides, G. M. *Chem. Rev.* **1994**, *94*, 2383-2420. https://doi.org/10.1021/cr00032a007

[9]Desiraju, G. R., Vittal, J. J. and Ramanan, A. *Crystal Engineering. A Textbook*, World Scientific Publishing, Singapore, **2011**. https://doi.org/10.1142/8060

[10]Steiner, T. and Desiraju, G. R. *Chem. Commun.*, **1998**, 891−892. https://doi.org/10.1039/a708099i

[11]Desiraju, G. R. *Acc. Chem. Res.* **2002**, *35*, 565−573. https://doi.org/10.1021/ar010054t

[12]Bernstein, J., Davis, R. E., Shimoni, L. and Chang, N.-L. *Angew. Chem., Int. Ed.* **1995**, *34*, 1555-1573. https://doi.org/10.1002/anie.199515551

[13]Biradha, K. and Mahata, G. *Cryst. Growth Des.*, **2005**, *5*, 61-63. https://doi.org/10.1021/cg049761u

[14]Price, S. L. *CrystEngComm* **2004**, *6*, 344-353. https://doi.org/10.1039/b406598k

[15]Hubbard, T. A., Brown, A. J., Bell, I. A. W. and Cockroft, S. L. *J. Am. Chem. Soc.*, **2016**, *138*, 15114. https://doi.org/10.1021/jacs.6b09130

[16]Tanabe, J., Taura, D., Yamada, H., Furusho, Y. and Yashima, E. *Chem. Sci.*, **2013**, *4*, 2960. https://doi.org/10.1039/c3sc50833a

[17]Narushima, S., Mohri, S., Yonezawa, N. and Okamoto, A. *Acta Cryst.*, **2014**, E70, 170. doi: 10.1107/S1600536814019758

[18]Siqingaowa, Tsumuki, T., Ogata, K., Yonezawa, N. and Okamoto, A. *Acta Cryst.* **2016**, *E72*, 1819. *Acta Cryst.* (2016). E**72**, 1819-1823 https://doi.org/10.1107/S2056989016018077

[19]Okamoto, A. and Yonezawa, N. *J. Synth. Org. Chem. Jpn.* **2015**, *73(4)*, 339. https://doi.org/10.5059/yukigoseikyokaishi.73.339

[20]Hijikata, D., Takada, T., Nagasawa, A., Okamoto, A. and Yonezawa, N., *Acta Cryst.,* **2010**, *E66*, o2902–o2903. doi: 10.1107/S1600536810042170

[21]Mitsui, R., Nagasawa, A., Noguchi, K., Okamoto, A. and Yonezawa, N., *Acta Cryst.,* **2010**, *E66*, o1790. *Acta Cryst.* (2010). E**66**, o1790 doi: 10.1107/S1600536810024074

[22]Sasagawa, K., Takeuchi, R., Kusakabe, T., Yonezawa, N. and Okamoto, A. *Acta Cryst.,* **2013**, *E69*, o444. doi: 10.1107/S1600536813004959

[23]CCDC-1526510 contains the supplementary crystallographic data for this paper. These data can be obtained free of charge from The Cambridge Crystallographic Data Centre via www.ccdc.cam.ac.uk/data_request/cif

[24]Sakamoto, R., Sasagawa, K., Hijikata, D., Okamoto, A. and Yonezawa, N. *Acta Cryst.*, **2012**, *E68*, o2454. doi: 10.1107/S1600536812030991

[25]Armarego, W. L. F.; Chai, C. L. L. *Purification of Laboratory Chemicals, Seventh edition*, **2013**, Elsevier Inc., Oxford.

[26]Mouri, S., Hijikata, D., Isozaki, K., Yonezawa, N., Okamoto, A., *Acta Cryst.,* **2013**, *E69*, o637. doi:10.1107/S1600536813008295

[27]Rigaku (1998). *PROCESS-AUTO*. Rigaku Corporation, Tokyo, Japan.

[28]Rigaku (2010). *CrystalStructure.* Rigaku Corporation, Tokyo, Japan.

[29]Burla, M. C., Caliandro, R., Camalli, M., Carrozzini, B., Cascarano, G. L., De Caro, L., Giacovazzo, C., Polidori, G., Siliqi, D. and Spagna, R. *J. Appl. Cryst.* **2007**, *40*, 609–613. https://doi.org/10.1107/S0021889807010941

[30]Sheldrick, G. M. *Acta Cryst.* **2008**, *A64*, 112–122. https://doi.org/10.1107/S0108767307043930

[31]Burnett, M. N. and Johnson, C. K. (1996). ORTEPIII. Report ORNL-6895. Oak Ridge National Laboratory, Tennessee, USA.

Received: 21.01.2017.
Accepted: 25.02.2017.

GRADIENT AND LAYERED BORON NITRIDE FORMATION UNDER EFFECT OF CONCENTRATED LIGHT IN A FLOW OF NITROGEN

L. L. Sartinska,[a]* A.M.Kasumov,[a] I. I. Timofeeva,[a] A. Yu. Koval',[a] E. V. Voynich,[a] O. Kutsay,[b] C. Jastrebski,[c] N. Maisuradze,[d] N. C. Danilenko[a] and G. A. Frolov[a]

Keywords: Light heating, powder, Boron, Boron nitride, gradient and layered nanostructures.

Results of the effect of concentrated light energy in a xenon high-flux optical furnace on transformation of boron nitride (BN) and boron (B) powders in a flow of nitrogen are presented. Raman, Auger Electron (AES), Fourier transform infrared spectroscopy (FTIR), X-ray diffraction (XRD), scanning and transmission electron microscopes (SEM and TEM), and the measurement of band gap using transmittance technique have been employed for investigation of the properties of produced nanostructures. According Raman, AES and FTIR study the surface of all prepared nano powders is composed of BN. XRD disclosed pure amorphous boron inside particle. Gradient transformation pure boron to BN in the framework of one particle as well as layered nanostructure was observed by TEM study. Dependence of a square of the optical absorption coefficient for a deposited BN film versus the photon energy of incident light has confirmed a gradient and layered nature of the prepared BN nanostructures.

* Corresponding Author
Fax: +380 (0) 44-4242131
E-Mail: sart@ipms.kiev.ua
[a]Frantsevich Institute for Problems of Materials Science of NAS of Ukraine, 3 Krzhyzhanovsky Str., Kiev-142, 03680 Ukraine.
[b]V.Bakul Institute for Superhard materials NASU of Ukraine, 2, Avtozavods'ka Str., Kiev, 04074, Ukraine.
[c] CEPHOMA Centre at Faculty of Physics Warsaw University of TechnologyKoszykowa 75, 00-662 Warszawa, Poland.
[d]Department of Engineering Physics, Georgian Technical University, 77 Kostava Ave., Tbilisi, 0175, Georgia.

Introduction

Boron nitride (BN) is a structural equivalent to carbon because of close polymorphism. Hexagonal and rhombohedral boron nitrides (h-BN and r-BN) are structurally similar to hexagonal and rhombohedral graphite. They are extremely soft, electrical insulators with poor thermal conductivities. Cubic and Wurtzite boron nitride (c-BN and w-BN) are structurally similar to diamond and lonsdalite. Consequently, c-BN is an extremely hard, electrical insulator with an excellent thermal conductivity. Another very common modification of BN is a quasi-amorphous phase called turbostratic boron nitride (t-BN) which often co-exist with c-BN.[1] One minor difference between BN and carbon is in their layer stacking. In h-BN, the layers are arranged so that boron atoms in one layer are located directly on top of nitrogen atoms in neighboring layers, and vice versa.[2]

All these modifications of BN can be considered as three-dimensional (3D) bulk substances. However, effect of architecture and grain size of BN result in different properties of powder materials because surface effect of nanostructure defines application. Therefore, a new class of material with reduced dimensionality, i.e., with one or more physical dimension(s) constrained to the nanometer scale should be recognized. Two-dimensional (2D) nanosheets, one-dimensional (1D) nanotubes, and zero-dimensional (0D) fullerenes represent typical examples of such materials. When compared to three-dimensional (3D) bulk substances, low-dimensional structures are anticipated to exhibit new properties due to quantum confinement and/or surface and interfacial effects.[3] Their unusual physical and chemical properties [4–6] can promote novel applications in engineering. Boron nitride low-dimensional materials are among the most promising inorganic nanosystems explored so far.

For boron nitride various approaches have been investigated, synthesis methods have been intensively studied, and significant achievements have been obtained in terms of quantity, structure quality and variety.[7] In order to prepare BN nanostructures, high and low temperature routes have been developed, for example, high temperature and high pressure (HTHP) method, chemical vapor deposition (CVD) method, physical vapor deposition (PVD) method, hydrothermal and solvothermal synthesis routes.[8] A comprehensive overview of the current status of the different synthesis processes for BN has demonstrated formation of different properties for BN powders highlighting the advantages of every synthetic methods.[9-20]

Solar heating is a promising alternative energy source for nanotechnology. A xenon high-flux optical simulator (also artificial sun) that provides illumination approximating natural sunlight in controllable indoor tests under laboratory conditions is a good model of this source. Optical simulator has numerous advantages. Its versatility, rapid heating and cooling rates, ability to adjust temperature profile along each axes, maximum operating temperatures and environmental adaptability stand out among others. Moreover, this technique can also be suitable for both conducting and non-conducting materials and is one of cleanest energy sources available. Since hard conditions of this furnace, can cause a new structure formation with new architecture, morphology, elemental and phase composition in the prepared boron nitride powder, it would be important to define the most valuable features, which may open a new opportunity for better BN powder application.

Experimental

Plate-like fine powder of h-BN (Chempur, CH070802) with thickness 0.001 μm and mean grain size ~ 0.3 μm and boron powder with particle size ≤ 0.05 μm have been used as a starting material. *These* powders exhibit uniform size and structure and high surface area.[21] Initially BN powder was annealed at 800 °C for 1 h in order to increase its chemical stability. Detailed description of the initial powders can be found in a number of previous papers.[21–23]

A quartz chamber was chosen for the process of heating. Surface of BN initial powder was treated in a xenon high-flux optical furnace in a flow of nitrogen at the density of energy in focal zone of set-up ~ 1.4×10^4 kW m^{-2} and ~ 0.7n $\times 10^4$ kW m^{-2}. Prepared BN powders precipitated on copper water-cooling screens and on a quartz surface of the chamber. Detailed description of the experiments was presented in the earlier papers.[4–28]

Dilor XY-800 Spectrometer in micro configuration recorded Raman spectra of prepared BN powders. As the excitation beam Ar^+ ion and Kr^+ ion lasers were used. 514.5 nm and 488 nm wavelengths of the Ar^+ laser and a 647 nm line of the Kr^+ laser were applied. Auger process was initiated by creation of a core hole carried out by exposing a sample to a beam of high energy electrons 3 keV (beam current – 120, 180, 200 μmA, modulation – 1-2 eV, time constant - 3 s, sensitivity – 50-100 μmV, scanning time - 1000 sec, energy rate - 500 eV). A process in an Auger spectrometer chamber was initiated by exposing a sample to a beam of high-energy electrons (3 keV), which has a sufficient energy to ionize proper levels of the researched elements.

IR spectra were examined with Nicolet 6700 FTIR spectrometer equipped with a Thermo Nicole Continuum microscope. Resulting structures were examined by transmission electron microscope JEM-2100F (ability to separate 0.1 nm) and scanning electron microscopy Superprobe-733 (electron beam diameter of 0.7 nm). Powders were analyzed using X-ray diffraction (diffractometer "DRON-3.0", radiation of K_α – Cu) and were examined microstructurally using optical microscopy. A detailed spectrophotometric study of spectral dependence of optical absorptionwas performed using a spectrophotometer "Specord UV-Vis".

Results and Discussion

White, glassy powder precipitated in a chamber during initial powders heating under concentrated light in flow of nitrogen. White threat-like and dark fullerene-like structures were found on a surface of the compacted h-BN sample around a crater (Fig. 1a). It is known that boron exists as a dark brown to black powder. BN, boron oxides and other boron compounds are mostly white and glassy powder. Therefore, dark fullerene-like structures were composed of boron with negligible amount of the boron oxides.[23]

SEM and TEM study disclosed complicated BN structures of significant diversity (Figures 1, 2). SEM images of 1D (Figure 1a), 2D (Figure 1b) and 3D (Figure 1c) structures of BN are typical for powders prepared under concentrated light at different conditions.

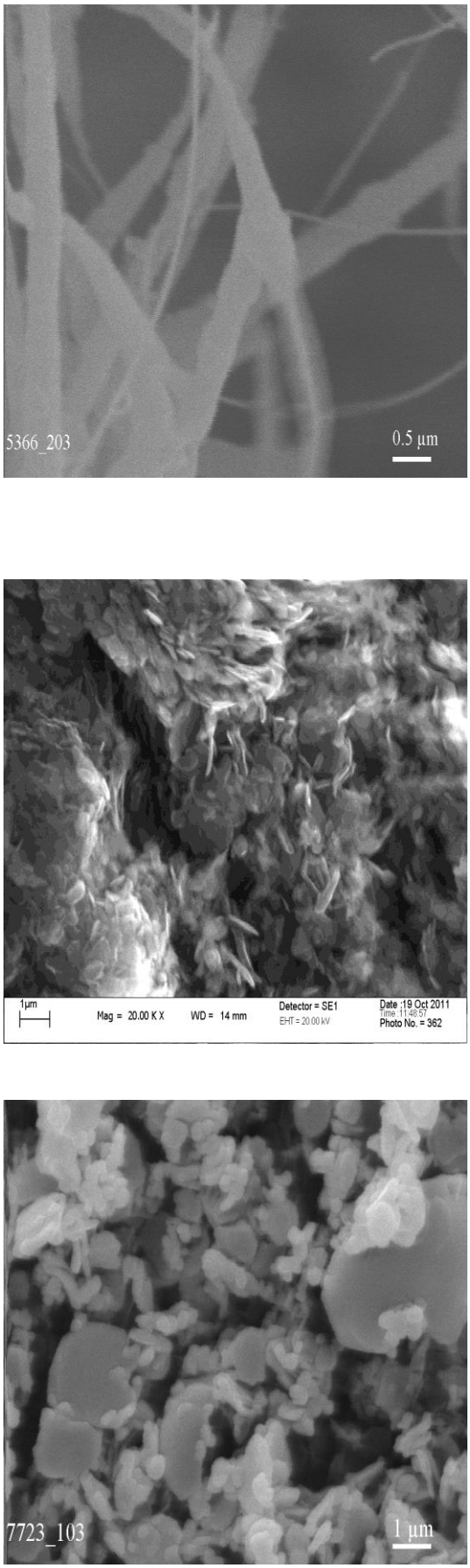

Figure 1. SEM image of 1D (a), 2D (b) and 3D (c) structures for BN powders prepared under concentrated light under different conditions.

0D nanostructures of BN were not found. TEM images of nanostructures have underlined the existence of gradient (Figure 3a) and layered (Figure 3b) nature for the low-dimensional structures of different architecture (Figure 2).

BN powder was characterized by a high transparency in a visible area of spectrum during exploration of an optical absorption. Dependence of a square of the optical absorption coefficient for a deposited BN film versus the photon energy of incident light can be a pure parabolic (Figure 3a) or with linear sections (Figure 3b).

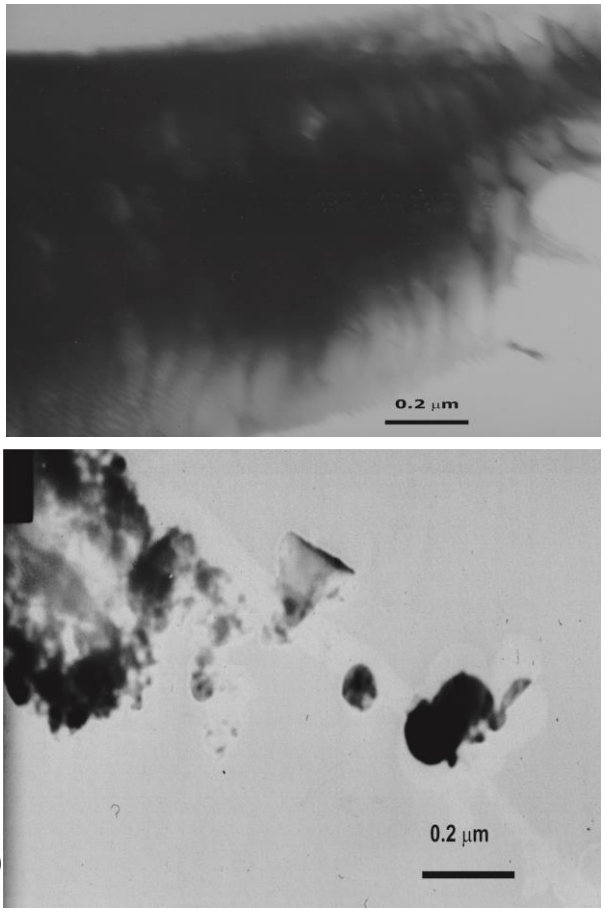

Figure 2. TEM image of gradient (a) and layered (b) nanostructures of BN powder of different architecture.

It is know that band gap for boron from different sources is 1,08 [29], 1,42 [30], 1,58 [31,32] eV in depend on purification. Boron of 99.9999% purity has been produced and is available commercially with band gap of 1.50 to 1.56 eV [32]. The band gap of h-BN remains in dispute, but recent reports seem to be converging close to 6 eV [33]. BN bad gap for graphene-like structures was estimated to be 5.6–5.8 eV [34] according to the optical absorption spectrum.For BNNTs can be 5,0 eV [35]; 5,5 – 5,8 eV [36,37] and higher – 6,0 eV [38]. Therefore, the peaks at ~5.5 eV are probably defect-induced and those at lower energies brought about by impurities [33].

Since BN was produced in conditions of a xenon high-flux optical furnace without any catalysts (impurities), therefore, a pure parabolic dependence (Figure 4a) has disclosed gradient nature of prepared powder (Figure 3a) from pure boron inside with band gap of 1.8 eV to BN with band gap of 5.1 eV

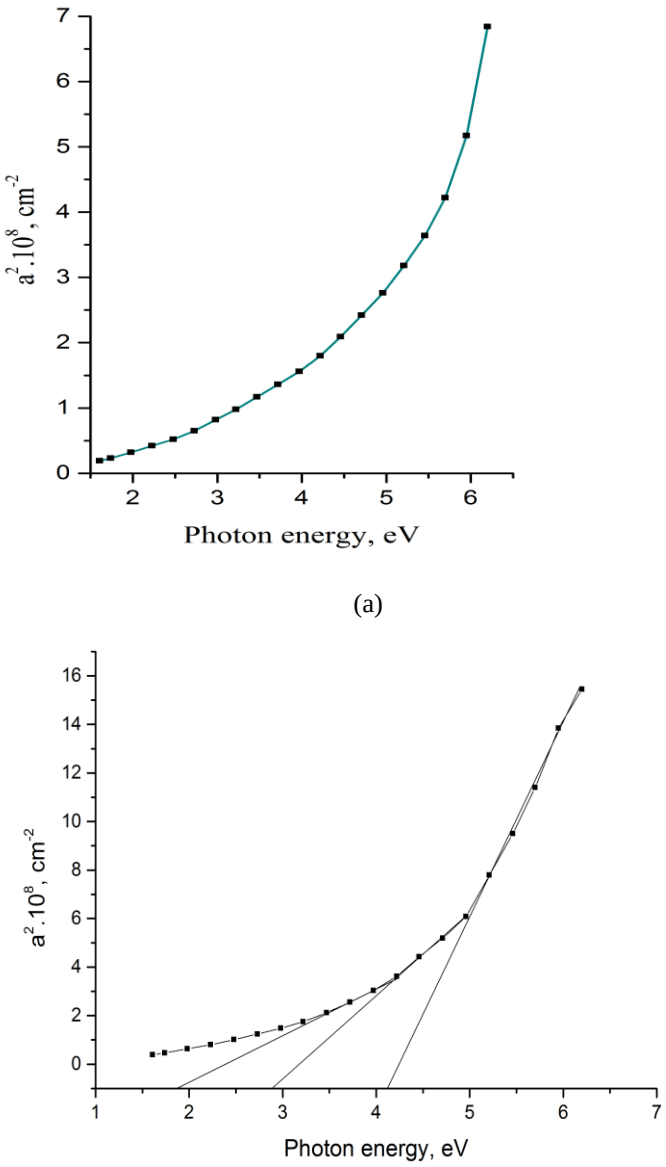

Figure 3. Square of the optical absorption coefficient, α, versus photon energy for the gradient (a) and layered (b) low-dimensional structures of BN powder.

Linear sections (Figure 4b) of the band gap, 2.4, 3.2 and 4.3 eV, accordingly, indicate the layered nature of structure of a prepared powder (Figure 3b). First-principles local-density calculations have shown that the lowest band gap (4.07 eV) is indirect, located near the Brillouin-zone edges. However, due to the quasi-two dimensional nature of the hexagonal structure, the lowest direct band gap is predicted to be close by 4.2 eV.[39] Therefore, band gap of 4.3 eV can be ascribed to BN layer with a deficit of nitrogen, that of 3.2 eV to the layer of tetragonal boron-enriched phase $B_{51,2}N$ and 2.4 eV to the layer of tetragonal and rhombohedric phases boron enriched nitrogen.[24] Lowest gap energies, such as 3.8 eV and 4.3 eV for BN have been reported by old experimental studies using various techniques.[39]

In contrast to SEM, which has a typical analysis depth of 1-3 μm, Auger electron spectroscopy (AES) is a surface analysis technique with an analysis depth of less than 5 nm and is therefore better suited for the compositional analysis of the features of ultra-thin layers and nanoscale samples.

Surface AES study of boron and BN powders has underlined these features.[40] Nitrogen implantation to boron results in splitting boron AES peak according preliminary studies.[40] This splitting was always observed for surfaces of all gradient and layered structures of prepared BN powders regardless of morphology difference (Figure 4).A curvature of a surface of 1D BN (Figure 2a) can explain just a negligible shifting peak at 171 eV for initial powder to lower values of the graph (Figure 1b). Low depth of nitrogen penetration in boron during heating can effect on surface structure, its activity and, as a result, on the quantity of absorbed carbon and oxygen (Figure 4).

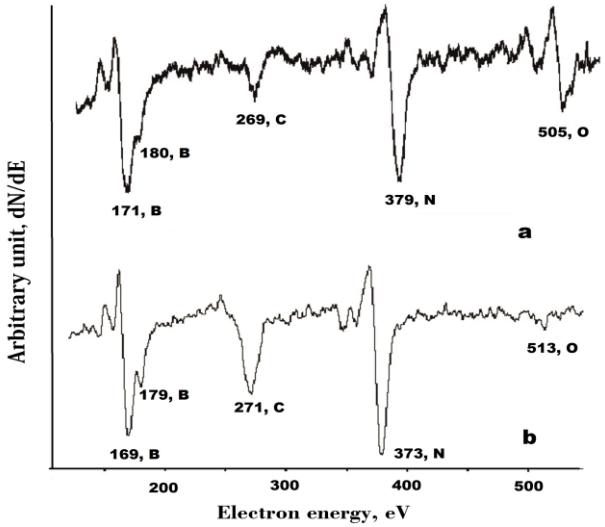

Figure 4. Differential Auger spectrum of the upper layer of the surface (a) 2D structure of initial h-BN powder,[1] (b) 1D threat-like structure of BN (Figure. 1a) prepared under concentrated light.

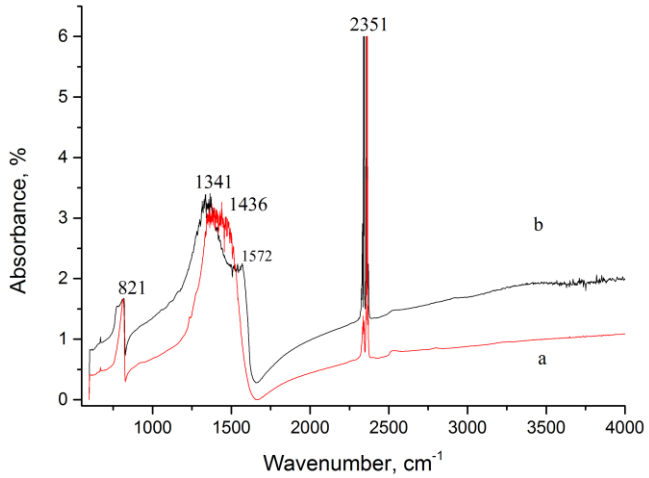

Figure 5. ATR-FTIR spectra (mid IR) with specific bands assignments for (a) an initial h-BN powder (2D structure) (b) prepared BN of 1D structure (Figure 2a).

In the mid-IR spectrum, the penetration depth typically is between 0.5 and 2μm with the exact value being determined by the wavelength of light, the angle of incidence and the indices of refraction for the medium being probed.[41]Two peaks at wave number of 821 and 2351 cm^{-1} of FT-IR spectra for initial h-BN and 1D BN (Figure 1a) are the same (Figure 6). The broadening, splitting and shift of the peak at 1436 cm^{-1} for initial h-BN into 2 peaks at 1341 and 1572 cm^{-1} for 1D BN was observed. Shift and broadening can be explained by the curvature of a surface of 1D BN, but look-like appearance of splitting may be ascribed to a new structure formation.

Raman spectroscopy is a valuable non-destructive analytical tool in detecting the different phases in mixed compounds. Depth of penetration for 514.5 nm and 488 nm wavelengths of the Ar^+ laser and a 647 nm line of the Kr^+ laser goes from 300 nm and higher for the best quantitatively studied silicon under effect of these lasers.[42] For initial h-BN and 1D BN (Figure 1a) Raman spectroscopy has disclosed that their spectra are very close (Figure 6). It is well known that bulk BN has an intrinsic E_{2g} vibration *at* 1367cm^{-1}.[43,44] In our research, the main peak, which corresponds to this E_{2g} vibration mode of h-BN was found at 1356 cm^{-1} because of laser wavelength of Dilor XY-800 Spectrometer. For prepared 1D BN (Figure 1a) broadening of its main peak occurs with a negligible shift at 1356 cm^{-1}(Figure 6). The shift and broadening in the Raman cross section for scattering from nanocrystals indicates that smaller crystal grain size because of the wave-vector uncertainty of the phonons. Preliminary research also has disclosed that an outer shell of 1D structures of BN (Figure 1b, Figure 2a) consists of polycrystalline nanosized h-BN. Some separate single crystals h-BN and $B_{51,2}N$ were also observed depending on the experimental conditions.[23] Therefore, Raman spectroscopy (Figure 6) also confirmes the presence of BN bonds on the surface of 1D structures prepared under concentrated light up to the depth up to 300 nm and higher.

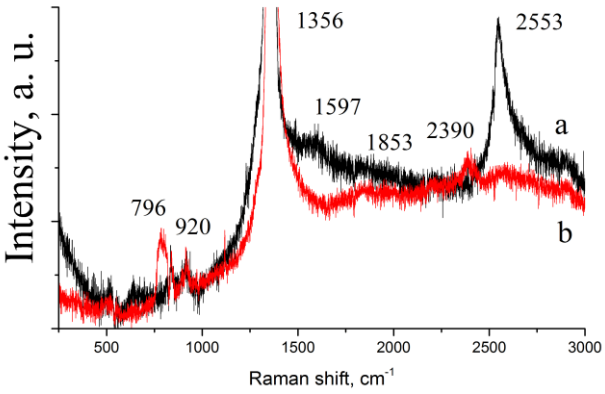

Figure 6. Raman spectra of (a) an initial h-BN powder (2D structure) and (b) prepared BN of 1D structure.

The depth of penetration for XRD study is much higher. Mass absorption coefficient of the BN sample and the incident angle of the X-ray beam effect on its spectra and penetration. Therefore, it is not unexpected that X-Ray diffractions pattern measured for prepared BN powder with pure parabolic dependence of a square of the optical absorption coefficient (Figure 3a) has disclosed only amorphous boron according to [44–47] with a small quantity of B_2O_3 (Figure 7).[45]

Based on all facts the structure of prepared BN nano-powders can be represented schematically as a boron particle with increase of nitrogen content from center to periphery occurring in agradient (Figure 9).

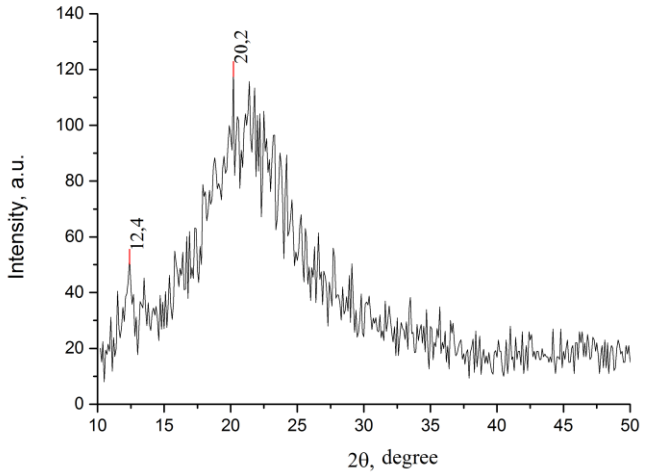

Figure 7. X-Ray diffractions pattern measured for BN of gradient nanostructure.

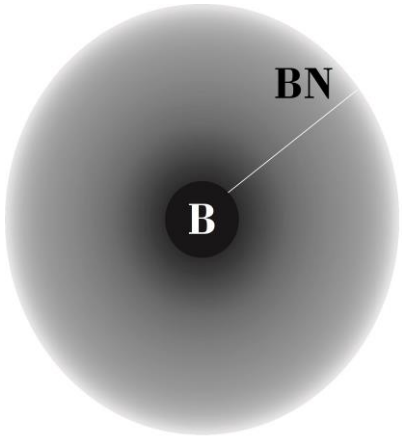

Figure 8. Schematic picture of the gradient structure of prepared BN nanoparticle.

X-Ray diffractions patterns for prepared BN powder of layered (Figure 2b) nature with linear sections of dependence of a square for the optical absorption coefficient were described before [21,24] and have demonstrated phases, as follows: h-BN, tetragonal boron-enriched phases $B_{51,2}N$ and $B_{25}N$; tetragonal and rhombohedral phases of pure boron and negligible amorphous boron content. Difference in heating condition under concentrated light may cause crystalline nanostructure formation on the surface in depend on a weight of the boron particle, its deposition velocity and velocity of nitrogen.

This conclusion does not conflict our previous "gaseous" model for 1D and 2D BN structures formation.[23,25] Heating h-BN or boron under concentrated light results in a melt of boron, boiling process and spattering melt boron drops or grow 1D nanostructure around a crater of the melt in flow of nitrogen.[21,23,25] SEM and TEM study has demonstrated diversity in BN particle size, its architecture and morphology (Figure 2, 3) caused impurity content, weight of the spattered boron particle, its deposition velocity and velocity of nitrogen.

Conclusion

Heating of boron and boron nitride powders under concentrated light, in a xenon high-flux optical furnace, in a flow of nitrogen, results in the formation of a BN powder with a new structure. Since rapid heating and cooling rate does not permit full penetration of nitrogen to boron grain, formed particle has gradient structure. Local annealing of such structure in the process of heating causes crystallization and transformation with a gradient distribution of nitrogen in boron particle to layered structure.

Thus, most of characterization challenges can be met by different research techniques of different analytical depth, which will permit one to understand the real picture of a structure of prepared powder as well as process of the formation of a new structure formation.

Acknowledgements

We acknowledge support of CRDF (UKE2-7034-KV-11) and JSPS. Our best acknowledgements are for support from Prof. Hirofumi Takikawa, Prof. Mototsugu Sakai and Associate Prof. Hiroyuki Muto.

This paper has been presented at the 4th International Conference "Nanotechnologies", October 24 – 27, 2016, Tbilisi, Georgia (Nano – 2016).

References

[1]Petrescu, M. L., Balint, M. G., *U. P. B. Sci. Bull., Ser. B*, 2007, 69, 35-42.

[2]Ishigami, M., Aloni, S., Zettl, A., *AIP Conference Proceedings* **2003**,94-99. https://doi.org/10.1063/1.1639682

[3]Pakdel, A., Zhi, C., Bando, Y., Golberg, D., *Mater Today*. **2012**, 15*(6)*, 256-265. https://doi.org/10.1016/S1369-7021(12)70116-5

[4]Chkhartishvili, L., *Mater. Sci. Appl*., **2010**, *1(4)*, 222-245.

[5]Chkhartishvili, L., *Phys. Solid State*, **2004**, *46 (11)*, 2126-2133. https://doi.org/10.1134/1.1825560

[6]Chkhartishvili, L., *J. Phys. Conf. Ser*., **2009**, *176(1)*, 12014. https://doi.org/10.1088/1742-6596/176/1/012014

[7]Kalay, S., Yilmaz, Z., Sen, O., Emanet, M., Kazanc, E., Çulha, M., S *Beilstein J. Nanotechnol*, **2015**, *6 (1)*, 84-102. https://doi.org/10.3762/bjnano.6.9

[8]Li, K., Jiang, H., Lian, G., Wang, Q., Zhao, X., Cui, D., Tao, X.., *Chin. Sci. Bull*., **2007**, *52(13)*, 1785-1790. https://doi.org/10.1007/s11434-007-0255-4

[9]Friedmann, T. A., Mirkarimi, P. B., Medlin, D. L., McCarty, K. F., Klaus, E. J., Boehme, D. R., Johnsen, H. A., Mills, M. J., Ottesen, D. K., Barbour, J. C. *J. Appl. Phys*., **1994**, *76(5)*, 3088-3101. https://doi.org/10.1063/1.357491

[10]Wang, X., Xie, Y., Guo, Q., *Chem. Commun*., **2003**, 2688. https://doi.org/10.1039/b308264d

[11]Wang, J., Li, Z., Gu, Y., Dua, X., Zhanga, Z., Wanga, W., Fua, Z.., *Ceram Int*., 2015. Volume 41, Issue 1, Part B, January 2015, Pages 1891–1896

[12]Hao, X., Yu, M., Cui, D., Xu, X., Wang, Q., Jiang, M., *J. Cryst. Growth*, **2002**, *241(1-2)*, 124-128. https://doi.org/10.1016/S0022-0248(02)01291-5

[13]Wang, J., Zhang, L., Gu, Y., Pan, X., Zhao, G., Zhang, Z., *Mater. Res. Bull.*, **2013**, *48(3)*, 943-947. https://doi.org/10.1016/j.materresbull.2012.11.012

[14]Budak, E., Bozkurt, Ç., *Phys. B Condens. Matter*., **2010**, *405(22)*, 4702-4705. https://doi.org/10.1016/j.physb.2010.08.067

[15]Li, L., Li, C. P., Chen, Y., *Physica E Low-dimens. Syst. Nanostruct.*, **2008**, *40(7)*, 2513-2516. https://doi.org/10.1016/j.physe.2007.06.065

[16]Pokropivny, V. V., Smolyar, A. S., Pokropivny, A. V., *Phys. Solid State*, **2007**, *49(3)*, 591-598. https://doi.org/10.1134/S1063783407030365

[17]Chen, L., Gu, Y., Shi, L., Yang, Z., Ma, J., Qian, Y., *Solid State Commun.*, **2004**, *130(8)*, 537-540. https://doi.org/10.1016/j.ssc.2004.03.009

[18]Lin, L.-X., Zheng, Y., Li, Z.,, Wei, K.-M., *Scr. Mater.*, **2008**, *59(10)*,1151-1154. https://doi.org/10.1016/j.scriptamat.2008.07.041

[19]Shi, L., Gu, Y., Chen, L., Qian, Y., Yang, Z., Ma, J., *J. Solid State Chem.*, **2004**, *177(3)*, 721-724. https://doi.org/10.1016/j.jssc.2003.08.026

[20]Li, Q., Liu, M., Zhang, Y., Liu, Z., *Small*. correct!!! (?) **2016**, *12(1)*, 32-50. https://doi.org/10.1002/smll.201501766

[21]Sartinska L. L., Frolov, A. A., Koval, A. Y., Danilenko, N. A., Timofeeva II, Rud' B. M., *Mater. Chem. Phys*., **2008**, *109(1)*, 20-25. https://doi.org/10.1016/j.matchemphys.2007.10.043

[22]Sartinska, L. L., Eren, T., Altay, E., Frolov, G. A., *Eur. Chem. Bull*., **2015**, *4(3)*, 165-168. *DOI: 10.17628/ecb.2015.4.165-168*

[23]Sartinska L. L., *Acta Mater*., **2011**, *59(11)*, 4395-4403. https://doi.org/10.1016/j.actamat.2011.03.063

[24]Sartinska, L. L., Frolov, A. A., Andreeva, A. F., Kasumov, A. M., Timofeeva, I. I., Danilenko, M. I., *Mater. Lett*., **2011**, *65(12)*, 1791-1793. https://doi.org/10.1016/j.matlet.2011.03.064

[25]Sartinska, L. L., *Superlattices Microstruct*., **2015**, *85*, 392-400. https://doi.org/10.1016/j.spmi.2015.05.042

[26]Sartinska, L. L., Vorobets, V. S., Frolov, G. A., Kolbasov, G.Ya., Jastrebski, C., Koval', A.Yu., Timofeeva, I.I., Karpenko, S.V. *Vacuum*, **2015**, *116*, 73-76. https://doi.org/10.1016/j.vacuum.2015.02.029

[27]Sartinska L. L., Bloschanevich, O. M., Timofeeva, I. I., Nishchenko, M. M., Shevchenko, N. A., *J. Non-Cryst. Solids*, **2011**, *357(6)*, 1504-1507. https://doi.org/10.1016/j.jnoncrysol.2010.12.035

[28]Frolov, A. A., Sartinska, L. L., Koval', A. Y., Danilenko, N. A., *Nanomaterials*, **2008**, *2*, 4.

[29]Semiconductor Materials (Полупроводниковые материалы). http://chem-bsu.narod.ru/ChemRadWeb/ch4/ch4.htm. Accessed January 3, 2017.

[30]General and Inorganic Chemistry, Общая и неорганическая химия - М. Х. Карапетьянц - Google книги. https://books.google.com.ua/books?id=axL7AgAAQBAJ&dq=ширина+запрещенной+зоны+бора&hl=uk&source=gbs_navlinks_s. Accessed January 3, 2017.

[31]Proeprties of elementary semiconductors (Свойства собственных элементарных полупроводников). http://worldofscience.ru/himija/5018-svojstva-sobstvennykh-elementarnykh-poluprovodnikov.html. Accessed January 3, 2017.

[32]*Periodic Table of Elements*: Los Alamos National Laboratory. http://periodic.lanl.gov/5.shtml. Accessed January 3, 2017.

[33]Edgar, J. H. Hoffman, T. B. Clubine, B. Currie, M. Du, X. Z.. Lin, J. Y. and Jiang, H. X. *J. Cryst. Growth*, **2014,** *403*, 110–113,

[34]Wang, L., Hang, R., Xu, Y., Guo, C., Qian, Y., *RSC Adv*., **2014**, *4(27)*, 14233. https://doi.org/10.1039/c3ra47005a

[35]Golberg, D., Bando, Y., Huang, Y., Terao,T., Mitome, M., Tang C., Zhi, C. *ACS Nano*, **2010**, *4(6)*, 2979-2993. https://doi.org/10.1021/nn1006495

[36]Blase, X., Rubio, A., Louie, G., Cohen, M. L., *EPL (Europhys. Lett.)*, 1994, *28(5)*, 335-340 · November 1994. https://doi.org/10.1209/0295-5075/28/5/007

[37]Singhal, S. K.; Srivastava, A. K.; Pant, R. P.; Halder, S. K.; Singh, B. P.; Gupta, Anil K., *Indian J. Eng. Mater.Sci*., **2008**, *15*, 419-424

[38]Lian, J., Kim, T., Liu, X., Ma, J., Zheng, W., *J. Phys. Chem. C*, **2009**, *113(21)*, 9135-9140. https://doi.org/10.1021/jp9004136

[39]Wu, J., Han, W.-Q., Walukiewicz, W., Ager III, J. W., Shan, W., Haller, E. E., Zettl, A., *Nano Lett.*, **2004**, *4(4)*, 647–650). https://doi.org/10.1021/nl049862e

[40]Sartinska, L. L., Stonis, V. V., Frolov, A. A., Stonis, V. V., Auger electron spectroscopy of boron nitride whiskers produced in optical furnace without catalysts. *Современные проблемы физического материаловедения*. 2009, 543-422.

[41]Mirabella, F. M., *Practical Spectroscopy Series: Internal Reflection Spectroscopy: Theory and Applications*, Marcel Dekker, Inc., New. York, **1993**, 17-52.

[42] Kreisel, J., Weber, M. C., Dix, N., Sánchez, F., Thomas, P. A., Fontcuberta, J., *Adv. Funct. Mater*., **2012**, *22(23)*, 5044-5049. https://doi.org/10.1002/adfm.201201272

[43]Chen, Z. G., Zou, J., Liu, G., Li, F., Cheng, H-M., Sekiguchi, T., Gu, M., Yao, X-D., Wang, L-Z., Lu, G. Q. *Appl. Phys. Lett*., **2009**. *94(2)*, 2014-2017. https://doi.org/10.1063/1.3069278

[44]Zhigadlo, N. D., *J. Cryst. Growth*, **2014**, 402, 308-311. https://doi.org/10.1016/j.jcrysgro.2014.06.038

[45]Jiang, J., Senkowicz, B. J., Larbalestier, D. C., Hellstrom, E. E., *Supercond. Sci. Technol*., **2006**, *19(8)*, L33-L36. https://doi.org/10.1088/0953-2048/19/8/L02

[46]Varin, R. A., Chiu, C., *J. Alloys Compd*., **2006**, *407(1)*, 268-273. https://doi.org/10.1016/j.jallcom.2005.06.026

[47]Li, L., Li, L., Chen, Y., Dai, X. J., Xing, T., Petravic M., Liu, X.. *Nanoscale Res. Lett*., **2012**, *7(1)*,417. https://doi.org/10.1186/1556-276X-7-417

Received:
Accepted:

SYNTHESIS OF A SERIES OF 2-INDOLYLMETHYLENE-LINKED COMPOUNDS BY THERMAL KNOEVENAGEL CONDENSATION UNDER CATALYST- AND SOLVENT-FREE CONDITIONS

Tapas Halder[a], Nayim Sepay[a] and Asok K. Mallik[a]*

Keywords: Knoevenagel condensation, 3-methylindole-2-aldehyde, cyclic active methylene compounds, catalyst- and solvent-free reaction

An efficient methodology has been developed by which a series of new 2-indolylmethylene-linked compounds can be readily synthesized by thermal Knoevenagel condensation of 3-methylindole-2-carboxaldehyde and cyclic active methylene compounds under catalyst- and solvent-free conditions.

* Corresponding Authors
E-Mail: mallikak52@yahoo.co.in
[a] Department of Chemistry, Jadavpur University, Kolkata-700 032, India

Introduction

Indole derivatives are well-known for their versatile biological activities[1-3]. This has made the synthesis of compounds containing indole moiety an interesting target for synthetic organic chemists. The Knoevenagel condensation[4] of substituted aromatic aldehydes with active methylene compounds is an important and widely employed method for carbon-carbon bond formation in organic synthesis with numerous applications in the construction of different types of organic molecules of biological significance. The reactions are usually catalyzed by bases[5] such as aliphatic amines, ethylenediamine and piperidine or their corresponding ammonium salts, ammonia or sodium ethoxide in organic solvents. Lewis acids[6-9], zeolites[10], surfactants[11], different types of nanoparticles[12,13] have also been employed to catalyze the reactions. Moreover, the uses of ionic liquids[14], microwave[15,16] and ultrasound[17] are found in the recent literature to effect this condensation under eco-friendly conditions.

Organic reactions under solvent-free and catalyst-free[18-23] conditions have increasingly attracted interest of chemists, particularly from the viewpoint of green chemistry. Though a number of solvent-free methodologies are known for effecting Knoevenagel condensation[13,15,16,24], only a few catalyst-free reaction conditions are reported[25,26]. Considering the importance of synthesis of new compounds containing an indole moiety and effecting Knoevenagel condensation under catalyst- and solvent-free conditions, we undertook the present work where 3-methylindole-2-carboxaldehyde (**1**) (readily available from a well-known indole compound skatole)[27], with different active methylene compounds under the influence of heat only. The interesting results obtained in this study are presented herein.

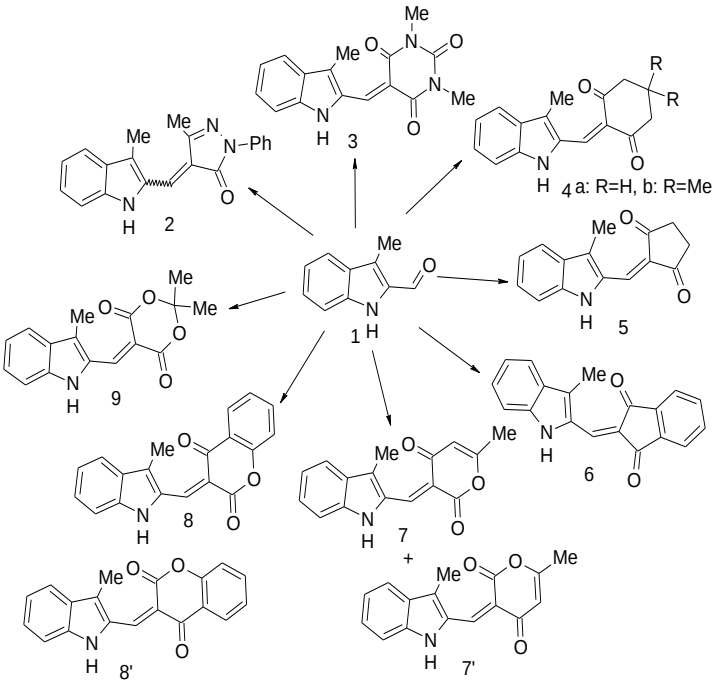

Scheme 1. Synthesis of 2-indolyl-methylene-linked compounds.

Experimentals

Melting points were recorded on a Köfler block. IR spectra were recorded on a Perkin Elmer FT-IR spectrophotometer (Spectrum BX II) in KBr pellets. ^{1}H and ^{13}C NMR spectra were recorded in $CDCl_3$ on a Bruker AV-300 (300 MHz) spectrometer. Analytical samples were routinely dried *in vacuo* at room temperature. Microanalytical data were recorded on two Perkin-Elmer 2400 Series II C, H, N analyzers. Mass spectra were measured with a Waters Xevo G2QTof HRMS spectrometer. TLC experiments were performed with silica gel G of SRL Pvt. Ltd make. Petroleum ether used had the boiling range of 60-80 °C.

Preparation of 3-methylindole-2-carboxaldehyde (1)

This compound was prepared by a known procedure.[26] A solution of 3-methylindole (1.64 g, 12.5 mmol) in DMF (1 mL) was added drop wise to a complex obtained from $POCl_3$ (2.3 g, 15 mmol) and DMF (7.76 g, 105 mmol). The reaction mixture was heated at 100 ° C for 3h. The crude product so obtained was cooled and subjected to column chromatography over silica gel (Spectrochem Pvt. Ltd., India, 100-200 mesh) using a mixture of petroleum ether and ether (19:1) as eluent gave first 3-methylindole-1-carboxaldehyde as a colourless oil. Further elution of the column with a mixture of petroleum ether and ether (17:3) gave **1** (0.42 g, 21 %) which was crystallised from petroleum ether as colourless needles, m.p. 138-140 °C (lit.[26] 139-140 °C), **1**H NMR (300 MHz, $CDCl_3$): δ 2.65 (s, 3H, indole-3-CH_3), 7.14-7.19 (m, 1H), 7.38 (br. d, 1H), 7.71 (d, J=8.1 Hz, 1H), 8.80 (br. s, 1H, indole-3-CH_3), 10.04 (s, 1H, -CHO).

Synthesis of 2-9

An intimate mixture of 3-methylindole-2-carboxaldehyde (**1**, 1 mmol) and an active methylene compound (1 mmol) was taken in a round-bottomed flask fitted with an air condenser, and it was heated in an oil bath at a temperature between 80-120°C for a time period of 10-40 min (*vide* Table 1). The reaction vessel was then cooled and the reaction mixture was subjected to column chromatography over silica gel. The pure product thus obtained was crystallized from dichloromethane-petroleum ether.

3-Methyl-4-((3-methyl-1*H*-indol-2-yl)methylene)-1-phenyl-1*H*-pyrazol-5(4*H*)-one (2)

Brick red crystals, IR (KBr): ν/cm^{-1} = 1672, 1578, 1330, 1216, 740. ^{1}H NMR (300 MHz, $CDCl_3$): δ 2.38 (s, 3H, pyrazolone-CH_3), 2.61 (3H, s, indole-3-CH_3), 7.11 (1H, t, J=7.4 Hz), 7.23 (t, J=7.0 Hz,1H), 7.37 (t, J=8.3 Hz,1H), 7.43-7.48 (m, 4H), 7.62 (d, J=7.9 Hz, 1H), 7.98 (d, J=8.0 Hz,1H), 7.99 (s, 1H, indole-2-CH=), 13.12 (br. s, 1H, indole-NH). ^{13}C NMR (75 MHz, $CDCl_3$): δ 9.8 (indole-3-CH_3), 13.1 (pyrazolone-CH_3), 112.9, 119.7, 120.4, 120.9, 125.3, 127.4, 128.2, 128.4, 128.9, 130.9, 131.7, 138.4, 139.2, 150.8, 163.8 (pyraozolone-C=O). HRMS *m/z* Calcd. for $C_{20}H_{18}N_3O$ $(M+H)^+$: 315.1450; Found: 316.1450. Anal. Calcd. for $C_{20}H_{17}N_3O$: C, 76.17; H, 5.43; N 13.32. Found: C, 75.92; H, 5.51; N, 13.15.

1,3-Dimethyl-5-((3-methyl-1*H*-indol-2-yl)methylene)-pyrimidine-2,4,6(1*H*,3*H*,5*H*)-trione (3)

Yellow crystals, ^{1}H NMR (300 MHz, $CDCl_3$): δ 2.68 (s, 3H, indole-3-CH_3), 3.42 (s, 3H, barbiturate-CH_3), 3.46 (s, 3H, barbiturate-CH_3), 7.12 (br. t, J= 7.1 Hz, 1H), 7.40-7.44 (m, 2H), 7.66 (d, J=8.2, 1H), 8.67 (s, 1H, indole-2-CH=), 12.43 (br. s, 1H, indole-N-H). ^{13}C NMR (75 MHz, $CDCl_3$): 10.0 (indole-3-CH_3), 28.5 (barbiturate-CH_3), 28.9 (barbiturate-CH_3), 108.1, 112.8, 120.7, 121.5, 128.2, 129.5, 130.3, 132.8, 139.6, 140.8, 151.2 (C=O), 163.1(C=O), 163.3 (C=O). HRMS *m/z* Calcd. for $C_{16}H_{16}N_3O_3$ $(M+H)^+$: 298.1192; Found: 298.0818. Anal. Calcd. for $C_{16}H_{15}N_3O_3$: C, 64.64; H, 5.09; N 14.13. Found: C, 64.72; H, 5.31; N, 14.25.

2-((3-Methyl-1*H*-indol-2-yl)methylene)cyclohexane-1,3-dione (4a)

Red crystals, ^{1}H NMR (300 MHz, $CDCl_3$): δ 2.05-2.13 (m, 2H), 2.66 (s, 3H, indole-3-CH_3), 2.66-2.73 (m, 2H), 2.75-2.82 (m, 2H), 7.09-7.15 (m, 1H), 7.38-7.42 (m, 2H), 7.65 (d, J=8.1Hz, 1H), 8.44 (s, 1H, indole-2-CH=), 12.38 (br. s, 1H, indole-NH). HRMS *m/z* Calcd. for $C_{16}H_{16}NO_2$ $(M+H)^+$: 254.1181; Found: 254.1168. Anal. Calcd. for $C_{16}H_{15}NO_2$: C, 75.57; H, 6.34; N, 5.51. Found: C, 76.02; H, 6.21; N, 5.34.

5,5-Dimethyl-2-((3-methyl-1*H*-indol-2-yl)methylene)-cyclohexane-1,3-dione (4b)

Orange crystals, ^{1}H NMR (300 MHz, $CDCl_3$): δ 1.13 (s, 6H, 2×CH_3 of dimidone moiety), 2.60-2.67 (m, 4H, 2×CH_2 of dimidone moiety), 2.67 (s, 3H, indole-3-CH_3), 7.10 (br. t, J=7.5 Hz,1H), 7.38-7.44 (m, 2H), 7.64 (br. d, J = 8.1 Hz, 1H), 8.42 (s, 1H, indole-2-CH=), 12.41 (br. s, 1H, indole-NH). Anal. Calcd. for $C_{18}H_{19}NO_2$: C, 76.84; H, 6.81; N 4.98. Found: C, 76.58; H, 6.64; N, 5.15.

2-((3-Methyl-1*H*-indol-2-yl)methylene)cyclopentane-1,3-dione (5)

Orange crystals, IR (KBr): ν /cm^{-1} = 1650, 1626, 1562, 1523, 1323, 1201, 1128, 1054, 746, 712. **1**H NMR (300 MHz, $CDCl_3$): δ 2.66 (s, 3H, indole-3-CH_3), 2.80 (s, 4H, 2×CH_2 of cyclopenta-1,3-dione moity), 7.09-7.13 (m, 1H), 7.44 (br. s, 2H), 7.64 (d, J=8.3, 1H), 7.91 (s, 1H, indole-2-CH=), 12.64 (br. s, 1H, indole-NH); ^{13}C NMR (75 MHz, $CDCl_3$): δ 10.0 (indole-3-CH_3), 34.3 (CH_2 of cyclopenta-1,3-dione moiety), 34.5 (CH_2 of cyclopenta-1,3-dione moiety), 113.1, 121.0, 121.6, 122.4, 128.7, 130.3, 132.5, 133.4, 134.2, 140.0, 203.2 (C=O), 205.2 (C=O). Anal. Calcd. for $C_{15}H_{13}NO_2$: C, 75.30; H, 5.48; N 5.85. Found: C, 74.99; H, 5.61; N, 5.58.

2-((3-Methyl-1*H*-indol-2-yl)methylene)-1*H*-indene-1,3(2*H*)-dione (6)

Red crystals, IR (KBr): ν /cm^{-1} = 1665, 1596, 1554, 1498, 1325, 1262, 1158, 991, 755. **1**H NMR (300 MHz, $CDCl_3$): δ 2.66 (s, 3H, indole-3-CH_3), 7.11 (t, J=7.5 Hz, 1H), 7.40 (t, J=7.5 Hz, 1H), 7.47 (d, J=8.1 Hz, 1H), 7.63 (d, J=8.1 Hz, 1H), 7.76-7.80 (m, 2H), 7.95-7.99 (m, 2H), 7.99 (s, 1H, indole-2-CH=), 12.31 (br. s, 1H, indole-NH); ^{13}C NMR (75 MHz, $CDCl_3$): δ 9.8 (indole-3-CH_3), 112.6, 120.5, 121.1, 122.5, 122.8, 128.5, 128.7, 129.5, 130.8, 131.6, 134.7, 135.1, 139.2, 140.3, 141.5, 162.3, 190.3 (C=O), 191.9 (C=O). Anal. Calcd. for $C_{19}H_{13}NO_2$: C, 79.43; H, 4.56; N 4.88. Found: C, 79.72; H, 4.51; N, 5.15.

(*E* and *Z*)-6-Methyl-3-((3-methyl-1*H*-indol-2-yl)methyl-ene)-2*H*-pyran-2,4(3*H*)-dione (7 and 7′)

Orange crystals, **1**H NMR (300 MHz, $CDCl_3$): δ 2.23 (s, 3H, pyrone-6-CH_3), 2.68 and 2.70 (each s, 3H (total), indole-3-CH_3), 5.86 and 5.90 (each s, 1H (total), pyrone-H-5), 7.09-7.13 (m, 1H), 7.42 and 7.43 (each br. s, 2H (total)), 7.65 and 7.67 (each d, J=7.5 Hz, 1H (total)), 8.61 and 8.75 (each s, 1H (total), indole-2-CH=), 12.10 and 13.16 (each br.

s, 1H (total), indole-NH) [Characteristic peaks: δ 2.68, 5.86, 8.60, 13.16 (major isomer *ca*. 72 %), δ 2.70, 5.90, 8.75, 12.10 (minor isomer *ca*. 28 %)].

(*E* and *Z*)-3-((3-methyl-1*H*-indol-2-yl)methylene)chrom an-2,4-dione (8 and 8′)

Red crystals, ^{1}H NMR (300 MHz, $CDCl_3$): δ 2.74 and 2.76 (each s, 3H (total), indole-3-CH_3), 7.14 (br. t, *J* = 6.6 Hz, 1H), 7.26-7.35 (m, 2H,), 7.45-7.50 (m, 2H), 7.63-7.70 (m, 2H), 8.14-8.20 (m, 1H), 8.83 and 8.95 (each s, 1H (total), indole-2-CH=), 12.25 (br. s, 1H, Indole-NH), 13.11 (br. s, 1H (total), indole-NH) [Characteristic peaks: δ 2.74, 8.83, 13.11 (major isomer *ca*. 75 %), δ 2.76, 8.86, 12.20 (minor isomer *ca*. 25 %)]. ^{13}C NMR (75 MHz, $CDCl_3$): 10.3 (indole-3-CH_3), 113.0, 113.3, 117.2, 117.4, 120.9, 121.0, 121.2, 122.0, 124.5, 124.8, 127.4, 128.2, 128.8, 131.0, 132.4, 135.2, 135.6, 135.8, 136.2, 140.2, 141.0, 141.7, 143.4, 154.5, 154.9, 163.7, 164.4, 180.4 (very much characteristic of a mixture). HRMS *m/z* Calcd. for $C_{19}H_{14}NO_3$ $(M+H)^+$: 304.0974; Found: 304.1276.

2,2-Dimethyl-5-((3-methyl-1*H*-indol-2-yl)methylene)-1,3-dioxane-4,6-dione (9)

Red crystals, ^{1}H NMR (300 MHz, $CDCl_3$): δ 1.80 (s, 6H**,** 2×CH_3 of the Meldrm's acid moiety), 2.67(s, 3H, indole-3-CH_3), 7.11-7.17 (m, 1H), 7.42-7.44 (m, 2H), 7.67 (d, J= 8.2 Hz, 1H), 11.86 (br. s, 1H, indole NH). ^{13}C NMR (75 MHz, $CDCl_3$): δ 10.0 (indole-3-CH_3), 27.4 (2×CH_3 of Meldrum's acid moiety), 103.5, 104.4, 112.9, 121.0, 121.7, 128.1, 129.6, 129.9, 133.4, 140.1, 141.3, 163.8 (C=O), 164.1 (C=O); HRMS *m/z* Calcd. for $C_{16}H_{16}NO_4$ $(M+H)^+$: 286.1079; Found: 286.1092.

9-(3-Methyl-1*H*-indol-2-yl)-3,4,5,6,7,9-hexahydro-1*H*-xanthene-1,8(2*H*)-dione (10)

Colorless crystals, m.p. 286-287 °C ^{1}H NMR (300 MHz, $CDCl_3$): δ 2.01-2.10 (m, 4H), 2.11 (s, 3H, indole-3-CH_3), 2.25-2.44 (m, 4H), 2.53-2.71 (m, 4H), 4.94 (s, 1H), 7.00 (t, 1H, J= 7.7 Hz), 7.08 (t, 1H, J= 7.4 Hz), 7.26 (d, 1H, merged with $CHCl_3$ signal), 7.42 (d, 1H, J=7.5 Hz), 8.36 (br. s, 1H, indole NH) Anal. Calcd. for $C_{22}H_{21}NO_3$: C, 76.06; H, 6.09; N, 4.03, Found: C, 75.89; H, 6.21; N, 4.24.

Results and Discussion

Our present method involves subjecting of an intimate mixture of 3-methylindole-2-carboxaldehyde (**1**) and a cyclic active methylene compound (1:1 mole ratio) directly to heat. A range of structurally diverse cyclic active methylene compounds, *viz.*, 3-methyl-1-phenyl-1*H*-pyrazol-5(4*H*)-one (**CAM-1,** pK_a = 6.90)[28], 1,3-dimethylbarbituric acid (**CAM-2,** pK_a = 4.68)[29], cyclohexan-1,3-dione (**CAM-3,** pKa = 10.3)[30], 5,5-dimethylcyclohexan-1,3-dione (dimedone) (**CAM-4,** pK_a = 11.2)[30], cyclopentan-1,3-dione (**CAM-5,** pK_a = 4.4)[31], indan-1,3-dione (**CAM-6,** pK_a = 7.82)[32], 6-methyl-4-hydroxy-2-pyrone (**CAM-7,** pK_a = 4.94)[33], 4-hydroxycoumarin (**CAM-8,** pK_a = 4.14)[34] and 2,2-dimethyl-1,3-dioxane-4,6-dione (Meldrum's acid) (**CAM-9,** pK_a = 7.3)[30] were taken to get the condensation products **2-9**, all of which are new compounds. The time and temperature for the reaction of **1** with each of the above cyclic active methylene compounds were optimized and the results are shown in Table 1. It is interesting to note that when 3-methyl-1-phenyl-1*H*-pyrazol-5(4*H*)-one was used, only one geometrical isomer of the condensation product was obtained. However, as the product did not give good quality crystals, settlement of its configuration by x-ray crystallography could not be done.

Table 1. Optimised reaction conditions for synthesis of **2-9**.

Methylene compound	Time (min)	Temp. (°C)	Product	Yield (%)	m.p. (°C)
CAM-1	20	120	2	65	154-155
CAM-2	40	120	3	90	208-209
CAM-3	20	80	4a§	25	94-96
CAM-4	20	95	4b	31	104-105
CAM-5	20	115	5	79	184-185
CAM-6	20	120	6	91	252-253
CAM-7	20	120	7+7′	45	186-190
CAM-8	140	120	8+8′	83	211-215
CAM-9	20	110	9	89	193-194

§ In this case, another product (**10**) was also obtained (Scheme 2).

In the condensation reaction of **1** with each of **CAM-7** and **CAM-8**, a mixture of two products were obtained in approx. 4:1 ratio, which were found to be inseparable by column chromatography. When the results of the reactions of **1** with cyclic 1,3-diones were analyzed, it was observed that Knoevenagel condensation products were formed in better yields from the 5-membered 1,3-diones as compared to the six-membered 1,3-diones. From the reaction mixture using **CAM-3** some amount of the new xanthene-1,8(2*H*)-dione derivative **10** could be isolated in low yield (16%, based on amount of **1** taken), which indicated the occurrence of a facile Michael reaction on **4a** under the applied reaction conditions (Scheme 2). It may, therefore, be expected that development of a method for synthesis of **10** or its analogs may be possible by use of **1** and cyclohexan-1,3-diones in 1:2 mole ratio. Furthermore, we wish to report here that attempted reaction of **1** with the acyclic 1,3-dione acetylacetone (pK_a = 13.3)[30] (120 °C, 3 h) did not afford any Knoevenagel condensation product. The pK_a values of the active methylene compounds as quoted above indicate that the acidity of these compounds possibly plays an important role on the ease of their Knoevenagel condensation with **1**.

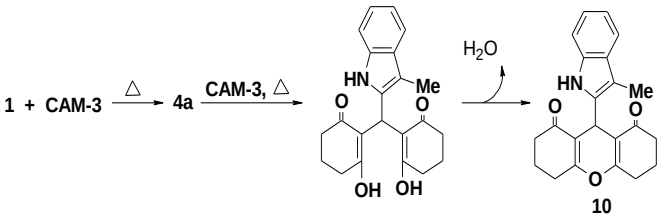

Scheme 2. Formation of 9-(3-methyl-1*H*-indol-2-yl)-3,4,5,6,7,9-hexahydro-1*H*-xanthene-1,8(2*H*)-dione (**10**)

The formatiom of 2-9 is expected to follow a path typical for acid-catalyzed Knoevenagel condensation. Possibly, the enol forms of the cyclic active methylene compounds are acting as acid catalysts.

Conclusions

We have developed a simple and efficient method for synthesis of a series of new 2-indolylmethylene-linked compounds by Knoevenagel condensation of 3-methylindole-2-carboxaldehyde and cyclic active methylene compounds under catalyst- and solvent-free conditions. Yields of the products were found to be moderate to very good in majority of cases.

Acknowledgments

The authors are grateful to the UPE-II and CAS programs of the UGC for financial support. Financial assistance and spectral facilities from the PURSE and FIST programs of the DST, New Delhi to the Department of Chemistry, Jadavpur University is also gratefully acknowledged. TH and NS are thankful to the UGC, New Delhi for their Research Fellowships.

Conflicts of interest

The authors declare that there is no conflict of interest regarding the publication of this manuscript.

References

[1]Sharma, V., Kumar, P., Pathak, D., *J. Heterocycl. Chem.*, **2010**, *47*, 491, DOI: 10.1002/jhet.349.

[2]Kaushik, N. K., Kaushik, N., Attri, P., Kumar, N., Kim C. H., Verma, A. K., Choi, E. H., *Molecules*, **2013**, *18*, 6620, doi:10.3390/molecules18066620.

[3]Kerzarea, D. R., Khedekar P. B., *J. Pharm. Sci. Bioscientific Res.* **2016**, *6*, 144.

[4]Knoevenagel, E., *Ber. Deutsch. Chem. Gesellschaft*, **1894**, ***27(2)***, 2345. https://doi.org/10.1002/cber.189402702229

[5]Jones, G. *Org. React.*, **1967**, *15*, 204, DOI: 10.1002/0471264180.or015.02.

[6]Leelavathi, P., Kumar, S. R., *J. Mol. Catal. A: Chem.*, **2004**, *240*, 99. doi:10.1016/j.molcata.2005.06.026.

[7]Abaee, M. S., Mojtahedi, M. M., Zahedi, M. M., Khanalizadeh, G., *ARKIVOC*, **2006**, (xv), 48. https://doi.org/10.3998/ark.5550190.0007.f06

[8]Kumbhare, R. M., Sridhar, M., *Catal. Commun.*, **2008**, *9*, 403. doi:10.1016/j.catcom.2007.07.027

[9]Vijender, M., Kishore, P., Satyanarayana, B., *ARKIVOC*, **2008**, (xiii), 122. https://doi.org/10.3998/ark.5550190.0009.d14

[10]Komura, K., Kawamura, T., Sugi, Y., *Catal. Commun.*, **2007**, *8*, 644. doi:10.1016/j.catcom.2006.08.015

[11]Bose, D. S., Narsaiah, A. V., *J. Chem. Res.* (S), **2001**, 36. doi.org/10.3184/030823401103168217

[12]Prashanth Kumar, P. N., Bhojya Naik, H. S., Harish K. N. Viswanath. R, *Arch. Appl. Sci. Res.*, **2013**, *5*, 132.

[13]Chaudhary, R. G., Tanna, J. A., Gandhare, N. V., Rai, A. R., Juneja, H. D., *Adv. Mater. Lett.* **2015**, *6*, 990. doi:10.5185/amlett.2015.5901

[14]Phan, N. T. S., Le, K. K. A., Nguyen, T. V., Le, N. T. H., *ISRN Org. Chem.* **2012**, *2012*, Article ID 928484, 9 pages. doi.org/10.5402/2012/928484

[15]Prajapati, D., Gohain M., *Catal. Lett.*, **2007**, *119*, 59. DOI 10.1007/s10562-007-9186-6.

[16]Mogilaiah, K., Sharath Babu, H., Vidya, K., Shiva Kumar, K., *Indian, J. Chem.*, **2010**, *49B*, 390.

[17]McNulty, J., Steere, J. A., Wolf, S., Tetrahedron Lett. **1998**, *39*, 8013 https://doi.org/10.1016/s0040-4039(98)01789-4

[18]Das Gupta, A., Samanta, S., Mondal, R., Mallik, A. K. *Bull. Korean Chem. Soc.*, **2012**, 33, 4239. http://dx.doi.org/10.5012/bkcs.2012.33.12.4239

[19]Galleti, P., Pori, M., Giacomini, D. *Eur. J. Org. Chem.*, **2011**, *2011*, 3896. DOI: 10.1002/ejoc.201100089

[20]Panda, S. S., Ibrahim, M. A., Oliferenko, A. A., Asiri, A. M.,Katritzky, A. R. *Green Chem.*, **2013**, *15*, 2709. **DOI:** 10.1039/C3GC41255E

[21]Das Gupta, A., Samanta, S., Mondal, R., Mallik, A. K. *Chem. Sci.Trans.*, **2013**, *2*, 524. DOI:10.7598/cst2013.388.

[22]Gutierrez, R. U., Correa, H. C., Bautista, R., Vargas, J. L., Jerezano, A.V., Delgado, F., Tamariz, J. *J. Org. Chem.*, **2013**, *78*, 9614. **DOI:** 10.1021/jo400973g

[23]Chandna, N., Chandak, N., Kumar, P., Kapoor, J. K., Sharma, P.K. *Green Chem.*, **2013**, *15*, 2294. **DOI:** 10.1039/C3GC40797G

[24]Banothu, V., Basude, M., Battu, S. *J. Chem. Pharm. Res.*, **2013**, *5*, 97.

[25]Jursic, B. S., *J. Heterocyclic Chem.*, **2001**, *38*, 655. DOI: 10.1002/jhet.5570380318

[26]Das Gupta, A., Pal, R., Mallik, A. K., *Green Chem. Lett. Rev.*, **2014**, *7*, 404, doi.org/10.1080/17518253.2014.970236.

[27]Chatterjee, A., Biswas, K. M., *J. Org., Chem.*, **1973**, *38*, 4002. **DOI:** 10.1021/jo00987a009

[28]Chegaev, K., Cena, C., Giorgis, M., Rolando, B., Tosco, P., Bertinaria, M., Fruttero, R., Carrupt, P.-A., Gasco A., *J. Med. Chem.* **2009,** *52*, 574. DOI: 10.1021/jm8007008

[29]Biggs, A. I., *J. Chem. Soc.*, **1956**, 2485. **DOI:** 10.1039/JR9560002485

[30]Carey, F. A., Sundburg, R. J., *Advanced Organic Chemistry*, *5th Ed., Part A: Structure and Mechanisms*, Springer, New York, 2007, pp. 593-624.

[31]Ballatore, C., Soper, J. H., Piscitelli, F., James, M., Huang, L., Atasoylu, O., Huryn, D. M., Trojanowski, J. Q., Lee, V. M.-Y., Brunden, K. R., Smith III, A. B., *J. Med. Chem.* **2011**, *54*, 6969. **DOI:** 10.1021/jm200980u.

[32]Berger, S. T. A., Seeliger, F. H., Hofbauer, F., Mayr, H., *Org. Biomol. Chem.*, **2007**, *5*, 3020. **DOI:** 10.1039/B708025E.

[33]Ang, K.-P., Tan, S.-F., *J.C.S. Perkin II*, **1979**, 1525. DOI: 10.1039/P29790001525.

[34]Wolibeis, O. S., Uray, G., *Monatsh. Chem.* **1978**, 109, 123. https://doi.org/10.1007/bf00911952

Received: 31.01.2017.
Accepted: 01.03.2017.

HYPOTHALAMIC PROLINE-RICH PEPTIDE-1 PROTECTS AGAINST MYOCARDIAL ISCHEMIA-REPERFUSION INJURY

A. G. Guevorgyan

Keywords: Hypothalamic proline-rich peptide-1; cardiac output; ischemia-reperfusion; myeloperoxidase; myocardial infarction; neutrophils

Hypothalamic proline-rich peptide-1 (PRP-1), a neurosecretory cytokine appeared to be involved in the multiple mechanisms of cardioprotection. Dose-dependent effects of PRP-1 (4 and 8 μg) were studied in an open-chest model of myocardial ischemia-reperfusion injury (IRI). Adult male Sprague-Dawley rats underwent 40-minute left anterior descending coronary artery occlusion, under isoflurane anesthesia followed by 2 and/or 24 h of reperfusion. Groups treated with PRP-1 were compared to control. It has been revealed that the efficient dose of PRP-1 can restore in a time-dependent manner the contractile activity of the myocardium and suppress the both inflammation and necrosis via amelioration of oxidative stress in the cardiac tissues therethrough contributing to the *in vivo* reduction of myocardial infarct volume and an improvement the cardiac hemodynamics and coronary circulation. New studies are needed to ascertain a beneficial effect of PRP-1 in humans and its future clinic use for the myocardial IRI treatment

* Corresponding Authors
E-Mail: artashes_72@rambler.ru
[a] Yerevan State Medical University called after M. Heratsi, 2 Koryun Street, 0025 Yerevan, Republic of Armenia

INTRODUCTION

Early reperfusion, the process of restoring blood flow to the ischemic myocardium is the most efficient way of prevention the deleterious impact of pathogenic factors associated with myocardial ischemia, to reduce the size of a myocardial infarct and improve the clinical outcome.[1] Although the beneficial effects of myocardial reperfusion are reduced because of the development of ischemia-reperfusion injury (IRI) that leads to arrhythmia, myocardial stunning (the reversible reduction of function of heart contraction after reperfusion), overproduction of reactive oxygen species (ROS). It is accompanied by necrosis apoptosis, and autophagy is contributing to the death of cardiomyocytes viable before myocardial reperfusion.[2,3] Mechanisms underlying IRI are complex and not well understood why there is still no effective, proven therapy against IRI.[4]

We have recently reported that hypothalamic proline-rich peptide-1 (PRP-1) discovered in H. Buniatyan Institute of Biochemistry NAS RA is involved in the mechanisms of cardioprotection by the maintenance of the calcium binding properties of the cardiomyocytes membrane proteins interfering with the standard molecular mechanisms of myocardial damage caused by pancreatic necrosis and/or muscle compression injury.[5,6] At the same time there is evidence that PRP-1 could protect heart tissues on the one hand via inhibition of the phospholipase A2 and the processes of ROS generation and lipid peroxidation, on the other via stimulation the activity of catalase and the energy metabolism, exhibiting membrane-stabilizing effects.[7] Notably, the increased lipoprotein-associated phospholipase A2 levels detected early after myocardial infarction are strongly and independently associated with mortality.[8] This study was performed to investigate whether administration of PRP-1 after induction of ischemia had any effect on the hemodynamic parameters, infarct size and inflammation following ischemic - reperfusion injury.

EXPERIMENTAL

Materials and Methods

The experiments were performed in accordance with the European Communities Council Directives (86/609/EC) on care and use of animals for experimental procedures. These directives are approved by the Animal Care and Ethics Committee of the Center for Vascular Research of Lowe Cancer Research Center of New South Wales University (Australia) and H. Buniatian Institute of Biochemistry (Republic of Armenia). Bovine serum albumin was purchased from Carl Roth (GmbH, Karlsruhe). Solid-phase synthesis of proline-rich peptide-1 (PRP-1) was performed at Moscow laboratory of academic A. A. Galoyan. The PRP-1 preparations were dissolved in saline and filtered (0.22 μm) before use. All other reagents were purchased from Sigma-Aldrich (USA). The work is done in the Center for Vascular Research of Lowe Cancer Research Center of New South Wales University during of June 2010 – August 2010.

Animals and study design

Adult male Sprague-Dawley rats weighing 200-240 g were randomly divided into groups (n=15/group). Control – intact rats; experimental – rats subjected to myocardial ischemia subdivided to untreated, treated with intraperitoneal (*ip*) injections of saline or PRP-1 dissolved in saline (4 or 8 μg) and studied following 2 and/or 24 h reperfusion.

Table 1. Dose-, and time-dependent effects of PRP-1 on cardiac output following myocardial ischemia/reperfusion.

Conditions	**Control**	**Ischemia**		**Ischemia/saline**		**Ischemia/4 μg PRP-1**		**Ischemia/8μg PRP-1**	
Time after releasing the ligature		2 h	24 h	2 h	24 h	2 h	24 h	2 h	24 h
Cardiac output (%)	98	54-57	62-68	54-56	62-67	64-68	96-97	56-58	68-70

A rat model of myocardial ischemia-reperfusion.

Prior to surgery rats were anesthetized with a mixture of ketamine and xylazine (25 and 75 μg kg^{-1} body weight *ip*, respectively). The PRP-1 impact on the heart was studied in an open-chest model of myocardial ischemia-reperfusion injury (IRI), and inhalational anesthesia with isoflurane was performed throughout the experiment.[9,10] Myocardial ischemia was induced by occlusion of the left anterior descending coronary artery (LAD) using a silk suture with a section of silica gel tubing and confirmed by regional cyanosis and ST-segment elevation. After 40 min of ischemia, reperfusion was initiated via releasing the ligature and removing the silica gel tubing. Reperfusion was confirmed by a rapid color change on the heart surface. In the drug treatment group 2 min after artery ligation and the beginning of surgical procedures, rats were *ip* injected with 0.2 ml PRP-1 diluted with normal saline to 4 or 8 μg. An equal volume of saline was used as a vehicle control. Indices of oxidative stress and inflammation were assayed and the myocardial IRI measured at the end of reperfusion.

Determination of myocardial IRI was performed following 2 and/or 24 h reperfusion. LAD was retied, and 2.0 % Evans blue (Sigma-Aldrich, St. Louis, MO, USA) was injected into the left ventricular cavity to delineate the area at risk of myocardial infarction retrospectively.[11] The heart was removed, washed in phosphate buffered saline, and then stained with 1.5 % 2,3,5-triphenyltetrazolium chloride (TTC) (Sigma-Aldrich) via incubation for 15 min at 37°C, to discriminate between the viable non-ischemic area (blue) and the zone at risk (white and red).

Echocardiography was performed prior to ligation and as 40 min ischemia followed by 2 and/or 24 h reperfusion using the Vevo 770 micro-ultrasound system High-Resolution In Vivo Micro-Imaging System (FujiFilm VisualSonics Inc.).Indices of oxidative stress referring to lipid peroxidation processes were established by measuring malondialdehyde (MDA) using thiobarbituric acid.[12] Briefly: Samples were deproteinized with 10 % TCA, and the precipitates were removed by centrifugation at 15000 rpm for 3 min, and supernatants were mixed with 0.72 % TBA and 0.6 N HCl, heated for 15 min in boiling water bath. After that, the absorbance of samples was measured at 535 nm against reagent blank containing all the reagents minus the sample.

The superoxide radical content was measured using cellular ROS/Superoxide Detection Assay Kit (ab139476). Quantification of neutrophil accumulation in the myocardial tissues using hematoxylin and eosin (H&E) staining.[13] Formalin-fixed, paraffin-embedded sections of myocardial tissues were stained with H&E and examined under a light microscope (magnification, ×400).

Myeloperoxidase assay in heart tissues was based on the cytochemical determination of oxybenzidine formed from the benzidine oxidized in the presence of myeloperoxidase.[14] Fresh smears were fixed by 4 % formalin-alcohol solution for 30 seconds, washed, dried, treated with peroxidase reagent for 5 min, washed again, dried and stained with Romanowsky-Giemsa dye. Myeloperoxidase is detected in the cytoplasm of cells as brown granules.

Results and discussion

Inflammation plays a pivotal role in the myocardial IRI pathophysiology, and anti-inflammatory compounds may attenuate detrimental consequences of infection-reperfusion [15, 16]. New hypothalamic cytokine, PRP-1 (primary structure, AGAPEPAEPAQPGVY and apparent molecular mass of 1475.26 Da) represented the C-terminal 25-39 fragment of neurophysin-vasopressin-associated glycoprotein, produced in hypothalamus nuclei (n. paraventricularis and n. supraopticus) and might be involved in the regulation of homeostasis via multiple mechanisms including anti-inflammatory/antioxidant effects.[7] Dose-dependent effects of PRP-1 (4 or 8 μg) were studied in an open-chest model of myocardial ischemia-reperfusion injury (IRI), which is the most acceptable and appropriate model for the reproduction of human myocardial infarction and screening of pharmacological activity of various compounds.[9,10] The different doses of PRP-1 were administered 2 min after artery ligation in accordance with recommendations to enhance the cardioprotective effects and reduce infarct size by introducing drugs before or during ischemia.[17] Quantification of cardiac output using ultrasound was performed prior to occlusion, and following 2 and/or 24 h reperfusion. Data on a left ventricular ejection fraction (LVEF) (the percentage, of blood that is pumped (or ejected) out of the ventricles with each contraction) measured by echocardiography are presented in Table 1.

We revealed that 2h after the release of ligature cardiac output in experimental animals decreased to 54-57 %, compared to control (98 %). Both saline and 8 μg PRP-1 could not improve the low cardiac output that remained approximately on the same level, while 4 μg PRP-1 appeared to be slightly increased LVEF up to 64-68 %. The more pronounced dose-dependent effect of PRP-1 on coronary outflow was observed following 24 h reperfusion, namely: almost restored normal cardiac output (96-97 %) detected in the groups that received 4 μg PRP-1, while no significant changes in the LVEF were seen in the case of the double dose of PRP-1. Time-dependent effects of 4 μg PRP-1 on cardiac output in experimental ischemia-reperfusion are presented in Figs 1 and 2. At this moment, the mentioned dose of PRP-1 appeared to be improved the cardiac hemodynamics and coronary circulation during 24 h reperfusion period.

The cellular and molecular mechanisms regulating the inflammatory response following myocardial ischemia and reperfusion, myocardial necrosis induces complement activation and free radical generation, triggering a cytokine cascade recruiting neutrophils in the ischemic and reperfused myocardium.[18, 19] Treatment with the only efficient dose of PRP-1 (4 µg, *ip*) could decrease the oxidative stress processes in cardiac muscle tissues at early reperfusion period causing the reduction in the reactive oxygen species, particularly superoxide anion ($O_2^{\cdot -}$) and the MDA levels up to 40-45 %, and 20-25 % compared respectively to the rest of groups.

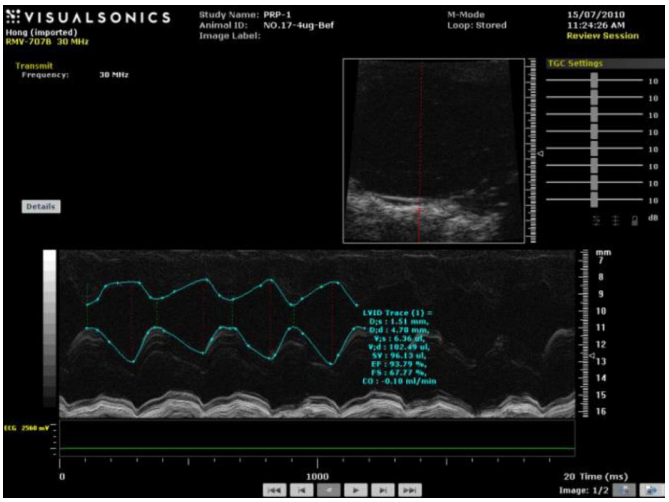

Figure 1. The PRP-1 (4 µg, *ip*) impact on cardiac output (left ventricle) following 2 h reperfusion after coronary artery occlusion in anesthetized rats. Results are shown as mean ± SEM of n = 15/group. $P < 0.05$ compared to control.

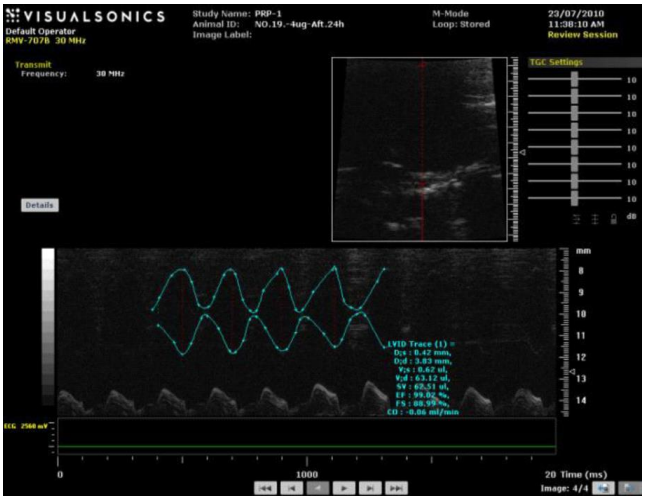

Fig. 2. The PRP-1 (4 µg, *ip*) impact on cardiac output (left ventricle) following 24 h reperfusion after coronary artery 40 min occlusion in anesthetized rats. Results are shown as mean ± SEM of n = 15/group. $P < 0.05$ compared to control.

Neutrophils are mainly contributed to a significant amount of myocardial injury induced by coronary artery occlusion followed by reperfusion.[20] Quantification of neutrophil accumulation in myocardial tissues as a marker of tissue damage showed that the effective dose of PRP-1 (4 µg µg, *ip*) caused a decrease in their number up to 7-8 in the field of view, compared to control following 24 h reperfusion (Fig. 3).

A

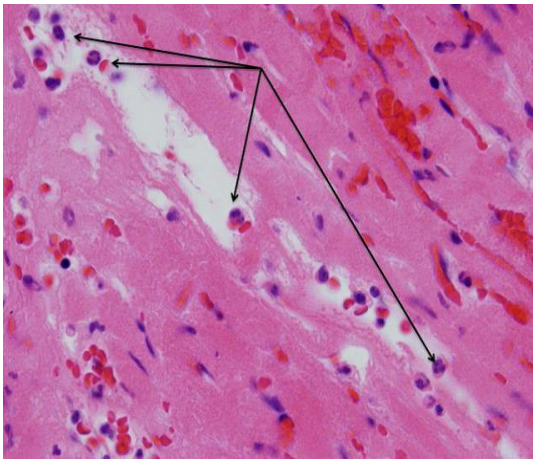

B

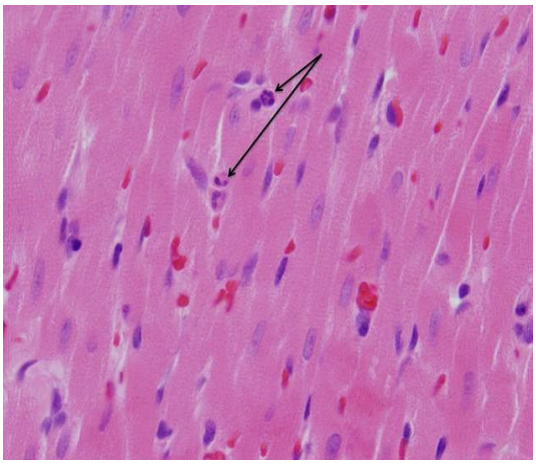

Figure 3. Neutrophil infiltration into cardiac tissues following 24 h reperfusion after coronary artery 40 min occlusion in anesthetized rats. (*A*) Saline-Treated rats (the number of neutrophils 40.3 ± 3.6 per field of view); (*B*) PRP-1-treated rats (4 µg, *ip*; the number of neutrophils per field of view – 7.9 ± 1.2). Hematoxylin and eosin staining (magnification, ×400). Results are shown as mean ± SEM of n = 15/group. $P < 0.05$ compared to control.

The results were confirmed by determination of the myeloperoxidase (MPO) level in the cardiac tissues. MPO is released by activated neutrophils from azurophilic granules and is recognized as a key regulator of neutrophil oxidant production, and an indicator for neutrophil infiltration in tissues; MPO may cause marked damage to cells, extracellular matrix, biological fluids and has been detected at sites of inflammation.[21] Targets and actions of the oxidants generated by MPO and mechanisms of its biological damage are reviewed elsewhere.[22] We found that only the effective dose of PRP-1 (4 µg) could decrease the MPO content in the myocardium during IRI in a time-dependent manner. Despite the administration of PRP-1, there are plenty of brown granules of oxybenzidine pointing to an unusual activity of MPO and indirectly confirm the infiltration of neutrophils following 2 h reperfusion, whereas they virtually disappear following 24 h reperfusion (Fig. 4).

The double dose of PRP-1 exhibited no effect on the MPO level in heart tissues under the same conditions, as well as saline-control.

A

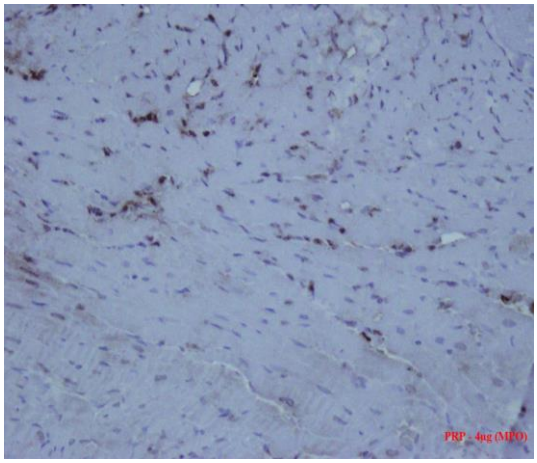

B

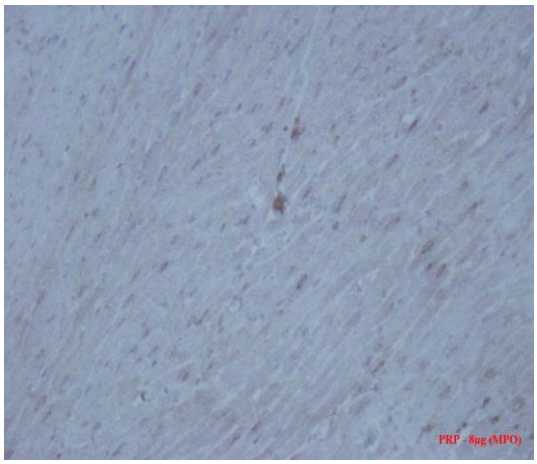

Figure 4. The impact of the effective dose of PRP-1 (4 μg) on the level of myeloperoxidase in cardiac tissues A. Following 2 hours reperfusion after coronary artery 40 min occlusion in anesthetized rats.; B. Following 24 h reperfusion after coronary artery 40 min occlusion in anesthetized rats.; (Hematoxylin staining, magnification, ×40). Results are shown as mean ± SEM of n = 15/group. $P < 0.05$ compared to control.

It should be noted that elevated levels of leukocyte- and blood-MPO are associated with the coronary artery disease.[23] High MPO activity is a risk factor for long-term mortality and adds prognostic value to LVEF measurements in patients with acute myocardial infarction.[24] On induction of IRI, MPO inhibition decreased postischemic apoptosis of cardiomyocytes and reduced cardiac infarct size.[25] Also, the infarct size was smaller in the PRP-1 (4 μg) groups compared to the rest of groups (Fig. 5).

Presumably, the antioxidant activity of the revealed dose of PRP-1 may contribute to the higher safety of cardiomyocytes and reduction of infarct zone. Our findings confirm the antioxidant potential of PRP-1 that could be used in myocardial IRI. However, be aware that not always it is possible to translate findings of animal experiments into clinical therapy.[1] Further research should be done to reproduce the PRP-1 ameliorating effects on myocardial IRI in the clinic.

A

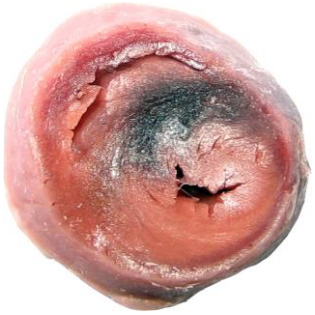

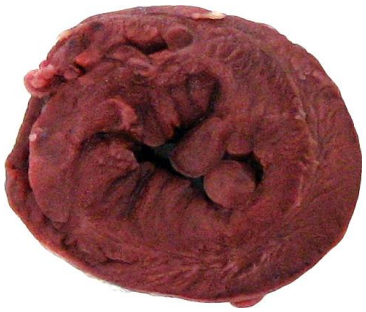

Figure 5. Myocardial ischemia-reperfusion injury (IRI) following 24 h reperfusion after transient occlusion of the left ventricle coronary artery in anesthetized rats. A. Myocardial infarction (the viable non-ischemic area (blue); B. an alleviation of myocardial IRI via ip injection of 4 μg PRP-1.

CONCLUSION

In conclusion, this study demonstrates that the hypothalamic cytokine PRP-1 could substantially reduce a reperfusion injury caused by regional ischemia-reperfusion in the rats in a dose and time-dependent manner. The effective dose of PRP-1 could restore the contractile activity of the myocardium and suppress the both inflammation and necrosis due to ameliorating of oxidative stress in the cardiac tissues and triggering the adaptation processes contributed to the improvement of heart structure and function. The data from this study clearly demonstrate that treatment with appropriate doses of PRP-1 may reduce the cardiomyocyte death, improve the cardiac hemodynamics and coronary circulation. In vivo, post-ischemic administration of PRP-1 significantly reduced myocardial infarct volume caused by transient occlusion of the coronary artery in rats, suggesting that this cytokine might be useful for the treatment of myocardial IRI and this possibility should be further investigated for introduction into clinical practice.

References

[1]Hausenloy, D. J., and Yellon, D. M. "Myocardial ischemia-reperfusion injury: a neglected therapeutic target," *J. Clin. Invest.*, **2013**, *123(1)*, 92–100. https://doi.org/10.1172/JCI62874

[2]Muntean, D. M. Sturza, A., Dănilă, M. D. Borza, C., Duicu, O. M. and Mornoș, C. "The Role of Mitochondrial Reactive Oxygen Species in Cardiovascular Injury and Protective Strategies," *Oxid. Med. Cell. Long.* **2016**, Article ID 8254942, 19 pages. https://doi.org/10.1155/2016/8254942

[3]Jennings, R. B. "Historical perspective on the pathology of myocardial ischemia/reperfusion injury," *Circ. Research.*, **2013**, *113(4)*, 428–438. https://doi.org/10.1161/circresaha.113.300987

[4]Bellanti, F. "Ischemia-reperfusion injury: evidences for translational research," *Ann. Trans. Med.*, **2016**, *4*(Suppl 1), S55. http://doi.org/10.21037/atm.2016.10.52

[5]Galoyan, A. A. "*Biochemistry of novel cardioactive hormones and immunomodulators of the functional system neurosecretory hypothalamus – endocrine heart*," Nauka Publishers. Moscow, 1997.

[6]Guevorkyan, A. G. Alchujyan N. Kh., Mikaelyan, H. M. Barseghyan, V. H. Hairapetyan, H. L. Khachatryan, H. F. Grigoryan, V. S. Melkonyan, L. H. Chailyan, S. G. Kevorkian, G. A. "Beneficial effects of hypothalamic proline-rich peptide-1 on the heart failure associated with experimental pancreatic necrosis and crush syndrome," *Eur. Chem. Bull.*, **2016**, *5(6)*, 259–265, DOI:10.17628/ecb.2016.5.259-265

[7]Galoyan, A. A. "*Brain Neurosecretory Cytokines: Immune Response and Neuronal Survival*," Kluwer Academic/Plenum Publishers, New York, **2004**. https://doi.org/10.1007/978-1-4419-8893-5

[8]Gerber, Y., McConnel, J. P. Jaffe, A. S. Weston, S. A. Killian, J. M. and. Roger, V. L "Lipoprotein-Associated Phospholipase A2 and Prognosis After Myocardial Infarction in the Community," *Arterioscler. Thromb. Vasc. Biol.*, **2006**, *26(11)*, 2517–2522. https://doi.org/10.1161/01.atv.0000240406.89440.0c

[9]Hayashida, K. Sano, S. Ohsawa, I. Shinmura, K. Tamaki, K. Kimura, K. Endo, J. Katayama, T. Kawamura, A. Kohsaka, S. Makino, Sh. Ohta, Sh. Ogawa, S. and Fukuda, K. "Inhalation of hydrogen gas reduces infarct size in the rat model of myocardial ischemia–reperfusion injury," *Biochem. Biophys. Res. Commun.*, **2008**, *373(1)*, 30–35. https://doi.org/10.1016/j.bbrc.2008.05.165

[10]Zhang, Q. Xiang, J. Wang, X. Liu, H. Hu, B. Feng, M. and Fu, Q. "Beta(2)-adrenoceptor agonist clenbuterol reduces infarct size and myocardial apoptosis after myocardial ischaemia/reperfusion in anaesthetized rats," *Br. J. Pharmacol.*, **2010**, *160(6)*, 1561–1572. https://doi.org/10.1111/j.1476-5381.2010.00813.x

[11]Yang, J. Chen, L. Yang, J. Ding, J. Li, S. Wu, H. Zhang, J. Fan, Z. Dong, W. and Li, X. "MicroRNA-22 targeting CBP protects against myocardial ischemia-reperfusion injury through anti-apoptosis in rats," *Mol. Biol. Rep.*, **2014**, *41*, 555–561. https://doi.org/10.1007/s11033-013-2891-x

[12]Buege, J. A. and Aust, S. D. "Microsomal lipid peroxidation," *Method Enzymol.*, **1978**, *52*, 302-310. https://doi.org/10.1016/S0076-6879(78)52032-6

[13]Wang, J., MacKenzie, J. D., Ramachandran, R. and D. Z. Chen, "Identifying neutrophils in H&E staining histology tissue images," P. Colland et al. (Eds): MICCAI 2014, part I, LNCS 8673, 73–80. Springer International Publishing Switzerland, **2014**. https://doi.org/10.1007/978-3-319-10404-1_10

[14]Kinkade, J. M. Pember, S. O. Barnes, K. C. Shapira, R. Spitznagel, J. K. and Martin, L. E. "Differential distribution of distinct forms of myeloperoxidase in different azurophilic granule subpopulations from human neutrophils," Biochem. Biophys. Res. Commun., vol. 114(1), pp. 296–303, 1983. https://doi.org/10.1016/0006-291X(83)91627-3

[15]Yang, J., Fan, Z., Yang, J., Ding, J., Yang, C. and Chen, L. "MicroRNA-22 attenuates myocardial ischemia-reperfusion injury via an anti-inflammatory mechanism in rats," *Experiment. Therap. Med.*, **2016**, *12(5)*, 3249-3255. https://doi.org/10.3892/etm.2016.3777

[16]Uysal, A., Sahna, E., Ozguler, I. M., Burma, O. and Ilhan, N. "Effects of apocynin, an NADPH oxidase inhibitor, on levels of ADMA, MPO, iNOS and TLR4 induced by myocardial ischemia-reperfusion," *Perfusion*, **2015**, *30(6)*, 472-477, 2015. https://doi.org/10.1177/0267659114559260

[17]Hausenloy, D. J. Mocanu, M. M. and Yellon, D. M. "Cross-talk between the survival kinases during early reperfusion: its contribution to ischemic preconditioning," *Cardiovasc. Res.*, **2004**, *63*, 305–312. https://doi.org/10.1016/j.cardiores.2004.04.011

[18]Frangogiannis, G. N., Smith, C. W. and Entman, M. L. "The inflammatory response in myocardial infarction," *Cardiovasc. Res.*, **2002**, *53(1)*, 31-47. https://doi.org/10.1016/S0008-6363(01)00434-5

[19]Bellanti, F. "Ischemia-reperfusion injury: evidences for translational research," *Ann. Transl. Med.*, **2016**, *4(Suppl 1)*, S55. https://doi.org/10.21037/atm.2016.10.52

[20]Jordan, J. E., Zhao, Z. Q. and Vinten-Johansen, J. "The role of neutrophils in myocardial ischemia–reperfusion injury," *Cardiovasc. Res.*, **1999**, *4*, 860-878. https://doi.org/10.1016/s0008-6363(99)00187-x

[21]van der Veen, B. S. de Winther, M. P. and Heeringa, P., "Myeloperoxidase: molecular mechanisms of action and their relevance to human health and disease," *Antioxid. Redox. Signal.*, **2009**, *11*, 2899–2937. https://doi.org/10.1089/ars.2009.2538

[22]Davies, M. J. "Myeloperoxidase-derived oxidation: mechanisms of biological damage and its prevention," *J. Clin. Biochem. Nutr.*, **2011**, *48(1)*, 8–19.

[23]Zhang, R., Brennan, M. L., Fu, X., Aviles, R. J., Pearce, G. L., Penn, M. S., Topol, E. J., Sprecher, D. L. and Hazen, S. L., "Association between myeloperoxidase levels and risk of coronary artery disease," *JAMA*, **2001**, *286(17)*, 2136–2142. https://doi.org/10.1001/jama.286.17.2136

[24]Mocatta, T. J. Pilbrow, A. P. Cameron, V. A. Senthilmohan, R. Frampton, C. M. Richards, A. M. and Winterbourn, C. C. "Plasma concentrations of myeloperoxidase predict mortality after myocardial infarction," *J. Am. Coll. Cardiol.*, **2007**, *49(20)*, 1993–2000. https://doi.org/10.1016/j.jacc.2007.02.040

[25]Liu, H. R., Tao, L., Gao, E., Qu, Y., Lau, W. B., Lopez, B. L., Christopher, T. A., Koch, W., Yue, T. L. and Ma, X. L. "Rosiglitazone inhibits hypercholesterolaemia-induced myeloperoxidase upregulation: a novel mechanism for the cardioprotective effects of PPAR agonists," *Cardiovasc. Res.*, **2009**, *81*, 344–352. https://doi.org/10.1093/cvr/cvn308

Received: 22.01.2017.
Accepted: 02.03.2017.